

# The Antiviral Role of USP10 in Response to Chikungunya and Mayaro Virus Infections

Inaugural-Dissertation  
to obtain the academic degree  
Doctor rerum naturalium (Dr. rer. nat.)

submitted to the Department of Biology, Chemistry, Pharmacy  
of Freie Universität Berlin

by

Elise Christiane Schüler

2024



The research for this thesis was conducted at

Charité Universitätsmedizin Berlin

Institute of Virology

from July 2019 to January 2024

under the supervision of Prof. Dr. Christine Goffinet

1st reviewer: Prof. Dr. Christine Goffinet, Liverpool School of Tropical Medicine

2nd reviewer: Prof. Dr. Gerhard Wolber, Freie Universität Berlin

Date of defense: 18.11.2024

Herewith I certify that I have prepared and written my thesis independently  
and that I have not used any sources and aids other than those indicated by me.

# Table of Contents

1	Introduction.....	1
1.1	Chikungunya virus and other alphaviruses.....	1
1.1.1	The (re-) emergence of Chikungunya and Mayaro virus.....	1
1.1.2	Phylogeny and epidemiology .....	1
1.1.3	Clinical manifestation and diagnostics of CHIKV .....	4
1.1.4	Vaccine development.....	5
1.2	Molecular biology of CHIKV.....	6
1.2.1	Structure and genomic organization .....	6
1.2.2	The replication cycle .....	8
1.2.3	The non-structural protein 3.....	10
1.2.4	Innate immune response to alphavirus infections .....	10
1.2.5	Stress granules in CHIKV infection .....	11
1.3	Cellular Factors .....	14
1.3.1	G3BP1 and 2 .....	14
1.3.2	USP10 .....	15
2	Materials and Methods .....	18
2.1	Materials.....	18
2.1.1	Cell lines .....	18
2.1.2	Bacteria.....	18
2.1.3	Viruses, Pseudotypes and Virus Replicons.....	19
2.1.4	Plasmids .....	19
2.1.5	Oligonucleotides .....	20
2.1.5.1	Cloning Primers.....	20
2.1.5.2	qPCR Primers and Probes .....	21
2.1.6	Enzymes .....	22

2.1.7	Antibodies .....	22
2.1.7.1	Primary Antibodies .....	22
2.1.7.2	Secondary Antibodies.....	23
2.1.8	Cell culture media and supplements .....	23
2.1.9	Disposable materials.....	24
2.1.10	Technical equipment.....	25
2.1.11	Software .....	27
2.2	Methods .....	28
2.2.1	Protein biochemistry .....	28
2.2.1.1	Tandem mass spectrometry .....	28
2.2.1.2	Co-Immunoprecipitation .....	28
2.2.2	Cell culture procedures .....	29
2.2.2.1	Cell lines and culture media .....	29
2.2.2.2	Plasmid transfection .....	30
2.2.2.3	RNA transfection .....	30
2.2.2.4	Virus stock production .....	31
2.2.2.5	Pseudoparticle production .....	31
2.2.2.6	Gene editing .....	32
2.2.3	Molecular biology methods .....	34
2.2.3.1	<i>In vitro</i> transcription .....	34
2.2.3.2	Molecular cloning .....	36
2.2.3.3	Bacterial transformation.....	39
2.2.3.4	Isolation of plasmid DNA .....	40
2.2.3.5	Sanger sequencing .....	40
2.2.3.6	Extraction of cellular RNA.....	40
2.2.3.7	Isolation of viral RNA .....	41
2.2.3.8	Agarose gel electrophoresis .....	41

2.2.4	Readout methods.....	41
2.2.4.1	Luciferase assay .....	41
2.2.4.2	Flow cytometry .....	42
2.2.4.3	Immunoblotting.....	42
2.2.4.4	Two-step reverse transcription qPCR.....	44
2.2.4.5	One-step reverse transcription qPCR.....	45
2.2.4.6	Plaque Assay .....	47
2.2.4.7	Confocal Microscopy .....	47
2.2.5	Next generation sequencing .....	48
2.2.6	Phylogenetic analysis .....	49
2.2.7	Statistical analysis.....	49
3	Results .....	50
3.1	Characterizing USP10 as a binding partner of nsP3 and G3BP.....	50
3.1.1	Tandem mass spectrometry identifies USP10 as a potential binding partner of nsP3.....	50
3.1.2	USP10 co-immunoprecipitates with nsP3 in presence of G3BP .....	51
3.1.3	Interaction between nsP3 and G3BP is driven by aromatic amino acids of a FGDF motif.....	52
3.1.4	USP10 and G3BP1 expression in response to type I IFN and vasopressin	53
3.1.5	Conservation of the USP10 FGxF motif among humans and across vertebrates .....	54
3.2	USP10 in the context of alphavirus infection .....	57
3.2.1	USP10 overexpression inhibits CHIKV and MAYV infections in a dose-dependent manner .....	57
3.2.2	The G3BP binding capability is essential for the antiviral effect of USP10	58

3.2.3	USP10 overexpression inhibits the assembly of G3BP condensates at both early and late time of infection .....	61
3.2.4	<i>USP10</i> knock-out has no significant effect on CHIKV infection.....	64
3.2.5	C-terminal truncation destabilizes USP10 and attenuates its antiviral effect	66
3.2.6	<i>USP10</i> and <i>G3BP1</i> are moderately upregulated upon CHIKV infection	67
3.3	Antiviral mechanisms of USP10 and viral evasion strategies .....	70
3.3.1	Transduction with CHIKV gp-pseudotyped lentiviruses reveals no CHIKV-specific USP10-mediated entry inhibition .....	70
3.3.2	Replication and protein translation in the CHIKV replicon system are unaffected by USP10 overexpression .....	72
3.3.3	Virus progeny is decreased in cells overexpressing wild type and DUB-deficient, but not G3BP-binding deficient USP10 .....	73
3.3.4	Influence of G3BP-binding deficiency in CHIKV nsP3 on virus kinetics and USP10-mediated antiviral response .....	75
3.3.5	Mutation analysis under selective pressure .....	78
4	Discussion .....	81
4.1	Characterization of USP10 and G3BP expression and inducibility .....	81
4.2	Impact of USP10 on alphavirus infection and SG formation.....	84
4.3	Antiviral mechanisms of USP10 and viral evasion strategies .....	89
5	Abbreviations.....	109
6	Acknowledgments .....	113
7	Curriculum Vitae.....	114
8	Appendix .....	115



## Summary

Mosquito-borne alphaviruses like Chikungunya virus (CHIKV) and Mayaro virus (MAYV), which caused endemic outbreaks involving millions of patients over the past decades, pose an emerging threat due to climate-driven expansion of the virus vectors. Recently, the first vaccine against CHIKV was approved by the FDA, however, the lack of antiviral treatments underscores the need for a deeper understanding of virus-host interactions, potentially leading to the development of novel antiviral strategies.

In this thesis, we investigate the role of ubiquitin-specific protease 10 (USP10) in the context of CHIKV and MAYV. Our findings demonstrate that USP10 overexpression significantly reduces infection rates for both alphaviruses. This antiviral effect is independent of USP10's deubiquitinase activity and instead relies on its interaction with the stress granule protein G3BP, mediated by a specific motif (FGDF) within USP10. Notably, USP10 overexpression disrupts the formation of stress granules during CHIKV infection, likely by sequestering G3BP and preventing its aggregation.

Exploring the impact of USP10 on different stages of the viral replication cycle, our findings suggest that USP10 primarily targets the later stages, inhibiting the formation and release of new virus particles. In contrast, CHIKV glycoprotein-mediated entry and viral RNA replication are not significantly affected by USP10. Analogously to USP10, CHIKV nonstructural protein 3 (nsP3) binds G3BP via two FGDF motifs. Cells infected with G3BP binding-deficient mutants displayed no reduction in viral infection upon USP10 overexpression, underlining a critical role of the G3BP-nsP3 interaction in the antiviral effect of USP10.

Finally, we explored the emergence of potential escape variants after serial passaging of CHIKV under selection pressure by USP10 overexpression. Notably, mutations were observed in the nsP2 and E2 proteins, suggesting potential rescue mutations in these proteins counteracting the antiviral activity of USP10. This highlights the selective pressure exerted by USP10, highlighting its importance as an antiviral factor.

In conclusion, this thesis establishes USP10 as a potent cellular inhibitor of alphavirus infection. By targeting the G3BP-nsP3 interaction, USP10 offers a promising path for the development of novel antiviral strategies.

## Zusammenfassung

Durch Mücken übertragene Alphaviren wie das Chikungunya-Virus (CHIKV) und das Mayaro-Virus (MAYV) verursachten in den letzten Jahrzehnten endemische Ausbrüche mit Millionen von Patienten und stellen aufgrund der klimabedingten Ausbreitung der Virusvektoren eine zunehmende Bedrohung dar. Der erste Impfstoff gegen CHIKV wurde jüngst von der FDA zugelassen. Das Fehlen antiviraler Behandlungsmöglichkeiten unterstreicht jedoch weiterhin die Notwendigkeit eines tieferen Verständnisses der Interaktion zwischen Virus und Wirt, welches zur Entwicklung neuer antiviraler Strategien führen könnte.

In dieser Arbeit wird die Rolle der ubiquitinspezifischen Protease 10 (USP10) im Zusammenhang mit CHIKV und MAYV untersucht. Unsere Ergebnisse zeigen, dass die Überexpression von USP10 die Infektionsraten für beide Alphaviren deutlich reduziert. Diese antivirale Wirkung ist unabhängig von der Deubiquitinase-Aktivität von USP10 und beruht stattdessen auf der Interaktion mit dem Stressgranulaprotein G3BP, die durch ein spezifisches Motiv (FGDF) innerhalb von USP10 vermittelt wird. Überexpression von USP10 unterbindet die Bildung von Stressgranula durch CHIKV-Infektion, mutmaßlich durch Sequestrierung von G3BP und Verhinderung seiner Aggregation.

Weiterhin zeigen unsere Untersuchungen der Auswirkungen von USP10 auf verschiedene Stadien des viralen Replikationszyklus, dass USP10 in erster Linie auf die späteren Stadien abzielt und die Bildung und Freisetzung neuer Viruspartikel hemmt. Der durch CHIKV-Glykoproteine vermittelte Zelleintritt und die virale RNA-Replikation werden durch USP10 nicht signifikant beeinflusst. Analog zu USP10 bindet das CHIKV Nichtstrukturprotein 3 (nsP3) G3BP über zwei FGDF-Motive. Zellen, die mit G3BP-bindungsdefizienten Mutanten infiziert wurden, zeigten bei Überexpression von USP10 keine Reduktion der viralen Infektion, was eine kritische Rolle der G3BP-nsP3-Interaktion für die antivirale Wirkung von USP10 unterstreicht.

Abschließend untersuchten wir die Entstehung potenzieller Escape-Varianten nach serieller Passage von CHIKV unter Selektionsdruck durch USP10-Überexpression. Insbesondere wurden Mutationen in den nsP2- und E2-Proteinen beobachtet, was auf mögliche Rescue-Mutationen in diesen Proteinen hindeutet, die der antiviralen Aktivität

von USP10 entgegenwirken. Dies verdeutlicht den durch USP10 ausgeübten Selektionsdruck, und verdeutlicht seine Bedeutung als antiviraler Faktor.

Zusammenfassend charakterisiert diese Arbeit USP10 als potenten zellulären Inhibitor von Alphavirusinfektionen. Indem es auf die G3BP-nsP3-Interaktion abzielt, bietet USP10 vielversprechende Möglichkeiten für die Entwicklung neuer antiviraler Strategien.



# 1 Introduction

## 1.1 Chikungunya virus and other alphaviruses

### 1.1.1 The (re-) emergence of Chikungunya and Mayaro virus

In the recent past, global health has been challenged by the emergence and re-emergence of arboviruses. Among these, Chikungunya virus (CHIKV) and Mayaro virus (MAYV) garnered increasing attention due to widespread epidemic outbreaks (1,2). In 2018, CHIKV was added to the World Health Organization's (WHO) priority list for research and development. Other alphaviruses, including MAYV, were mentioned as a significant concern, indicating an advancing recognition of the risks posed by these viruses (3). CHIKV and MAYV are both arthritogenic alphaviruses, belonging to the *Togaviridae* family. Both viruses display similar clinical manifestations, often including fever, joint pain, and rash (4). Despite their similarities, CHIKV and MAYV differ in their genetic characteristics, transmission vectors, and geographical distributions.

### 1.1.2 Phylogeny and epidemiology

Alphaviruses are categorized into Old World and New World alphaviruses, based on their geographic origin. An overview of the phylogenetics of selected alphaviruses is given in Figure 1A.

Old World alphaviruses, including Chikungunya virus (CHIKV), Semliki Forest virus (SFV), and Sindbis virus (SINV), primarily circulate in Europe, Asia, and Africa. These viruses are transmitted through *Aedes* and *Culex* mosquitoes and are often maintained in a sylvatic cycle, with humans serving as incidental hosts. CHIKV was first identified in 1952 in a patient serum from the Makonde Plateau in today's Tanzania (5,6). Historically confined to Africa and Asia, in the past decades an increasing number of autochthonous infections have occurred in the Americas and Europe. To date, the virus has been reported in more than 110 countries (7). Global expansion is facilitated by the widespread distribution of its primary vectors, *Aedes aegypti* and *Aedes albopictus*.

## Introduction

---

Further spread across the globe is expected due to globalization, urbanization, and climate change (8).

Phylogenetic analysis of CHIKV identified four distinct lineages: West African (WA), East Central South African (ECSA), Asian, and the Indian Ocean Lineage (IOL) (9). As depicted in Figure 1B, each lineage is associated with specific geographic areas. The WA lineage is considered to be the ancestral form of CHIKV. Maintained in an enzootic cycle involving non-human primates and *Aedes* mosquitoes, the WA lineage has primarily been confined to West Africa, causing sporadic outbreaks with relatively limited spread. The Asian lineage emerged in the 1950s and has caused extensive outbreaks in Southeast Asia and the Pacific Islands (10). In 2013, a major outbreak of the Asian lineage spread from the Caribbean islands to more than 50 countries in South America (11). The ECSA lineage had been circulating since the late 20<sup>th</sup> century but gained prominence in 2004-2006 due to major outbreaks on the Indian Ocean islands. The most severe outbreak occurred on La Réunion, where around 35% of the island population was affected. The rapid spread was facilitated by a key mutation in the E1 glycoprotein, A226V, which allowed for the infection of *Aedes albopictus* mosquitoes (12,13). Further, a new distinct lineage, IOL, was identified in patient serum isolates from La Réunion, which further spread to more temperate regions, including Europe and the Americas (14).

New World alphaviruses are predominantly found in the Americas. Many prominent examples are associated with encephalitic symptoms, including Eastern equine encephalitis virus (EEEV), Western equine encephalitis virus (WEEV), and Venezuelan equine encephalitis virus (VEEV). These viruses are mainly transmitted by *Culiseta* and *Culex* mosquitoes and cause the infection of equines, with spillover into human populations (15). MAYV, an arthritogenic New World alphavirus, has caused several outbreaks in South American countries, including Brazil, Peru, and Venezuela (2). MAYV is primarily maintained in a sylvatic cycle involving non-human primates and forest-dwelling mosquitoes such as *Haemagogus* species. However, the potential adaptation to urban mosquito vectors like *Aedes* species raises concerns about the possibility of urban outbreaks, similar to those seen with CHIKV.

Climate change and global travel pose additional challenges, potentially expanding the natural habitats of the transmission vectors and accelerating the spread of alphaviruses (16).

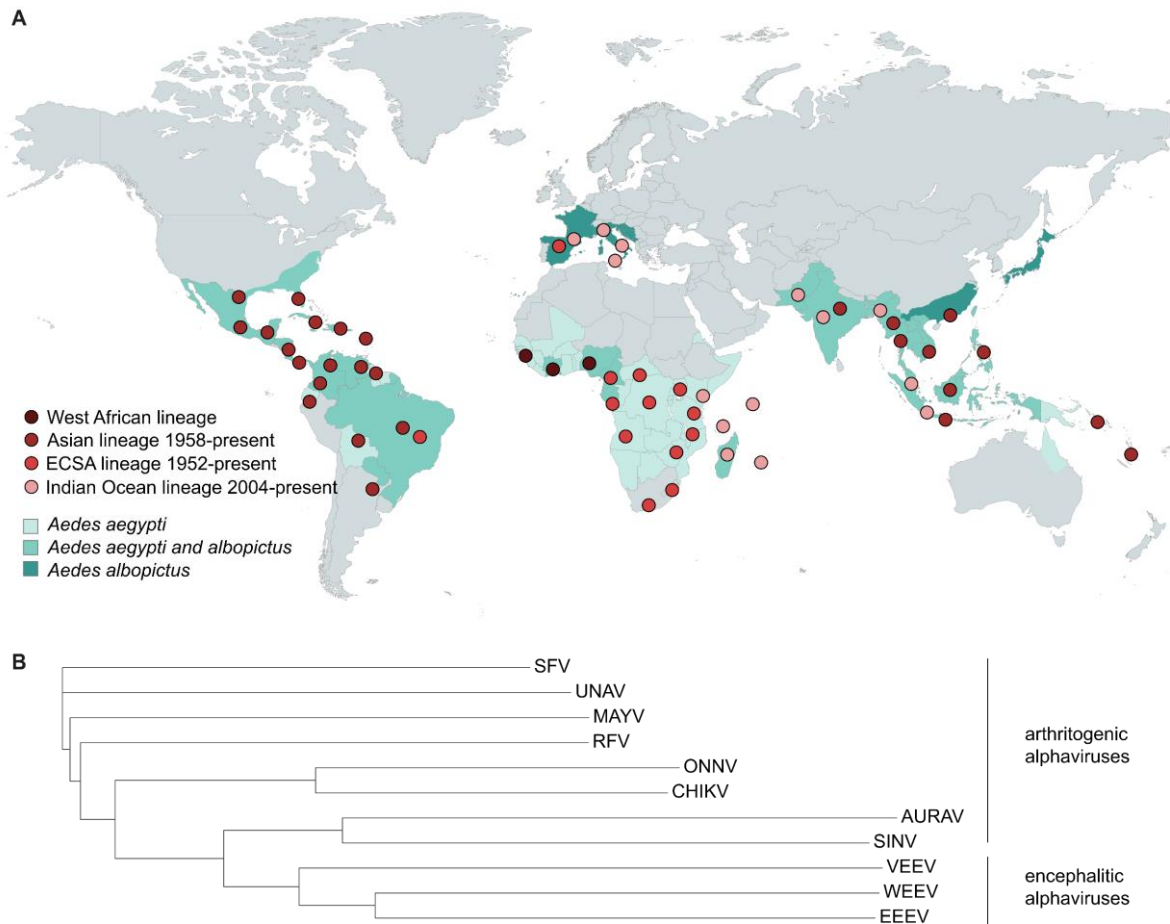


**Figure 1: Global spread of CHIKV and evolutionary relationship to other mosquito-borne alphaviruses. (A)** World map representing autochthonous CHIKV transmission and spread of the transmission vectors. Data from Rezza et al. 2019 (17), updated with data from the World Health Organization (8) and NCBI Virus (18). Created with MapChart and modified with Inkscape 1.3.2. **(B)** Phylogenetic tree of selected mosquito-borne alphaviruses: Chikungunya virus (CHIKV) GenBank NC\_004162, Mayaro virus (MAYV) GenBank NC\_003417, Sindbis virus (SINV) GenBank NC\_001547, Semliki Forest virus (SFV) GenBank NC\_003215, O'nyong-n'yong virus (ONNV) GenBank NC\_075006, Ross River virus (RFV) GenBank NC\_075016, Venezuelan equine encephalitis virus (VEEV) GenBank NC\_075022, Eastern equine encephalitis virus (EEEV) GenBank NC\_003899, Western equine encephalitis virus (WEEV) GenBank NC\_075015, Aura virus (AURAV) GenBank NC\_003900, Una virus (UNAV) GenBank NC\_043403. Created with iTOL v6 (19) and modified with Inkscape 1.3.2.

### 1.1.3 Clinical manifestation and diagnostics of CHIKV

CHIKV infection is categorized into acute, post-acute, and chronic stage, based on the duration after symptom onset. In a proportion of cases (3-25%), the infection remains asymptomatic.

The acute phase of infection begins after an incubation period of 2-10 days, depending on the variant (20), and is characterized by febrile illness, often accompanied by rash, myalgia, and polyarthralgia (4,21). This phase is marked by high-level viremia and a robust innate immune response. Despite a low fatality rate of about 0.1% during this phase, a significant proportion of patients endure prolonged disease manifestations that can last from three months to several years. The underlying mechanism leading to chronic disease manifestation is not fully understood. However, the chronic state of CHIKV typically resembles rheumatoid arthritis in terms of inflammatory pathogenesis and clinical features. Elevated levels of cytokines such as IL-6 and IL-17, suggest a continuous inflammatory state contributing to symptom persistence (22).

The tissue tropism of CHIKV includes epithelial and endothelial cells of various organs, synovial fibroblasts, dendritic cells, and macrophages. In rare cases, particularly in severe or fatal disease outcomes, viral RNA can be detected in the central nervous system (23).

Given the symptomatic overlap with other arboviruses, confirmation of the clinical diagnosis via PCR or serological testing is required. In the initial eight days of infection, reverse transcription-PCR (RT-PCR) is recommended for detecting viral RNA in serum or plasma samples with high specificity and sensitivity (24). Serological testing for CHIKV-specific IgM antibodies is feasible from four days after symptom onset up to two months. Diagnostics via serological assays are limited due to cross-neutralization with other closely related alphaviruses. Compared to IgM antibody tests, plaque reduction neutralization testing (PRNT) for neutralizing antibodies offers more specific evidence of infection but is technically demanding (25).



#### **1.1.4 Vaccine development**

In November 2023, the first vaccine against CHIKV was approved by the FDA (26). Ixchiq, a live-attenuated, single-dose vaccine, is derived from an ECSA strain isolate of the La Réunion outbreak in 2006. Clinical trials demonstrated nearly 100% seroconversion with high safety and tolerability (27,28). Despite these advantages, the application of live-attenuated vaccines bears the risk of systemic reactogenicity, emphasizing the importance of post-market studies.

Several alternative vaccine platforms are progressing through phase II and III clinical trials. Vector-based vaccines are increasingly recognized, after their successful application against SARS-CoV-2 (29–32) and Ebola virus (33). This technique utilizes non-pathogenic viral vectors for the delivery of antigens. Among these, a promising vaccine candidate that is based on the measles vector is V184, also known as MV-CHIK (34). Similarly, virus-like particle (VLP) vaccines deliver antigens via nanoparticles that structurally resemble virions. A notable candidate is VRC-CHKVLP059-00-VP (35), developed by the U.S. National Institutes of Health. Both VLP- and measles-based vaccines have demonstrated safety and immunogenicity in clinical trials, but require multiple doses for optimal efficacy.

Inactivated vaccines like BBV87, based on an Indian strain of CHIKV (36), offer thermostability and safety for use in all populations, including pregnant and immunocompromised individuals. Similarly, DNA vaccines offer numerous advantages in terms of safety, stability, and simplicity in development. On the downside, inactivated and DNA vaccine candidates elicit less immunogenicity compared to live-virus vaccines (37). However, the DNA vaccine candidate pCHIKV-7 demonstrated rapid protection in mice, when combined with monoclonal antibody adjuvants (38,39).

The success of mRNA vaccines in the COVID-19 pandemic has paved the way for this approach in CHIKV vaccine development. mRNA-based vaccines utilize lipid nanoparticles carrying genetically optimized nucleic acids, which deliver the genetic code of immunogenic viral fragments into human cells. Phase I studies of mRNA-1388, encoding the full native structural polyprotein, achieved 100% seroconversion after the second vaccination. These results demonstrate the potential of mRNA technology in CHIKV vaccine development (40).

### 1.2 Molecular biology of CHIKV

#### 1.2.1 Structure and genomic organization

Common for all alphaviruses, CHIKV forms enveloped spherical particles of icosahedral symmetry, measuring 60-70 nm in diameter (41,42). The outer glycoprotein shell contains 240 heterodimers of the viral envelope proteins E1-E2 and is embedded in a host-cell derived membrane, arranged in trimeric surface spikes (35,41,42). The inner core, or nucleocapsid, is composed of 240 capsid proteins encapsulating the ~11.8 kb long positive-sense single-stranded RNA genome (43).

The genome is organized in two open reading frames (ORFs), encoding for the non-structural and the structural polyproteins. Both ends of the genomic RNA are flanked by untranslated regions (UTRs), carrying a 5' cap and a 3' polyadenylated tail (44).

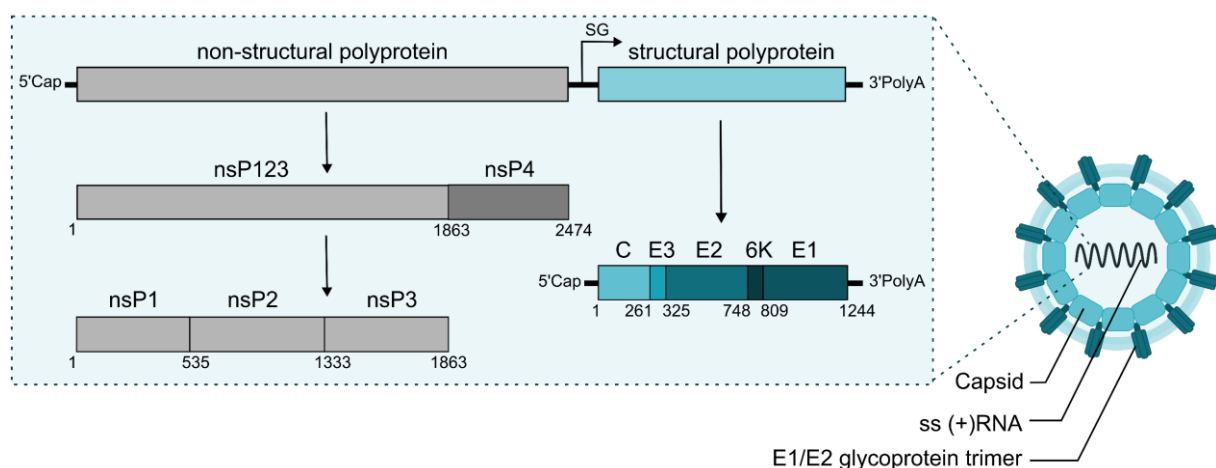


**Figure 2: CHIKV genomic organization.** CHIKV genomic organization and schematic overview of the virion. Created with Inkscape 1.3.2.

The first ORF encodes the non-structural polyprotein (p1234), later cleaved into the individual non-structural proteins (nsPs) (45,46). All four non-structural proteins are involved in the replicase complex that catalyzes the production of new viral RNA.

nsP1 serves as an RNA-capping enzyme (47,48). In concerted action with nsP2, nsP1 adds a 5' cap to the newly formed positive-strand viral RNA (49). Capping prevents RNA degradation by cellular 5' exonucleases and is crucial for ribosomal recognition.

nsP2 is a multifunctional protein, including protease, helicase, and triphosphatase activities (50,51,49,52). The protein cleaves the non-structural polyprotein into functional units. nsP2 is further involved in RNA capping and modulation of the host immune responses (49). nsP3 is the least studied non-structural protein. The protein has an ADP-ribosylhydrolase activity that is crucial for viral replication and a hypervariable domain, which serves as an interaction hub for cellular proteins and is involved in evasion of the innate immune response (53). More details will be discussed in chapter 1.2.3. nsP4 acts as the viral RNA-dependent RNA polymerase, synthesizing both genomic and subgenomic RNAs (54,55).

The second ORF, downstream of a subgenomic promoter, encodes the structural polyprotein consisting of the viral capsid (C), the envelope glycoproteins E1-E3, 6K, and, as an alternative splicing variant, the trans-frame (TF) protein (C-E3-E2-6K/TF-E1).

The capsid protein encapsulates the viral RNA genome and is crucial for virus assembly. The glycoproteins E1 and E2 form the viral envelope (41). E1 mediates membrane fusion during cell entry, while E2 facilitates entry and is involved in receptor binding, thereby determining host tropism (41). E3 is associated with E2 during virus particle maturation, stabilizing the E1-E2 heterodimer and preventing premature fusion (56,57). 6K and the trans frame (TF) protein, which is an alternative frame reading product of 6K, form ion channels in the endoplasmic reticulum (ER) and stimulate virus budding and release (58,59).

**Table 1: CHIKV non-structural and structural proteins with functional domains.**

<b>Protein</b>	<b>Length</b>	<b>Functional Domains</b>	<b>References</b>
nsP1	535 aa	methyltransferase	(60)
		guanylyltransferase	(47)
		membrane-binding domain	(61)
nsP2	798 aa	RNA helicase	(51)
		triphosphatase	(49,50)
		cysteine protease	(52)

## Introduction

---

nsP3	530 aa	ADP-ribosylhydrolase interaction with cellular proteins	(53)
nsP4	611 aa	RNA-dependent RNA polymerase	(54,55)
C	261 aa	RNA binding domain serine protease	(62) (63)
E3	64 aa	E2 transport and budding	(64)
E2	423 aa	receptor binding domains A-C	(65)
6K/TF	61/76 aa	ion channel	(66,67)
E1	435 aa	type II fusion domain Ig-like domain transmembrane domain	(68,69)

---

### 1.2.2 The replication cycle

The replication cycle of CHIKV begins with binding of the surface glycoprotein E2 to a cellular receptor. Various cellular factors have been identified as possible entry-assisting receptors, including prohibitin (70), the matrix-remodeling-associated protein 8 (MXRA8) in vertebrates (71,72), and the ATP synthase  $\beta$  subunit (ATPS $\beta$ ) in insects (73). Virions are primarily internalized via clathrin-mediated endocytosis. A sudden decrease in the endosomal pH triggers the disruption of E1-E2 heterodimers, thereby promoting the fusion of viral and endosomal membranes. Subsequently, viral genomic RNA (gRNA) is released into the cytoplasm and immediately translated into the non-structural polyprotein. This polyprotein undergoes cleavage by the protease activity of nsP2. Matured nsP1, nsP2, nsP3 and nsP4 form the replicase complex, which translocates to the plasma membrane and forms replication spherules. These spherules catalyze the synthesis of negative-sense RNA intermediates, which serve as templates for the production of both the full-length genome and the subgenomic (26S) RNA. The newly synthesized positive-strand RNAs are capped at the 5' end with m7GMP through concerted action of nsP1 and nsP2, and 3' polyadenylation is facilitated by nsP4.

After release from the replication complex, subgenomic RNA is translated into the structural polyprotein (C-E3-E2-6K-E1). The capsid (C) is autoproteolytically cleaved through its inherent protease activity and remains in the cytoplasm to induce packaging of viral gRNA into new virions. The envelope proteins (E1-E3) undergo cleavage by furin proteases and further processing at the ER and the trans-Golgi network. The transmembrane proteins E1 and E2 assemble into heterodimers, that form the glycoprotein shell. 6K and TF, which is produced after a frameshift of the 6K gene, form ion channels in the endoplasmic reticulum, thereby enhance efficient budding and release of virions.

Notably, the replication cycle of CHIKV progresses more rapidly than in other RNA arboviruses, with the first newly formed virions observed after around 5 hours post infection (h. p.i.) in vertebrate cells (74).

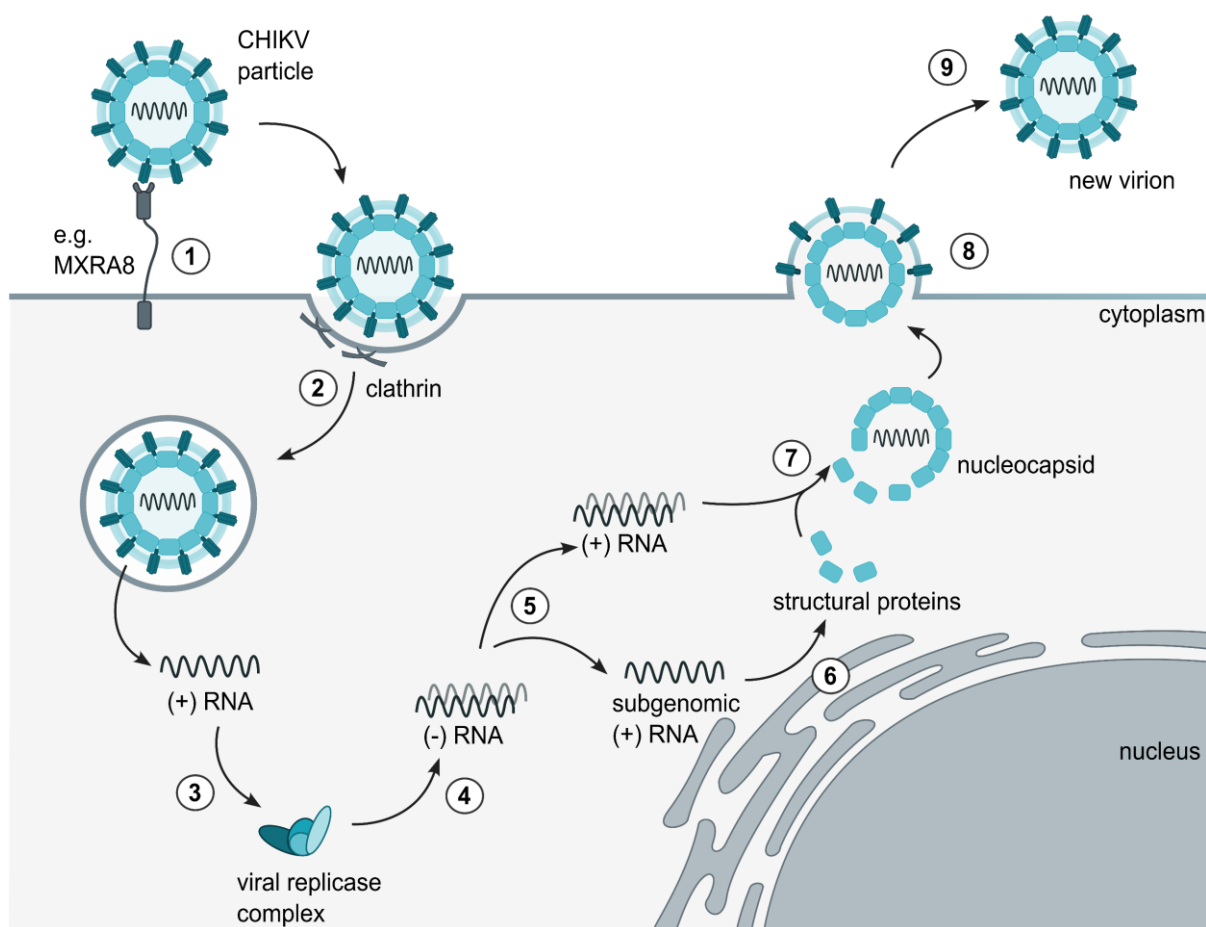


**Figure 3: Schematic overview of the CHIKV replication cycle.** CHIKV E2 glycoprotein binds to host cell entry receptors (1), and the virus enters the cell via clathrin-mediated endocytosis (2). The endosomal membrane disrupts upon a sudden lowering of the pH, and the single stranded positive-

## Introduction

---

sense RNA is released into the cytoplasm. The viral RNA is translated to produce the non-structural proteins (3), which form the viral replicase complex. The viral replicase complex catalyzes the synthesis of negative-sense RNA intermediates (4), which serve as templates for the synthesis of full-length and subgenomic RNA (5). Subgenomic RNA is translated and processed into structural proteins (6). The capsid protein binds genomic viral RNA at the host plasma membrane (7). Mature virions are formed and released by budding through the host plasma membrane (8,9). Created with Inkscape 1.3.2.

### 1.2.3 The non-structural protein 3

The non-structural protein 3 (nsP3) is a multifunctional protein that comprises three domains: The N-terminal macro domain (MD), followed by the zinc-binding alphavirus unique domain (AUD), and the C-terminal hypervariable domain (HVD). The macro domain, a conserved feature across RNA viruses, is involved in the processing of ADP-ribose conjugates (53,75). The AUD is specific to alphaviruses and relatively conserved within the genus. This domain displays a zinc-binding capacity, which is essential for maintaining the structural integrity of nsP3 and contributes to virus genome replication and assembly (76).

The HVD is intrinsically disordered and highly divergent among alphaviruses. However, it harbors several conserved amino acid regions, which serve as specific binding motifs to cellular proteins. The interaction with host factors modulates various cellular pathways and functions during infection, thereby contributing to alphavirus immune evasion strategies (77). Examples include PARP-1 binding to SINV nsP3 HVD, independent of its enzymatic activity and VEEV nsP3 HVD interacting with DDX1/3, promoting viral mRNA translation. This promiscuous binding by the HVD suggests its role in alphavirus adaptation to new hosts. A proviral interaction partner of the HVD is the Four and a half LIM domains protein 1 (FHL1), a cellular protein that is essential for CHIKV replication (78,79). Further, interaction of the HVD with G3BP and Fragile X mental retardation protein (FMRP) (80,81) causes sequestration of these two stress granule components. The interaction with G3BP (82–84) is detailed in chapter 1.3.1.

### 1.2.4 Innate immune response to alphavirus infections

The innate immune system serves as the first line of defense against invading pathogens and is characterized by immediate, non-specific responses. Upon infection,

host cells sense CHIKV components by pattern recognition receptors (PRRs), such as Toll-like receptors (TLRs) and RIG-I-like receptors (RLRs) (85). The presence of single-stranded RNA in the endosome is detected by TLR7 and TLR8, activating MYD88-dependent pathways as an early immune response (86,87). As the infection progresses, double-stranded RNA, a byproduct of viral replication, is sensed by RIG-I and MDA5 (88,89). PRR activation triggers a cascade of signaling pathways, leading eventually to the nuclear translocation of the transcription factors NF- $\kappa$ B, IRF3, and IRF7 (85). IRF3 and IRF7 drive the expression of type I and type III interferons, while NF- $\kappa$ B leads to secretion of pro-inflammatory cytokines.

Released IFNs activate the Janus kinase 1 / signal transducer and activator of transcription (JAK-STAT) pathway in infected and bystander cells by binding to the heterodimeric IFN- $\alpha/\beta$  receptor (IFNAR1/IFNAR2) in case of type I (90), and the IFN- $\lambda$  receptor (IFNLR) in case of type III IFNs (85). JAK-STAT signaling leads to the expression of interferon-stimulated genes (ISGs), such as PRRs, interferon regulatory factors (IRFs), cytokines, chemokines, and proapoptotic molecules. ISGs play various roles in promoting an antiviral state in infected and bystander cells, e.g. by restricting viral replication or inducing apoptosis to prevent further spread of the virus (91,92).

In parallel, NF- $\kappa$ B upregulates genes essential for the recruitment and activation of innate immune cells, including macrophages, dendritic cells, and neutrophils, and influences the activation and differentiation of inflammatory T cells (93). Additionally, NF- $\kappa$ B promotes the transcription of pro-inflammatory cytokines such as IL-1 $\beta$ , IL-6, and tumor necrosis factor  $\alpha$  (TNF- $\alpha$ ), alongside with chemokines including IL-8, CCL2, CCL5, and the growth factor GM-CSF (94). Hence, this pathway plays a dual role in pathogenesis: promoting viral clearance on the one hand, while at the same time contributing to the inflammatory state in infected individuals.

### **1.2.5 Stress granules in CHIKV infection**

Stress granules (SGs) are membrane-less condensates of RNA, RNA-binding proteins (RBPs), and translation factors, formed in response to acute stress, such as oxidation, heat, toxin exposure, or viral infections (95). To manage these stressors, the cell prioritizes survival by shutting down normal protein translation. SG formation is

## Introduction

---

primarily achieved by the inhibition of preinitiation complexes (PICs) through phosphorylation of the eukaryotic initiation factor 2 (eIF2) (96). Depending on the stressor, activation of eIF4-binding proteins may cause additional disruption of the eIF4 translation complex (97).

Early upon CHIKV infection, double-stranded viral RNAs trigger the activation of protein kinase R (PKR) (98). The kinase then phosphorylates the eukaryotic initiation factor 2 $\alpha$  (eIF2 $\alpha$ ), leading to the depletion of translation-initiating ternary complexes at the ribosomal 40S subunit and subsequent polysome disassembly (99). The released mRNAs and 40S subunits form non-canonical complexes, which recruit nucleating proteins such as the stress granule initiation factors G3BP1/2 and the T-cell restricted intracellular antigen-1-related protein (TIA-1/R) (95). Following post-transcriptional and post-translational modifications of mRNAs and proteins, respectively, SG seeds are formed. These SG seeds condensate to larger foci, driven by liquid-liquid phase separation (LLPS) (100). The size, shape, and composition of SG foci varies depending on the stressor. The assembly and disassembly of SGs is regulated by numerous proteins. Known factors for component recruitment and assembly are the Ubiquitin associated protein 2 like (UBAP2L), T-cell restricted intracellular antigen-1 (TIA-1), FMRP, and the FMR1 interacting protein 2 (NUFIP2) (101–103). The Poly(A) binding protein cytoplasmic 1 (PABP1) and Ataxin-2 (ATXN2), two primary SG components, regulate mRNA stability and translation (104,105). Further, the DEAD box 1 protein (DDX1) binds and protects mRNAs upon oxidative stress (106). G3BP1/2, further referred to as G3BPs, play a key role in SG initiation. Overexpression of G3BPs promotes (107), while G3BP knockdown inhibits SG formation (108). Notably, G3BPs are key initiators for SG assembly mediated via eIF2 $\alpha$ /4A inhibition, while heat- or osmotic stress-induced SG formation is G3BP-independent (99). SGs play an important role in the innate immune response to many viruses, including alphaviruses (109), Influenza A virus (110), and the severe acute respiratory syndrome coronavirus 2 (SARS-CoV-2) (111,112).

While SG assembly is induced early after CHIKV infection, the virus counteracts SGs at later stages of infection (113). Three hypotheses for the inhibition mechanism have been discussed in the literature:



(i) The first hypothesis proposes that the hypervariable domain (HVD) of CHIKV nsP3 binds the pivotal SG initiation factors G3BP1 and 2. The nsP3-G3BP complexes sequester the entire pool of G3BPs, thereby hindering SG development and indirectly promoting viral replication (114,115).

(ii) A second hypothesis discussed in the literature indicated that the macro domain of CHIKV nsP3 reduced ADP-ribosylation of G3BP1, resulting in a downregulating of SG formation (116).

(iii) Lastly, a recent study suggests that the inhibition of stress granule formation is a result of transcriptional and translational shutoffs in alphaviruses. The study indicates that, while G3BP binding plays a proviral role in the replication of alphaviruses, it is not crucial for SG clearance (117).

### 1.3 Cellular Factors

#### 1.3.1 G3BP1 and 2

The Ras-GTPase-activating protein SH3-domain-binding proteins 1 and 2 (G3BP1/2), jointly referred to as G3BP, are critical mediators in the cellular stress response, particularly in the formation of stress granules (SGs). The function of G3BP, however, extends well beyond the stress response, impacting various cellular processes such as signal transduction, RNA metabolism, and viral replication.

Members of the G3BP family are characterized by a significant degree of structural disorder. Yet, five functional domains or motifs have been identified (118): the nuclear transport factor 2 (NTF2)-like domain located at the N-terminus, followed by an acidic-rich region, one or several proline-rich (PxxP) motifs, two RNA recognition motifs (RRM), and an arginine-glycine-glycine (RGG) cluster region at the C-terminus (Figure 4).

The NTF2-like domain is highly conserved among the G3BP family and plays a crucial role for the formation of G3BP homodimers, facilitating nuclear transport by binding to nucleoporins (119). Moreover, binding of the alphaviral nsP3 HVD to the NTF2-like domain leads to sequestration G3BP (120). The acidic-rich region acts as an autoinhibitor for stress granule formation by negatively regulating phase separation and can be mitigated by RNA binding (121). The PxxP domain promotes the nucleation of SGs and the recruitment of PKR, which is involved in the antiviral response (122). The RRM domain, comprising two short hydrophobic motifs, and the RGG region, are thought to be involved in RNA binding (123). Further, the presence of the RGG region is essential for the accumulation of G3BP-nsP3 clusters with the host translation initiation machinery, as shown for SFV (83).



**Figure 4: Genomic structure of G3BP.** Schematic representation of G3BP with its known domains. Created with Inkscape 1.3.2.

In response to cellular stress, G3BP rapidly recruits mRNA and other RNA-binding proteins. Thereby, it triggers RNA-dependent liquid-liquid phase separation (LLPS), which leads to the assembly of SG foci. This process is finely tuned by phosphorylation and other post-translational modifications of G3BP (113). The formation of SGs is crucial for cell survival under adverse conditions, as it helps to maintain protein synthesis and protect RNA from degradation.

Beyond stress response, G3BPs are multifunctional proteins, involved in cellular homeostasis and immune signaling pathways. G3BPs are thought to influence Ras signaling, thus playing a role in the regulation of cell proliferation, differentiation, and survival (124). However, G3BP showed no binding to Ras-GTPase-activating proteins (Ras-GAPs) in a later study, contradicting with a direct interaction between G3BP and Ras-GAP (125).

The role of G3BPs in viral infection has been the subject of interest and debated in numerous studies. One important antiviral mechanism is the formation of SGs for mRNA protection and modulation of translation of antiviral proteins. Apart from the role in SG induction, G3BP promotes the cGAS-mediated interferon induction in response to DNA virus and retrovirus infection (126).

Interestingly, proviral roles connected to viral replication and RNA metabolism have been described for G3BP in the context of CHIKV and other RNA viruses (82–84). For instance, the interaction with G3BP is thought to facilitate the assembly of viral replication complexes and potentially modulate SG formation to favor viral replication. In SARS-CoV-2, the nucleocapsid protein interacts with G3BP to facilitate viral replication (111,112,127). Murigneux et al. demonstrated that G3BPs are incorporated in SARS-CoV-2 virions and are required for virus particle assembly (128). These interactions underline the dual role of G3BP in viral pathogenesis, acting both as a host defense factor and a facilitator of viral replication.

### **1.3.2 USP10**

The ubiquitin-specific peptidase 10 (USP10) is ubiquitously expressed and involved in numerous cellular processes, including protein homeostasis, ubiquitin recycling, DNA damage response, and stress granule formation (129). As a member of the

## Introduction

---

deubiquitinase (DUB) family, the enzyme plays a pivotal role in the regulation of protein ubiquitination, a post-translational modification critical for regulating protein stability, localization, and function (130,131).

The protein is highly conserved, with about 99% sequence homology among humans, rats, and mice (129). The human USP10 is 798 amino acids long and features an N-terminal Ataxin 2C domain and a C-terminal deubiquitinase domain, sometimes referred to as catalytic or core domain. The deubiquitinase domain is further partitioned into three regions - palm, thumb, and fingers – reminiscent of a hand's structure (132). The active center is nestled between palm and thumb regions and comprises a cysteine protease, characterized by a catalytic dyad of a cysteine and a histidine residue. A schematic overview is given in Figure 5.

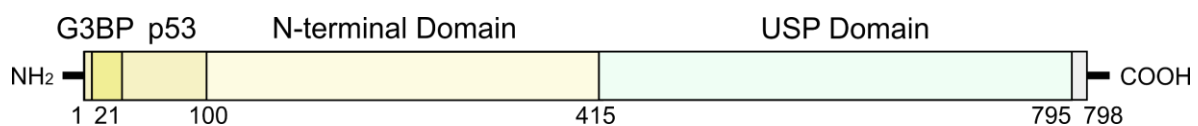


**Figure 5: Genomic structure of USP10.** Schematic representation of USP10 with its known domains. Created with Inkscape 1.3.2.

The ubiquitin-proteasome pathway displays the most important cellular mechanism for protein degradation, used for approximately 90% of intracellular proteins (129). Ubiquitination not only marks proteins for degradation but can also modulate their function and localization. The dynamic interplay between ubiquitination and deubiquitination ensures the precise control of protein function and turnover, which is essential for cellular homeostasis.

USP10 has been shown to deubiquitinate several pivotal proteins, including the tumor suppressor protein p53 (133), cystic fibrosis transmembrane conductance regulator (CFTR), AMP-activated protein kinase alpha (AMPK $\alpha$ ), and the NF- $\kappa$ B-essential modulator (NEMO). These proteins are involved in critical functions such as metabolic regulation, immune response modulation, and tumor suppression. Studies have revealed diverse roles for USP10 in cancer progression. In some cancers, such as colon cancer, USP10 antagonizes the transcription of oncogenes, thereby suppressing tumor growth (134). Similarly, USP10 can inhibit lung cancer cell proliferation by

stabilizing tumor suppressor genes (135). However, USP10 can also act as an oncogene in other cancers, such as prostate cancer, by modulating p53 activity (136).

In addition to its involvement in protein deubiquitylation, USP10 plays a role in the formation of cytoplasmic stress granules by interacting with the G3BP family, leading to the formation of G3BP-USP10 complexes. This interaction is competitive with Caprin-1 for the same binding site within the NTF2-like domain in G3BP. While Caprin-1 promotes stress granule formation, USP10's interaction inhibits it, suggesting a regulatory balance between the soluble and insoluble states of G3BP in complex with either USP10 or Caprin-1 (99,137). Remarkably, previously published crystal structures showed that the same hydrophobic pocket of G3BP interacted with alphaviral nsP3<sub>449-471</sub> and SARS-CoV-2 N<sub>1-25</sub>, underscoring the complex interplay between viral infection and stress granule dynamics mediated by USP10 (120,127,138).

## 2 Materials and Methods

### 2.1 Materials

#### 2.1.1 Cell lines

Cell line	Species	Cell Type	Tissue	Source
BHK-21	<i>Mesocricetus auratus</i>	Fibroblast	Kidney	ATCC CCL-10
CaCo-2	<i>Homo sapiens</i>	Epithelial	Colon (adenocarcinoma)	ATCC HTB-37
CI-huFIB	<i>Homo sapiens</i>	Fibroblast	Skin	InSCREENeX INS-CI-1010
HEK-293	<i>Homo sapiens</i>	Epithelial	Embryonal kidney	Korn Lab, RWTH Aachen
HEK-293T	<i>Homo sapiens</i>	Epithelial	Embryonal kidney	ATCC CRL-3216
HeLa	<i>Homo sapiens</i>	Epithelial	Uterus cervix	ATCC CCL-2
hTert Fib	<i>Homo sapiens</i>	Fibroblast	Skin	Pessler Lab, MH Hannover
U2OS	<i>Homo sapiens</i>	Epithelial	Bone (osteosarcoma)	ATCC HTB-96
Vero E6	<i>African green monkey</i>	Epithelial	Kidney	ATCC CRL-1586

#### 2.1.2 Bacteria

Name	Source
ElectroMAX™ Stbl4™ competent cells	Thermo Fisher Scientific, Waltham, USA
MAX Efficiency™ Stbl2™ competent cells	Thermo Fisher Scientific, Waltham, USA
Stellar™ competent cells	Takara Bio, Kusatsu, Japan

### 2.1.3 Viruses, Pseudotypes and Virus Replicons

Name	Strain	Reporter	Reference
eGFP-CHIKV	LR2006 OPY1	eGFP at 5' end under a subgenomic promoter	(13)
eGFP-MAYV	BeAr 20290	eGFP between ORFs under a subgenomic promoter	(139)
CHIKV E3-E1 Pseudotype	S27-African prototype	eGFP downstream of E3-E1 cassette	(140)
CHIKV-eGFP Replicon	s37997	eGFP downstream of nsP1234 under a subgenomic promoter	(141)

### 2.1.4 Plasmids

Name	Source
GW-pFlag (empty vector)	Generated in-house
GW-pFlag G3BP1	Patricia Korn, RWTH Aachen
GW-pFlag G3BP2	Patricia Korn, RWTH Aachen
GW-pFlag-USP10 C424A	Patricia Korn, RWTH Aachen
GW-pFlag-USP10 F10A	Patricia Korn, RWTH Aachen
GW-pFlag-USP10 fragment01	Generated in-house
GW-pFlag-USP10 fragment02	Generated in-house
GW-pFlag-USP10 fragment03	Generated in-house
GW-pFlag-USP10 fragment04	Generated in-house
GW-pFlag-USP10 wt	Patricia Korn, RWTH Aachen
pACYC-MAYV-eGFP	Bo Zhang, IOV Wuhan
pcDNA 3.1 hCD317-Flag	n/a
pcDNA3.1 (empty vector)	Jerry Kaplan, TheU Salt Lake City
pCHIK-LR2006-OPY 5'eGFP	Graham Simmons, UC San Francisco

## Materials and Methods

---

pCHIKrep1 3'eGFP	Gorben Pijlman, WUR Wageningen
pCMV DR8.91	n/a
pCMV-VSV-G	n/a
pHR-CSII Luciferase	Nikunj Somia, UMN Minnesota
pIRES2-eGFP-CHIKV E3-E1	Babara Schnierle, PEI Erlangen
pLVX-IRES Puro USP10-C424A	Generated in-house
pLVX-IRES Puro USP10-F10A	Generated in-house
pLVX-IRES Puro USP10wt	Generated in-house
pLVX-IRES_Puro	Oya Cingöz, RKI Berlin
pQCXIP human IFITM3-HA	Generated in-house
pHR-CSII Luciferase	Nikunj Somia, UMN Minnesota

---

### 2.1.5 Oligonucleotides

#### 2.1.5.1 Cloning Primers

Description	Sequence 5'-3'
forward primer for USP10 fragments 1-4	GTTAGGCGTTTTGCGCTGCTTCG
reverse primer for fragment 1 (USP10 1-414)	ACTGTCTAGATTAGGGTTGCAACGACACTGG
reverse primer for fragment 2 (USP10 1-100)	ACTGTCTAGATCAGGTTATTTTGGAGCTGTACAAC
reverse primer for fragment 3 (USP10 1-26)	TCTGTCTAGATCATCGAGGAGTCACAAAGAATTG
reverse primer for fragment 4 (USP10 1-17)	TCTGTCTAGATCATTTCATCAGGGCTAAAATCTCC
forward primer for USP10 knock-out in HEK-293T cells	AAACCCATGCAGTGGAACAGTTCTC

---



---

reverse primer for USP10 knock-out in HEK-293T cells	CACCGAGAACTGTTCCACTGCATGG
forward primer for CHIKV ORF1 F1812A mutant	TTCCCCATTACAGCTGGGGACTTCAACGAAGGA
reverse primer for CHIKV ORF1 F1812A mutant	TCCTTCGTTGAAGTCCCCAGCTGTAATGGGGAA
forward primer for CHIKV ORF1 F1830A mutant	TCTGAGCTACTAACTGCCGGAGACTTCTTACCA
reverse primer for CHIKV ORF1 F1830A mutant	TGGTAAGAAGTCTCCGGCAGTTAGTAGCTCAGA

---

### 2.1.5.2 qPCR Primers and Probes

---

<b>Description</b>	<b>Sequence 5'-3'</b>
CHIKV forward	CATCTGCACYCAAGTGTACCA
CHIKV reverse	GCGCATTTCCTTCGTAATG
CHIKV probe	6-FAM/GCGGTGTACACTGCCTGTGACYGC/TAMRA
G3BP1 forward	AGATTCCACCACAAAGACCTCA
G3BP1 reverse	TTCAATGTCACCTTGCTCACC
G3BP1 probe	6-FAM/CTCACGGATTGGTCTGGGTCCCCTTT/TAMRA
USP10 forward	ATTGAGTTTGGTGTGATGAAGT
USP10 reverse	GGAGCCATAGCTTGCTTCTTTAG
USP10 probe	6-FAM/ACCATCAGGGGTATTTTGAAGCTGTAC/TAMRA
MAYV forward	AAGCTCTTCCTCTGCATTGC
MAYV reverse	TGCTGGAAACGCTCTCTGTA
MAYV probe	6-FAM/GCCGAGAGCCCGTTTTTAAAATCAC/TAMRA

---

**2.1.6 Enzymes**

---

<b>Name</b>	<b>Source</b>
BsmBI	New England Biolabs, Ipswich, USA
Q5® High-Fidelity DNA polymerase	New England Biolabs, Ipswich, USA
Antarctic phosphatase	New England Biolabs, Ipswich, USA
NotI-HF	New England Biolabs, Ipswich, USA
SP6 RNA polymerase	New England Biolabs, Ipswich, USA
PfuTurbo DNA polymerase	Agilent, Santa Clara, USA
Platinum™ Taq DNA polymerase	Thermo Fisher Scientific, Waltham, USA
DNase I	Thermo Fisher Scientific, Waltham, USA
MluI-HF	Thermo Fisher Scientific, Waltham, USA
XbaI	Thermo Fisher Scientific, Waltham, USA
T4 Ligase	Thermo Fisher Scientific, Waltham, USA

---

**2.1.7 Antibodies****2.1.7.1 Primary Antibodies**

---

<b>Name</b>	<b>Dilution</b>	<b>Application</b>	<b>Source</b>
monoclonal mouse anti-Flag [M2]	1:500	FC	Sigma-Aldrich, Merck KGaA, Darmstadt
monoclonal mouse anti-G3BP1 [2F3]	1:1000	IF	abcam, Cambridge, UK
monoclonal mouse anti- $\beta$ -actin [8226]	1:2000	WB	abcam, Cambridge, UK
monoclonal rabbit anti-TIA1 [EPR9304]	1:1000	IF	abcam, Cambridge, UK
monoclonal rabbit anti-USP10 [EPR4261]	1:2000/1:250	WB/IF	abcam, Cambridge, UK

---

polyclonal rabbit anti-CHIKV antiserum	1:2000	WB	IBT Bio Services, Rockville, USA
--	--------	----	----------------------------------

FC: Flow Cytometry, IF: Immunofluorescence, WB: Western Blot

### 2.1.7.2 Secondary Antibodies

Name	Dilution	Application	Source
Donkey anti-mouse IgG (H+L) Alexa Fluor 647	1:1000/1:4000	IF/FC	Thermo Fisher Scientific, Waltham, USA
Donkey anti-rabbit IgG (H+L) Alexa Fluor 568	1:1000	IF	Thermo Fisher Scientific, Waltham, USA
Goat anti-Mouse IRDye 800CW 1mg/ml (WB)	1:10000	WB	LI-COR Corporate, Lincoln, USA
Goat anti-Rabbit IRDye 680RD 1mg/ml (WB)	1:10000	WB	LI-COR Corporate, Lincoln, USA
Goat anti-Rabbit IRDye 800CW 1mg/ml (WB)	1:10000	WB	LI-COR Corporate, Lincoln, USA
Goat-anti-Mouse IRDye 680RD 1mg/ml (WB)	1:10000	WB	LI-COR Corporate, Lincoln, USA

FC: Flow Cytometry, IF: Immunofluorescence, WB: Western Blot

### 2.1.8 Cell culture media and supplements

Name	Source
Dulbecco's Modified Eagles Medium	Sigma-Aldrich, Merck KGaA, Darmstadt
Dulbecco's Phosphate Buffered Saline	Sigma-Aldrich, Merck KGaA, Darmstadt
Fetal Calf Serum	Thermo Fisher Scientific, Waltham, USA
L-Glutamine (200 mM)	Thermo Fisher Scientific, Waltham, USA
OptiMEM Reduced Serum Medium	Thermo Fisher Scientific, Waltham, USA
Penicillin-Streptomycin (10,000 U/mL)	Thermo Fisher Scientific, Waltham, USA

## Materials and Methods

---

---

Poly-L-Lysine	Sigma-Aldrich, Merck KGaA, Darmstadt
Trypsin-EDTA (0.5%)	Thermo Fisher Scientific, Waltham, USA

---

### 2.1.9 Disposable materials

---

Name	Source
Cell culture flask with filter cap (25, 75, 175 cm <sup>2</sup> )	Sarstedt AG & Co., Nümbrecht
Cell culture plates (6-, 12-, 24-, 96-well)	Greiner Bio-One, Kremsmünster, Austria
Centrifuge tubes (15, 50 mL)	Sarstedt AG & Co., Nümbrecht
Centrifuge tubes (15, 50 mL)	Corning Inc., USA
Microscopy $\mu$ -slides (8-well)	ibidi GmbH, Gräfelfing
Reaction tubes (1.5, 2 mL)	Sarstedt AG & Co., Nümbrecht
Electroporation cuvettes, 4 mm	Bio-Rad Laboratories Inc., Hercules, USA
Lumitrac 600 Micro-Plates (96-well)	VWR, Darmstadt
PCR plates (96-well)	Agilent, Santa Clara, USA
Bottle top filter, 0.45 $\mu$ m polystyrene membrane	Thermo Fisher Scientific GmbH, Schwerte
Serological pipettes (2, 5, 10, 25, 50 mL)	Sarstedt AG & Co., Nümbrecht
Pipette tips (10, 100, 200, 1000 $\mu$ L)	Sarstedt AG & Co., Nümbrecht
Petri dishes	Sarstedt AG & Co., Nümbrecht
Cryotubes	Sarstedt AG & Co., Nümbrecht

---

**2.1.10 Technical equipment**

<b>Application</b>	<b>Model</b>	<b>Company</b>
Agarose gel electrophoresis system	Perfect Blue Gel System Mini	VWR Biotechnologie GmbH, Erlangen
Autoclave	Varioklav® Typ 500	H+P Labortechnik, Oberschleisheim
	S1000	Matachana GmbH, Selmsdorf
	System VX-100	System GmbH, Linden
Centrifuges	Centrifuge 5424	Eppendorf, Hamburg
	Centrifuge 5810R	Eppendorf, Hamburg
	Centrifuge 5430	Eppendorf, Hamburg
Chemiluminescence reader	Synergy™ 2	BioTek, Vermont, USA
CO <sub>2</sub> incubators	HERAcell® 240	Fisher Scientific GmbH, Schwerte
	Heraeus® B6126	Fisher Scientific GmbH, Schwerte
	Mini-PROTEAN® Tetra Cell	Bio-Rad Laboratories GmbH, Feldkirchen
Electroporation system	GenePulser Xcell Electroporation System	Bio-Rad Laboratories GmbH, Feldkirchen
Freezer	Liebherr Premium -20°C	Liebherr, Biberach a. d. Riß
	Typ499 -80°C	Kaltis Europe GmbH, Niederweningen, Switzerland
	Innova® U725 -80°C	Eppendorf, Hamburg
Gel Documentation	ChemiDoc XRS+	Bio-Rad Laboratories GmbH, Feldkirchen
Heat block	Thermomixer comfort	Eppendorf, Hamburg

## Materials and Methods

---

Magnetic stirrer	REO basic IKAMAG	IKA®-Werke GmbH & CO, KG, Staufen
Microscopes (Confocal)	Zeiss LSM 800	Carl Zeiss Jena GmbH, Jena
	Leica TCS SP8	Leica Microsystems, Wetzlar
Microscopes (Epifluorescence)	Axio IMAGER M1	Carl Zeiss Jena GmbH, Jena
	Leica DMI8 S	Leica Microsystems, Wetzlar
Microscopes (Brightfield)	TELAVAL 31	Carl Zeiss Jena GmbH, Jena
	Axio Vert.A1	Carl Zeiss Jena GmbH, Jena
PCR cycler	Mastercycler® nexus	Eppendorf, Hamburg
PCR cycler, real-time	LightCycler® 480	Roche Diagnostics, Mannheim
pH meter	766 Calimatic	Knick Elektronische Meßgeräte GmbH, Berlin
Pipettes	Research® PhysioCare (0.5-10 µl, 10-100 µl, 100-1000µl)	Eppendorf, Hamburg
	Research® PhysioCare Multichannel	Eppendorf, Hamburg
	Accujet® pro	Brand, Wertheim
Spectrophotometer	NanoDrop 2000c	VWR, Darmstadt
Thermo mixer	Comfort 5355	Eppendorf, Hamburg
Vortex mixer	VV3	VWR, Darmstadt
Water bath	1092	GFL, Burgwedel
	51221029	Precision Westlock, Alberta, Canada

---

---

Water purification system	Milli-Q® Biocel	Merck KGaA, Darmstadt
Western Blot System	Trans-Blot® Turbo™ Transfer System	Bio-Rad Laboratories GmbH, Feldkirchen

---

### 2.1.11 Software

---

<b>Software</b>	<b>Developer</b>	<b>Version</b>
Adobe Illustrator	Adobe	27.4.1
Adobe Photoshop	Adobe	25.4
Biomatters Geneious	Biomatters	9.1.8
Biorender	BioRender	© 2024
Biotek Gen5	Agilent	3.0
CellProfiler	Broad Institute Inc.	4.2.6
FlowJo	BD Biosciences	10.7.1
GraphPad Prism	GraphPad	9.5.1
ImageJ	NIH	1.54f
Inkscape	Inkscape	1.3.2
JACoP Plugin for ImageJ	Bolte S, Cordelières FP	2.1.4
Leica LAS X	Leica	5.1.0
LightCycler 480	Roche	1.5
Microsoft Office	Microsoft	365
PyMOL	Schrödinger, LLC	2.5.2
Zen blue edition	Carl Zeiss	3.0
Zotero	Digital Scholar	6.0.30

---

## 2.2 Methods

### 2.2.1 Protein biochemistry

#### 2.2.1.1 Tandem mass spectrometry

Tandem mass spectrometry (MS/MS) was used to identify protein-protein binding. Sample preparation involved two distinct approaches:

(i) Tandem Affinity Purification (TAP) was used for the purification of protein complexes under near-physiological conditions. The TAP tag comprised a calmodulin-binding peptide (CBP) and the IgG-binding domains of *Staphylococcus aureus* protein A, separated by a tobacco etch virus (TEV) protease cleavage site. The initial purification step was performed using IgG Sepharose beads, followed by cleavage with the TEV protease. The first eluate was further purified over a calmodulin-binding resin and eluted with ethylene glycol tetraacetic acid (EGTA). This approach primarily identifies stable protein-protein interactions.

(ii) Secondly, proximity labeling experiments were conducted via BirA biotinylation. The *E. coli* biotin ligase BirA was fused to the target protein, enabling the biotinylation of proximate proteins. Streptavidin was used for the isolation of biotinylated proteins, thereby including both stable and transient interaction partners of the protein of interest.

Tandem mass spectrometry and initial analysis with MaxQuant software (142) were conducted by our collaboration partner Prof. Dr. Patricia Korn and her lab at RWTH Aachen University.

#### 2.2.1.2 Co-Immunoprecipitation

HEK-293T cells were plated and cultured for 48 hours before transfection with plasmids encoding eGFP-tagged CHIKV nsP3 (wildtype, V33E, or Y114V variants) via calcium phosphate precipitation. The GFP tag was located at the N-terminus of CHIKV nsP3. Transfection efficiency was monitored by GFP fluorescence.

At 48 hours post-transfection (h p.t.), cells were lysed in Co-IP lysis buffer containing 50 mM Tris (pH 7.5), 150 mM NaCl, 1 mM EDTA, 10% glycerol, 1% NP-40, 2 mM



Tris(2-carboxyethyl)phosphine (TCEP), and a protease inhibitor cocktail (PIC) to ensure protein integrity. The cell lysates were centrifuged for 30 minutes at 4 °C to remove cell debris.

For immunoprecipitation, eGFP-CHIKV nsP3 complexes were isolated using anti-GFP antibodies conjugated to protein G beads. The antibody-bead mixture was incubated with the cell lysates for 1 hour at 4 °C. Subsequently, the beads were first washed with Co-IP lysis buffer and then with Co-IP reaction buffer containing 50 mM Tris (pH 8.0), 2 mM TCEP, and 4 mM MgCl<sub>2</sub>. The immunoprecipitated proteins, along with whole cell lysates (WCL), were separated using SDS-PAGE and analyzed by Western blotting.

Co-immunoprecipitation analysis was conducted by our collaboration partner Prof. Dr. Patricia Korn and her lab at RWTH Aachen University.

### 2.2.2 Cell culture procedures

#### 2.2.2.1 Cell lines and culture media

HEK-293 cells (Korn Lab, RWTH Aachen) were cultivated in Dulbecco's modified Eagle's medium (DMEM) containing 4.5 g/L glucose and supplemented with 10% heat-inactivated fetal calf serum (FCS) at 37 °C and 5% CO<sub>2</sub>.

HEK-293T (ATCC CRL-3216), CI-huFIB (InSCREENeX, Cat. No.: INS-CI-1010), hTert Fib (kind gift from Frank Pessler's lab, MH Hannover), CaCo-2 (ATCC HTB-37), U2OS (ATCC HTB-96), HeLa (ATCC CCL-2) and Vero E6 (ATCC CRL-1586) cells were cultivated in DMEM containing 4.5 g/L glucose, supplemented with 10% heat-inactivated FCS, 100 µg/mL streptomycin and 2 mM L-glutamine at 37 °C and 5% CO<sub>2</sub>. HEK-293T-USP10KO cells were additionally supplemented with 1 µg/ml Puromycin.

CI-huFIB (InSCREENeX, Cat. No.: INS-CI-1010) is a human dermal fibroblast cell line, immortalized using the CI-SCREEN technology (143). The hTert Fib cell line, a kind gift from Frank Pessler's lab, MH Hannover, is an SV40-transformed and hTert-immortalized human dermal fibroblast cell line derived from healthy donors (144). Both cell lines were cultivated in DMEM containing 4.5 g/L glucose, supplemented with 10% heat-inactivated FCS, 100 µg/mL streptomycin, and 2 mM L-glutamine at 37 °C and 5% CO<sub>2</sub>.

All experiments in eukaryotic cell lines were performed under sterile conditions using laminar flow workstations described in the Materials section.

### 2.2.2.2 Plasmid transfection

Plasmids encoding USP10 wild type, F10A, or C424A were transfected into HEK-293T cells using the plasmids GW-pFlag-USP10 via Lipofectamine 3000 according to the manufacturer's protocol. In short, cells were seeded at a density of  $2.5 \times 10^5$  cells per mL in a 6-well plate, 12-well plate, 96-well plate, or ibidi microscopy slide format. After 24 hours, cells reached 60-80% confluency, as confirmed under microscope observation. Cells were washed once and fresh medium was added. For each transfection, two separate tubes were prepared: In tube A, plasmid DNA and P3000 reagent were mixed in Opti-MEM in a 1:2 ratio (e.g. 3  $\mu$ g plasmid DNA mixed with 6  $\mu$ l P3000 in 62  $\mu$ l Opti-MEM). In tube B, Lipofectamine 3000 was mixed in Opti-MEM in the same volume as P3000 (e.g. 6  $\mu$ l Lipofectamine 3000 in 62  $\mu$ l Opti-MEM). Tube A was mixed gently into tube B in a 1:1 ratio. After an incubation period of 15 minutes at room temperature, the DNA/Lipofectamine/P3000 mixture was added dropwise to each well. Cells were incubated at 37 °C and 5% CO<sub>2</sub> for 24 hours for further use in infection experiments. At the same time, transfection control cells were harvested and prepared for Western Blot (WB) or FACS assay. For microscopy experiments, cells were washed twice after 16-18 hours and cultivated in fresh DMEM including supplements. Microscopy slides were further used for infection experiments after 48 hours.

### 2.2.2.3 RNA transfection

Replicon RNA was *in vitro* transcribed as described in chapter 2.2.3.1. RNA was transfected into HEK-293T cells via a Lipofectamine 2000 transfection kit, according to the manufacturer's instructions. For transfection of HEK-293T cells in 6 well plate format, 3  $\mu$ g of *in vitro* transcribed RNA was mixed with 100  $\mu$ L Opti-MEM. In a separate reaction tube, 6  $\mu$ L Lipofectamine 2000 was mixed with 100  $\mu$ L Opti-MEM. Both tubes were mixed together in a 1:1 ratio and incubated for 15-20 minutes, before dropwise addition to the cells. Transfected cells were washed in phosphate buffer saline (PBS)

after four hours and cultivated in DMEM supplemented with 10% heat-inactivated FCS, 100 µg/mL streptomycin, and 2 mM L-glutamine at 37 °C and 5% CO<sub>2</sub> for 48 hours. To validate successful RNA transfection, eGFP expression was quantified as a surrogate of replicon translation at 48 h. p.t. via flow cytometry.

#### **2.2.2.4 Virus stock production**

Virus stocks were produced by electroporation of *in vitro*-transcribed RNA into BHK-21 cells, using pCHIK-LR2006-OPY-5'eGFP (Tsetsarkin et al., 2007) or pACYC-MAYV-eGFP (Li et al., 2019) for eGFP-CHIKV and eGFP-MAYV virus stocks, respectively. Electroporation was performed in a 4 mm electroporation cuvette using “square wave” modus with the following settings: 250 V, 15 milliseconds pulse length, two pulses with an interval of 1 second. Cells were cultivated in fresh medium immediately after electroporation. After two days, cells were observed under the microscope to check for cell death as a sign of cytopathic effect (CPE) of viral infection. The supernatant of electroporated BHK-21 cells was collected and centrifuged at 5000g for 5 minutes, followed by filtering through a sterile 0.45 µm membrane filter. The purified virus suspension was aliquoted and stored at -80 °C. Virus titer was determined via plaque assay on Vero E6 cells. Additionally, the virus was titrated on HEK-293T cells, followed by eGFP quantification via flow cytometry after 24 hours, for determination of a cell line-specific titer.

#### **2.2.2.5 Pseudoparticle production**

Lentiviral vector particles pseudotyped with either chikungunya virus glycoprotein (CHIKV-gp) or vesicular stomatitis virus glycoprotein (VSV-G) and encoding for luciferase were generated by calcium phosphate-based transfection of HEK-293T cells with the packaging plasmid pCMV ΔR8.91 (Zufferey et al., 1997), the lentiviral transfer plasmid pie-EF-luciferase (Agarwal et al., 2006) and either pCMV-VSV-G (Stewart et al., 2003) or IRES2-eGFP-CHIKV E3-E1 (Weber et al., 2017).

For the generation of lentiviral particles, HEK-293T cells were seeded in 10 cm cell culture dishes (3 x10<sup>7</sup> cells/dish). After 24 hours, cells were transfected via calcium

## Materials and Methods

---

phosphate transfection reagent (Takara Bio) according to the manufacturer's protocol. In short, CaCl<sub>2</sub>-solution was mixed into sterile H<sub>2</sub>O and all three plasmids were added in the following amounts:

---

Component	Input per reaction
Sterile H <sub>2</sub> O	615 µL
CaCl <sub>2</sub> solution	85 µL
pCMV ΔR8.91	0.5 µg
pie-EF-luciferase	10 µg
pCMV-VSV-G or IRES2-eGFP-CHIKV E3-E1	5 µg

---

The reaction mix was dropwise mixed into 2X HBS buffer in a 1:1 ratio and incubated for 20 minutes at room temperature. Subsequently, the final transfection mix was carefully added to the HEK-293T cells (1.4 mL/dish). Cells were incubated at 37 °C and 5% CO<sub>2</sub>. After 16-18 hours, cells were washed in PBS and fresh medium was added. Another 24 hours later, the supernatant was filtered using a 0.45 µm sterile filter cup and centrifuged over 20% sucrose in a vacuum ultracentrifuge with 30000 rpm at 4 °C for 90 minutes. The supernatant was aspirated carefully. Lentiviral particles, attached to the bottom of the centrifuge tubes, were resuspended in 350 µL medium and stored in aliquots at -80 °C.

### 2.2.2.6 Gene editing

*USP10* knock-out (KO) was introduced into HEK-293T cells via CRISPR/Cas9-mediated gene editing using the lentiCRISPRv2-puro vector. The knock-out targeted the following sequence on the antisense strand of *USP10*: GAGAACTGTTCCACTGCATGGGAGG. The protospacer adjacent motif, short PAM, is underlined.

To clone the target sequence into the lentiCRISPRv2-puro backbone, two gRNAs were designed that included the target sequence and included restriction sites for the

restriction enzyme BsmBI (USP10\_gRNA-B2\_rv: CACCGAGAACTGTTCCACTGC ATGG and USP10\_gRNA-B2\_fw: AAACCCATGCAGTGGAACAGTTCTC).

The lentiCRISPRv2-puro vector (Addgene plasmid #98290) was mixed with BsmBI and NEB buffer 3.1 in the following setup and incubated at 55 °C overnight for a complete digestion:

<b>Component</b>	<b>Input per reaction</b>
lentiCRISPRv2-puro plasmid DNA	2 µg
BsmBI restriction enzyme	1 µL
NEB buffer 3.1	2.5 µL
Nuclease-free H <sub>2</sub> O	Ad 25 µL

On the next day, the linearized DNA was subjected to agarose gel electrophoresis (0.7% agarose gel) for size separation. The DNA product with the expected size was cut out and extracted using the NucleoSpin™ Gel and PCR clean-up kit according to the manufacturer's protocol.

In parallel, the oligonucleotides were prepared for annealing in the following setup:

<b>Component</b>	<b>Input per reaction</b>
USP10_gRNA-B2_rv (100 µM)	2 µL
USP10_gRNA-B2_fw (100 µM)	2 µL
10X T4 Ligation buffer	2 µL
Nuclease-free H <sub>2</sub> O	14 µL

Oligonucleotide mix was heated in a thermocycler up to 95 °C for 5 minutes, followed by a continuous temperature decrease of 5 °C/minute until the temperature reached 25°C. Annealed oligonucleotides were diluted 1:200 in nuclease-free water.

The ligation reaction was set up as follows:

---

Component	Input per reaction
Linearized lentiCRISPRv2-puro	50 ng
Oligonucleotide duplex (10 $\mu$ M)	1 $\mu$ L
10X T4 Ligation buffer	1.2 $\mu$ L
T4 DNA Ligase	0.8 $\mu$ L
Nuclease-free H <sub>2</sub> O	Ad 12 $\mu$ L

---

Ligation mix was incubated at 16 °C overnight. Ligated DNA was immediately used for bacterial transformation (see 2.2.3.2 Bacterial transformation).

HEK-293T cells were transduced with lentiviral particles and kept in culture for 72 h prior to selection with puromycin (1  $\mu$ g/mL). Medium was changed every 2-3 days. After 7 days of selection, cells were seeded in 96-well plates with a calculated concentration of 0.5 cell/ well to obtain single cell clones. After 2-3 weeks of propagation, single cell clones were analyzed for successful gene knock-out in Sanger sequencing (Microsynth SeqLab, Göttingen, Germany) using the following standard primer: hU6-f GAGGGCCTATTTCCCATGATT. Additionally, knock-out was validated via immunoblotting.

### 2.2.3 Molecular biology methods

#### 2.2.3.1 *In vitro* transcription

*In vitro* transcription was performed on eGFP-expressing CHIKV replicon plasmids to obtain replicon RNA, further used for transfection. Plasmids containing different versions of CHIKV replicon, a kind gift from Gorben Pijlman, were previously described by Fros et al. (141). For linearization of plasmid DNA, the following components were mixed into a reaction tube:

<b>Component</b>	<b>Input per reaction</b>
eGFP-CHIKV replicon plasmid	10 µg
NotI-HF restriction enzyme	1 µL
10X SmartCut buffer	10 µL
Nuclease-free H <sub>2</sub> O	ad 100 µL

Plasmid DNA restriction digestion mix was incubated overnight at 37 °C under constant agitation. Linearized DNA was purified using the NucleoSpin Gel and PCR Clean-up kit from Macherey-Nagel according to the manufacturer's instructions. Purified DNA was eluted in 30 µL nuclease-free H<sub>2</sub>O. DNA concentration was measured via photometric analysis with the Nanodrop 2000c system. The size and integrity of the linearized DNA was validated by gel electrophoresis.

Reaction mix for *in vitro* transcription was set up in the following order:

<b>Component</b>	<b>Input per reaction</b>
Linearized DNA	2 µg
Polymerase buffer	10 µL
RNasin RNase inhibitor (Promega)	2.5 µL
rNTP mix (UTP 2.5 µL, ATP 2.5 µL, CTP 2.5 µL, GTP 1.25 µL, H <sub>2</sub> O 1.25 µL)	10 µL
3' cap analogues (Promega)	5 µL
Nuclease-free H <sub>2</sub> O	ad 94 µL

In the last step, 6 µL SP6 polymerase (New England Biolabs) were added to the reaction mix, immediately followed by incubation at 37 °C for 4 hours. Another 4 µL SP6 polymerase were added after 2 hours. By the end of 4 hours, 7.5 µL DNase (Promega) were added to digest the template DNA. The final RNA concentration was measured via photometric analysis with the Nanodrop 2000c system. RNA was aliquoted and stored at -80° C for further use or immediately used for RNA transfection.

### 2.2.3.2 Molecular cloning

#### USP10 F10A and C424A

GW-pFlag-USP10 construct was created by LR reaction with pDONRZeo-USP10iso1, inserting human USP10iso1 into the parental vector GW-pFlag (AC 521). F10A and C424A mutations were introduced into the GW-pFlag-USP10 plasmid via gateway cloning strategy by Patricia Korn's lab, RWTH Aachen. Sequences were verified by Sanger sequencing.

#### CHIKV mutants

CHIKV variants with a mutated G3BP-binding motif of nsP3 (CHIKV ORF1 F1812A and CHIKV ORF1 F1830A) were engineered via site-directed mutagenesis. For each mutation, two complimentary oligonucleotides were designed to introduce a single base pair exchange at the desired position. The sequences of these oligonucleotides, which served as forward and reverse primers, are shown in the materials section (chapter 2.1.5).

The mutations were introduced into the genome via PCR, using the eGFP-CHIKV plasmid as a template. Reagents were mixed in the following order:

---

<b>Component</b>	<b>Input per reaction</b>
10X reaction buffer	5 $\mu$ L
Template DNA (10ng/ $\mu$ L)	20-80 ng
Forward primer (10 $\mu$ M)	1.22 $\mu$ L
Reverse primer (10 $\mu$ M)	1.22 $\mu$ L
dNTP mix	1 $\mu$ L
Nuclease-free H <sub>2</sub> O	Ad 49 $\mu$ L
PfuTurbo DNA polymerase (2.5 U/ $\mu$ L)	1 $\mu$ L

---



Reagent mix was set up for thermal cycling:

<b>Cycles</b>	<b>Step</b>	<b>Temperature</b>	<b>Time</b>
1	Initial Denaturation	95 °C	30 sec
18	Denaturation	95 °C	30 sec
	Annealing	55 °C*	1 min
	Elongation	68 °C	15 min**
1	Cool down	10 °C	infinite

\* according to the primer melting temperature

\*\* according to the amplicon length

After PCR amplification, 1  $\mu$ L DpnI restriction enzyme was mixed directly into the reaction tube. Each reaction mix was incubated at 37 °C for 1 hour to digest the parental supercoiled dsDNA. For bacterial transformation, 5-8  $\mu$ L of the DpnI-treated DNA product was mixed with 50 mL XL1-blue supercompetent E. coli cells and kept on ice for 30 minutes. Subsequently, XL1-blue cells were heat-shocked at 42 °C for 45 seconds, followed by recovery on ice for 2 minutes. SOC medium (300-600  $\mu$ L) was added to the transformed cells, followed by a one-hour incubation at 37 °C under constant agitation. Bacteria suspension was cultivated overnight on prewarmed LB agar plates containing ampicillin or kanamycin, depending on the resistance gene of the transformed plasmid.

Successful mutation of the eGFP-CHIKV plasmid via site-directed mutagenesis was validated via Sanger sequencing.

### USP10 fragments

Four Flag-tagged USP10 fragments were cloned via directional restriction enzyme cloning, using the Flag-tagged USP10 wildtype plasmid as a template. The restriction enzyme recognition sites were inserted via PCR with specifically designed oligonucleotides. These oligonucleotides, used as PCR primers, were designed with the following properties:

## Materials and Methods

---

- Primer length between 18-24 bases
- G/C content should be 40-60%
- At least one G/C pair should be at 3' and 5' end of each primer
- Primer pairs should have a melting temperature within 5°C of each other
- Primer pairs should not be complementary to each other

Each USP10 fragment was amplified from the template DNA using Q5 High Fidelity DNA polymerase and the respective forward and reverse primers (see 2.1 Materials). Reagents were mixed in 0.2 µL PCR reaction tubes in the following order:

---

Component	Input per reaction	Final Concentration
5X Q5 reaction buffer	4.25 µL	1X
10 mM dNTPs	0.5 µL	200 µM
Nuclease-free H <sub>2</sub> O	16.25 µL	
Forward primer (10 µM)	1.25 µL	0.5 µM
Reverse primer (10 µM)	1.25 µL	0.5 µM
Template DNA (10ng/µL)	0.5 µL	0.2ng/µL
Q5 HiFi DNA Pol	0.25 µL	0.02 U/µL

---

DNA was amplified in a PCR cycler according to the following protocol:

---

Cycles	Step	Temperature	Time
1	Initial Denaturation	98 °C	30 sec
40	Denaturation	98 °C	10 sec
	Annealing	70 °C*	20 sec
	Elongation	72 °C	50 sec**
1	Final Extension	72 °C	120 sec

---

\* according to the primer melting temperature

\*\* according to the amplicon length

The amplified DNA product was subjected to agarose gel electrophoresis (0.7% agarose gel) for size separation. DNA products with the expected size were cut out and extracted using the NucleoSpin™ Gel and PCR Clean-up Kit according to the manufacturer's instructions. The cleaned PCR product was subjected to restriction digestion over night at 37 °C. Simultaneously, the plasmid vector was prepared for insertion by restriction digestion:

<b>Component</b>	<b>Input per reaction</b>
PCR product or Plasmid DNA	5 µg
Restriction Enzyme MluI-HF	2 µL
Restriction Enzyme XbaI	2 µL
10X CutSmart buffer	5 µL
Nuclease-free H <sub>2</sub> O	Add to 50 µL

To avoid self-ligation, the linearized vector was additionally treated with alkaline phosphatase. Therefore, 5.5 µL of 10X Antarctic Phosphatase reaction buffer and 1 µL Antarctic Phosphatase were added to the linearized plasmid DNA. The tube was incubated at 37 °C for 60 minutes, followed by heat inactivation at 80 °C for 3 minutes.

Linearized and dephosphorylated vector and insert DNA were ligated using T4 Ligase from Thermo Fisher Scientific according to the manufacturer's protocol for sticky end DNA insert ligation. Briefly, vector and insert were mixed at a molar ratio between 1:1 to 1:5. Ligation buffer, T4 DNA ligase, and nuclease-free water were added to a total volume of 20 µL and incubated at room temperature for 10 min. Ligated DNA was immediately used for bacterial transformation (see 2.2.3.2 Bacterial transformation). Successful cloning was validated via Sanger sequencing and agarose gel electrophoresis.

### **2.2.3.3 Bacterial transformation**

For bacterial transformation of plasmid DNA, MAX Efficiency™ Stbl2™ chemically competent cells (Thermo Fisher Scientific) were thawed on ice. 5-10 ng of the desired

plasmid DNA was mixed with 30  $\mu$ L bacteria suspension and incubated on ice for 15 minutes. DNA was transformed into bacteria cells via heat shock, therefore cells were heated up to 42°C for 45 seconds. For recovery, heat-shocked cells were put on ice for 5 minutes. After adding 300  $\mu$ L SOC medium, the bacteria suspension was incubated for 1 hour at 37°C under constant agitation. Transformed bacteria cells were cultivated overnight on LB agar plates containing ampicillin or kanamycin, depending on the resistance gene of the transformed plasmid.

### 2.2.3.4 Isolation of plasmid DNA

Bacterial colonies from bacterial transformation (chapter 2.2.3.2) or retransformation (chapter 2.2.3.3) were individually picked and cultivated overnight in TB medium.

On the next day, plasmid DNA isolation was performed using the NucleoBond Xtra Midi kit according to the manufacturer's protocol. DNA concentrations were measured by photometric analysis with the Nanodrop 2000c system.

### 2.2.3.5 Sanger sequencing

To validate DNA samples, samples containing the DNA of interest mixed with the appropriate sequencing primers were sent to Microsynth SeqLab for Sanger sequencing analysis. Briefly, this sequencing technique is based on the stochastic integration of dye-labeled dideoxynucleotides (ddNTPs) during *in vitro* DNA replication. These chain-terminating nucleotides prevent further elongation of the DNA strand due to the absence of a 3' hydroxyl group. The resulting DNA fragments are separated based on size via gel electrophoresis, allowing to conclude on the original DNA sequence from the order of termination events.

### 2.2.3.6 Extraction of cellular RNA

Cellular RNA was extracted using TRIzol™ reagent kit, which solubilizes biological material while simultaneously denaturing proteins in a phenol and guanidinium isothiocyanate solution over columns. To prepare samples for extraction, cultured cells

were detached from each well by trypsin treatment and collected in RNase-free reaction tubes. Cell lysates were centrifuged at 1200 g for 5 minutes. The cell pellet was resuspended in 300  $\mu$ L TRIzol™ reagent and RNA was extracted according to manufacturer's protocol.

### **2.2.3.7 Isolation of viral RNA**

Isolation of viral RNA was performed on supernatant samples of infected cells using the NucleoSpin® RNA virus kit. For each sample, 50  $\mu$ L cell culture supernatant was mixed with 300  $\mu$ L RAV-1 extraction buffer (Macherey-Nagel). Samples were heated to 70°C for 10 minutes for complete virus inactivation. Viral RNA was isolated according to the manufacturer's protocol.

### **2.2.3.8 Agarose gel electrophoresis**

Agarose gel electrophoresis was used for size-based DNA separation. Gels were prepared by dissolving agarose powder in Tris-acetate EDTA (TAE) buffer, with the agarose concentration ranging between 0.7-1%, depending on the size of DNA fragments. Midori green advance DNA stain was incorporated at a 1:20,000 dilution. Once the gel solidified, a sufficient quantity of DNA (at least 20 ng for plasmid or linearized DNA, and 5  $\mu$ L of PCR products) was loaded into individual wells. One-kb plus DNA ladder from New England Biolabs (NEB) served as a reference. DNA separation was conducted at 80-140 V for approximately 45 minutes, depending on the gel size and applied voltage. For analysis, DNA bands were visualized using a ChemiDoc XRS+ gel documentation system under UV light. In cloning experiments, a UV-to-blue light conversion screen was used to reduce DNA damage.

## **2.2.4 Readout methods**

### **2.2.4.1 Luciferase assay**

Cells were transduced with CHIKV-gp or VSV-G pseudotyped lentiviral vector particles. For each well of a 96-well plate, 0.1  $\mu$ L particle suspension and 100  $\mu$ L fresh

medium were added. The plates were centrifuged for 1 hour at 1000 g to enhance transduction efficiency. After 48 hours, cells were washed with PBS and lysed in 40  $\mu$ L cell culture lysis buffer (Promega) per well. After incubation for 5 minutes, 10  $\mu$ L of cell suspension were transferred into a white-bottom luminometric plate. 30  $\mu$ L of luciferase substrate (Promega) were added. Luciferase activity was quantified using the Synergy™ 2 chemiluminescence reader (BioTek).

### 2.2.4.2 Flow cytometry

Non-infectious cell samples were fixed in 2% paraformaldehyde (PFA) for 10-15 minutes at room temperature. Infectious samples were fixed in 6% PFA for 30 minutes to ensure complete inactivation. Fixed cells were washed in PBS and centrifuged at 1200 g for 5 minutes. Subsequently, samples were resuspended in 200-300  $\mu$ L FACS buffer (0.5% BSA in PBS) for direct analysis.

For cytometric analysis of intracellular proteins, samples underwent further steps for binding of primary and secondary antibodies: Primary antibody was added in combination with permeabilization buffer, which disrupts the cellular membrane and enables intracellular immunolabeling. Therefore, cells were resuspended in 100  $\mu$ L PBS including 0.1% Triton X-100 (Thermo Scientific) and primary antibody in the appropriate concentration, and incubated for 20 minutes on ice. After 20 minutes, samples were washed in PBS and centrifuged at 1200 g for 5 minutes. The secondary antibody was diluted in PBS at the appropriate concentration. Samples were resuspended in 100  $\mu$ L of the secondary antibody dilution and incubated for 20 minutes on ice. Finally, samples were washed in PBS and centrifuged at 1200 g for 5 minutes, followed by resuspension in 200-300  $\mu$ L FACS buffer (0.5% BSA in PBS). Cytometric analysis was performed on a FACSCelesta cell analyzer (Becton Dickinson).

### 2.2.4.3 Immunoblotting

For sample preparation, cells were lysed in Mammalian Protein Extraction Reagent (M-PER™, Thermo Fisher Scientific) for 20 minutes. Cellular debris was removed via centrifugation at 14000 g for 20 minutes. Samples were mixed with sodium dodecyl

sulfate (SDS) and heated up to 95 °C for 10 minutes to achieve protein denaturation and coating in negative-charged SDS molecules proportional to the protein length. The negative-charged proteins were subjected to separation via SDS polyacrylamide gel electrophoresis, in short SDS-PAGE.

The SDS-polyacrylamide gel consists of a stacking gel on the top layer, where the samples are loaded, and a separation gel on the bottom layer. Separation and stacking gel were prepared as detailed in the following table:

<b>Component</b>	<b>Separation gel</b>	<b>Stacking gel</b>
Acrylamide (30%)	2 mL	0.33 mL
1.88 M Tris/HCl, pH 8.8	1.2 mL	-
0.625 M Tris/HCl, pH 6.8	-	0.4 mL
SDS (0.5%)	1.2 mL	0.4 mL
Deionized H <sub>2</sub> O	1.6 mL	0.87 mL
TEMED	5 µL	2 µL
APS (10 %)	30 µL	10 µL

Electrophoresis commenced at 100 V until proteins entered the separation gel, at which point the voltage was raised to 120 V. Following this, proteins were electroblotted onto a nitrocellulose membrane equilibrated in transfer buffer (3% Tris, 15% Glycin, 1% SDS, 20% Methanol) using the Trans-Blot Turbo system (BioRad) in accordance with the standard protocol provided by the manufacturer. After blotting, the membrane was blocked in a solution of 5% BSA in Tris-buffered saline with 0.2% Tween-20 (TBS-T) for one hour to prevent non-specific binding. Primary antibodies, diluted in TBS-T with 1% BSA, were applied to target the desired proteins, and incubated overnight at 4 °C. Membranes were washed three times for 10 minutes in TBS-T. Secondary antibodies conjugated with IRDye® 680RD or 800CW were diluted in TBS-T with 1% BSA and added to the membrane for one hour. Detection and quantification of proteins were executed using the Odyssey Infrared Imaging System (Li-Cor Biosciences, Lincoln, Nebraska, USA).

### 2.2.4.4 Two-step reverse transcription qPCR

Cellular mRNA levels of *USP10*, *G3BP*, and *IFIT1* were quantified via two-step reverse transcription quantitative PCR (RT-qPCR). Cell samples were lysed and mRNA was extracted using TRIzol™ extraction kit as detailed in chapter 2.2.3.6.

For cDNA synthesis, extracted mRNA was mixed with the following reagents in a 0.5 mL PCR reaction tube:

Component	Input per reaction
Isolated mRNA	20 µL
dNTPs (10 mM)	2 µL
Random hexamers (100 µM)	2 µL
Nuclease-free H <sub>2</sub> O	8 µL

The reaction mix was incubated at 75 °C for 3 minutes, then put on ice while the reverse transcription master mix was set up:

Component	Input per reaction (+RT)	Input per reaction (-RT)
RT buffer (10X)	2 µL	2 µL
M-MuLV RT	0.5 µL	-
Nuclease-free H <sub>2</sub> O	1.5 µL	2 µL

Each sample was divided into two PCR reaction tubes and mixed with 4 µL master mix, either with or without RT enzyme. Samples were incubated at 42 °C for 1 hour to enable cDNA synthesis, then heated up to 90 °C for 10 minutes to denature the RT enzyme.

In the second step, cDNA was mixed with the following reagents in a 96-well qPCR plate in technical triplicates:



<b>Component</b>	<b>Input per reaction</b>
Sample (cDNA, Standard or H <sub>2</sub> O)	2 µL
Forward primer (10 µM)	0.5 µL
Reverse primer (10 µM)	0.5 µL
Probe FAM (10 µM)	0.25 µL
RNase P primer/probe (VIC)	1 µL
LightCycler® TaqMan® Mastermix	10 µL
Nuclease-free H <sub>2</sub> O	5.75 µL

Thermal cycling was performed on a LightCycler® 480 Real-Time PCR cycler using the following protocol:

<b>Cycles</b>	<b>Step</b>	<b>Temperature</b>	<b>Time</b>
1	Initial Denaturation	95 °C	30 sec
40	Denaturation	95 °C	15 sec
	Annealing/Extension	55 °C	60 sec
	Cooldown	10 °C	-

Relative mRNA levels were calculated with the  $\Delta\Delta C_t$  method, using human RNaseP as a reference. Each sample was analyzed in technical triplicates. For two-step qPCR, an omitting reverse transcriptase control was included for each sample. Assays were performed on a LightCycler 480 II (Roche, Basel, Switzerland), using LightCycler 480 software (version 1.5) for data analysis.

#### **2.2.4.5 One-step reverse transcription qPCR**

Viral RNA was isolated from the supernatant of infected cells using the NucleoSpin® RNA virus kit, as detailed in chapter 2.2.3.7. For the quantitative analysis of viral RNA, a one-step qPCR was performed. The following reagents were mixed and transferred

## Materials and Methods

---

into a 96-well qPCR reaction plate. Primers and probes for CHIKV and MAYV detection were previously described in the literature (145,146).

---

<b>Component</b>	<b>Input per reaction</b>
Nuclease-free H <sub>2</sub> O	8.25 µL
MgSO <sub>4</sub> (50 mM)	0.5 µL
2X Reaction buffer	12.5 µL
Forward primer (10 µM)	0.5 µL
Reverse primer (10 µM)	0.5 µL
Probe FAM (10 µM)	0.25 µL
RNase P primer/probe (VIC)	1 µL
SSIII PlatinumTaq Polymerase (5 U/µL)	0.5 µL
Sample (RNA, Standard, or H <sub>2</sub> O)	1 µL

---

Thermal cycling was performed on a LightCycler® 480 Real-Time PCR cycler using the following protocol:

---

<b>Cycles</b>	<b>Step</b>	<b>Temperature</b>	<b>Time</b>
1	Reverse transcription	52 °C	15 min
1	Initial denaturation	94 °C	2 min
45	Denaturation	94 °C	15 sec
	Annealing	55 °C	40 sec
	Elongation	68 °C	20 sec
	Cooldown	10 °C	-

---

For absolute quantification of the sample RNA, a standard curve was generated with previously diluted standards for Chikungunya virus RNA from Paul-Ehrlich-Institute, PEI code 11785/16 (147).

#### **2.2.4.6 Plaque Assay**

Vero E6 cells were seeded in 24-well plate format ( $3.5 \times 10^5$  cells/mL) 1 day prior to infection. Confluent cells were infected with serially diluted supernatants from infected cells and incubated at 37 °C and 5% CO<sub>2</sub> for 1 hour. Supernatant was carefully removed, followed by a wash in PBS. Cells were overlaid with highly viscous overlay medium, freshly made as a 1:1 mix of 2.4% Avicel (Merck) and 2X DMEM supplemented with 20% fetal calf serum (FCS), 200 µg/mL streptomycin and 4 mM L-glutamine. After incubation for 3 days at 37 °C and 5% CO<sub>2</sub>, overlay medium was aspirated and cells were fixed in 6% PFA for 30 minutes. Inactivated and fixed cells were washed in deionized water and stained with crystal violet solution for 20 minutes. Plaques were counted manually in technical duplicates.

#### **2.2.4.7 Confocal Microscopy**

Confocal microscopy was used for microscopic analysis of stress granules and nsP3-G3BP foci. HEK-293T cells were seeded in 8-well microscopy slides ( $6.3 \times 10^4$  cells/well). Slides were previously coated with poly-L-lysine for 20 minutes at 37 °C, followed by three washes in PBS, to enhance cell attachment. After 24 hours, cells were transfected with USP10 (WT, F10A, or C424A) or the empty vector as detailed in chapter 2.2.2.2 and incubated for 24 hours at 37 °C and 5% CO<sub>2</sub>. Subsequently, cells were infected with eGFP-CHIKV (MOI 5) and incubated at 37 °C and 5% CO<sub>2</sub> for 4, 8 or 24 hours. For positive control, sodium arsenite was diluted to 0.5 mM in fresh medium and added to the cells, followed by incubation for 1 hour. At the indicated time points, cells were fixed in 6% PFA for 30 minutes at room temperature, followed by three washes in PBS.

Fixed cells were permeabilized in 0.3% Triton-X in PBS for 10 minutes, then blocked in 5% BSA in PBS for 30 minutes. After washing in PBS, cells were incubated with primary antibodies, diluted in PBS containing 2.5% BSA, overnight at 4 °C under constant agitation. Slides were washed three times in PBS. Secondary antibody dilution in PBS was added and incubated for 1 hour at room temperature, followed by three washes in PBS. 5-6 drops of microscopy dilution, including DAPI (1:10.000), were added to each well, and incubated for 10 minutes, prior to confocal microscopy.

Primary and secondary antibodies are detailed in the materials section. Slides were analyzed on a Leica TCS SP8 confocal microscope, kindly provided by the Charité microscopy core facility, using a 63X magnification oil immersion objective. Microscopy images were analyzed on Fiji software with JaCoP Plugin and CellProfiler.

### 2.2.5 Next generation sequencing

eGFP-CHIKV was passaged over HEK-293T cells transfected with USP10 wild-type or F10A mutant. Plasmid transfection was performed as detailed in chapter 2.2.2.2, using 1.5 µg plasmid DNA per well of a 12-well plate. 24 h p.t., cells were infected with eGFP-CHIKV (MOI 0.1), designated as passage zero. Every 48 hours, 2 µL of the infectious supernatant were transferred onto naïve HEK-293T cells, previously transfected with USP10 wild-type or F10A, until the virus was passaged ten times. At the same time, supernatant samples were collected for qPCR analysis of viral RNA (chapter 2.2.4.5), and cells were lysed and fixed in 6% PFA for cytometric analysis (chapter 2.2.4.2).

For next generation sequencing (NGS), 50 µL of the infectious supernatant from passage 10 were collected at 48 hours post-infection (h p.i.), and viral RNA was extracted as detailed in chapter 2.2.3.7. The isolated RNA samples were sent to Azenza Genewiz (Leipzig) for library preparation and NGS using an Illumina® NovaSeq™ sequencer. Library preparation included rRNA removal via Poly(A) selection, followed by cDNA synthesis and Illumina-specific adapter ligation. Sequencing was configured for 2x150 bp reads with a depth of 10 million paired-end reads per sample.

NGS results were obtained in .fastq format and further processed as follows: The quality of illumina paired end .fastq files was analyzed using fastqc and 3' sequencing adapters were trimmed using Cutadapt 4.6 (148). The reads were mapped to the parental CHIKV sequence (GenBank accession no. DQ443544) using “bwa mem” version 0.7.17 (149). Mate coordinates were filled in and reads were sorted for further processing using “samtools fixmate” and “samtools sort” version 1.19 (150). Variant determination was performed using LoFreq\* 2.1.5 (151), following the pipeline recommended by the authors. In short, reads were realigned using “lofreq viterbi” to

correct mapping errors, alignment qualities were inserted using “lofreq alnqual” and a quality score for indels determined using “lofreq indelqual”. Variants were called using “lofreq call-parallel –call-indels -d 10000”. The resulting .vcf files were aggregated, converted to a table, and plotted using Python 3.11 with the libraries pandas, pyplot, and seaborn (152–154). Amino acid exchanges that occurred with < 10% frequency in all replicates were excluded from further analysis.

### **2.2.6 Phylogenetic analysis**

To analyze the sequence conservation of the FGDF motif across species, protein sequences of USP10 orthologs from 590 vertebrate species were downloaded from NCBI and aligned using ClustalO 1.2.4 (155,156). The phylogenetic tree for the included species was retrieved from NCBI taxonomy and visualized using iTOL (19)

### **2.2.7 Statistical analysis**

Statistical analyses were performed using Graph Pad Prism version 7 (GraphPad Software Inc.).

Unpaired t-tests were employed for comparisons between two datasets, assuming a parametric (Gaussian) distribution. For the statistical analysis of multiple groups, one-way analysis of variance (ANOVA) was used, followed by Dunnett’s multiple comparison test. Error bars in all figures represent the standard deviation.

Statistical significance is indicated using the following symbols:

<b>Symbol</b>	<b>p-value</b>
n. s.	$p > 0.05$
*	$p \leq 0.05$
**	$p \leq 0.01$
***	$p \leq 0.001$
****	$p \leq 0.0001$

### 3 Results

#### 3.1 Characterizing USP10 as a binding partner of nsP3 and G3BP

##### 3.1.1 Tandem mass spectrometry identifies USP10 as a potential binding partner of nsP3

Given the essential role of nsP3 in viral replication and immune evasion, the protein represents a promising target for antiviral drug development. Inhibitors that disrupt nsP3 functions or its interactions with host proteins could effectively impair CHIKV replication and spread, offering a potential therapeutic strategy against CHIKV infection. As discussed in chapter 1.2.3, the HVD of nsP3 serves as an interaction hub for many cellular proteins, which may be proviral or restrictive to the virus. Further, the MD may be an interesting interaction partner for cellular proteins, as it displays MAR hydrolase activity which is able to reverse the MARYlation of viral or cellular substrates (157).

Our collaboration partners Maud Verheirstraeten and Patricia Korn from RWTH Aachen used tandem Mass Spectrometry (MS) with two different sample preparation approaches: (i) Tandem affinity purification (TAP) -tagging to identify cellular proteins that form stable interactions with CHIKV nsP3, and (ii) BirA proximity labeling to detect both transient and stable interactions. The TAP-tagging approach was used on the whole nsP3 protein, while BirA proximity labeling was conducted on either the whole nsP3 protein or the isolated macro domain.

Analysis of the tandem MS data revealed 18 cellular proteins that interacted with the whole nsP3 protein in both TAP-tagging and BirA proximity labeling approach. Among these, we identified the known proviral host cell protein FHL1, underlining the validity of this approach. One of the hits, USP10, raised our interest as this protein is known to play a role in G3BP-binding and SG formation, but no studies on the effects of USP10 in the context of CHIKV were reported to date. The binding of USP10 to nsP3 seems independent of the MD since the interaction was only observed in the full-length nsP3 proximity assay. The presence of other interaction partners that are involved in SG formation and regulation, such as G3BP1/2, DDX1, and ATXN2, underlines the importance of this regulatory process for CHIKV infection and nsP3 as an interaction

hub that interferes with SG formation. A list of all hits is shown in the Appendix, Table S 1.

### 3.1.2 USP10 co-immunoprecipitates with nsP3 in presence of G3BP

The interaction between USP10 and nsP3 was validated via co-immunoprecipitation (Co-IP). Here, Patricia Korn's lab transfected HEK-293 cells with expression vectors containing GFP-expressing CHIKV-nsP3 wild type versus two mutants with hydrolase-deficient macrodomains (V33E and Y114V) (157,158). Samples were prepared either as whole cell lysate (WCL) or eluate of a GFP-trap for further analysis in Western Blot. Immunodetection revealed USP10 and G3BP in all lysates of the GFP trap. The data confirms the interaction between USP10 and CHIKV-nsP3. However, it is not clear if there is a direct interaction between USP10 and nsP3, or if the interaction is mediated via G3BP.

Further, both USP10 and G3BP were found in GFP-trap lysates of cells expressing the nsP3 mutants with interfered MD functionality, underlining the previous hypothesis that the MD is not involved in the interaction with USP10.

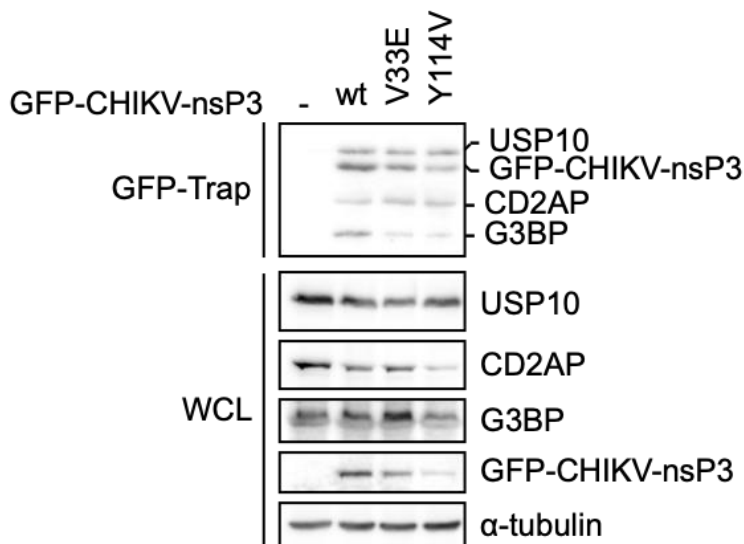


**Figure 6: Confirmation of potential nsP3 binding partners by co-immunoprecipitation.** HEK-293 cells were transfected with plasmids encoding GFP-CHIKV-nsP3 wild type, V33E or Y114V. After 24 hours, cells were lysed and immunoprecipitated via GFP-Trap (Chromotek). Co-immunoprecipitated interactors were analyzed via immunoblotting with specific antibodies. Endogenous and overexpressed GFP-fusion proteins were detected in whole cell lysates (WCL) for reference.

## Results

### 3.1.3 Interaction between nsP3 and G3BP is driven by aromatic amino acids of a FGDF motif

The interaction between G3BP and the alphaviral nsP3 has been extensively studied in recent years. Schulte et al. unveiled the crystal structure of G3BP1's NTF2-like domain in complex with a 25 amino acids long peptide derived from SFV nsP3 (120). This peptide contains two FGDF motifs, a signature feature that is also present in CHIKV nsP3. Crystallographic analysis (PDB: 5FW5) revealed the binding mode between the NTF2-like domain and the first FGDF motif to be mainly promoted by aromatic amino acids, particularly phenylalanines. As represented in Figure 7, distances between the FGDF motif and three proximal phenylalanine residues of the NTF2-like domain (F15, F33, and F124) range from 3.6 Å to 4.3 Å, falling in typical distances for aromatic interactions (159).

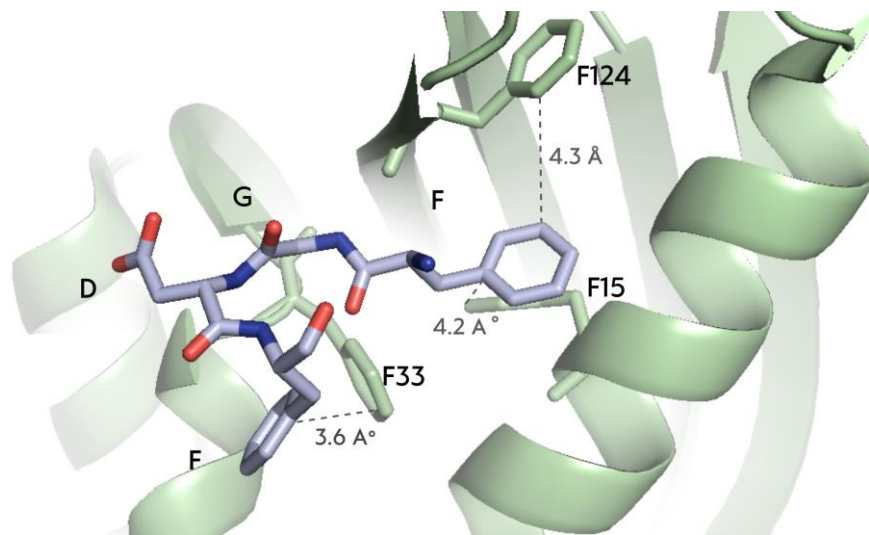


**Figure 7: Interaction of FGDF peptide with G3BP1-NTF2-like domain.** Semliki Forest virus nsP3<sub>3-6</sub> FGDF motif is represented in purple, G3BP1 NTF2-like domain is represented in green. Distances between the FGDF motif and nsP3 phenylalanine residues F15, F33, and F124 are detailed. Created with PyMOL.



### 3.1.4 USP10 and G3BP1 expression in response to type I IFN and vasopressin

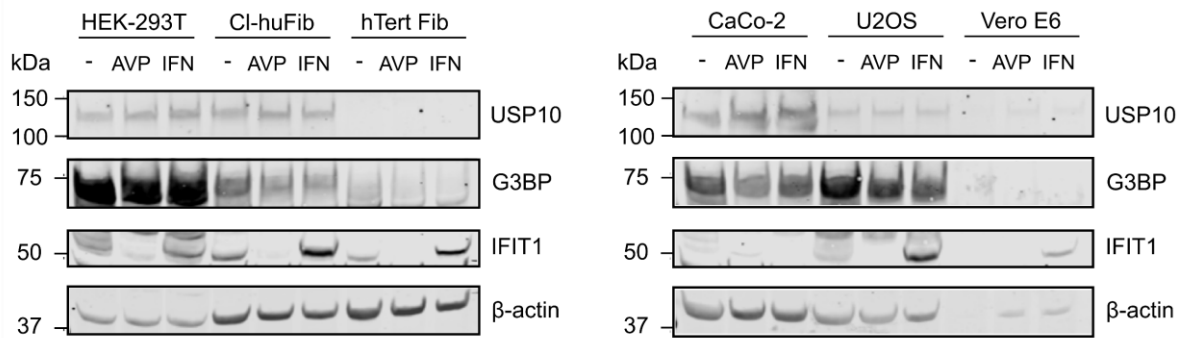
Type I interferons (IFNs) play a critical role in the innate immune response by upregulating interferon-stimulated genes (ISGs) with antiviral properties. Conversely, upregulation by IFN can be an indicator for an antiviral role of the encoded protein. To evaluate whether *USP10* and *G3BP* are ISGs, we treated several human cell lines (HEK-293T, dermal fibroblasts (CI-huFIB and hTert Fib), CaCo-2, U2OS) and Vero E6 cells (African green monkey kidney) with IFN- $\alpha$ 2 and arginine vasopressin (AVP), a polypeptide protein previously described to induce *USP10* expression in renal cells via the V<sub>2</sub> receptor (160). *USP10* and *G3BP1* expression levels were assessed via immunoblotting or qPCR following treatment of IFN- $\alpha$ 2 or AVP for 48 hours.

Immunoblot analysis revealed abundant expression of *G3BP1* across all tested human cell lines. The highest basal *G3BP* expression was observed in HEK-293T cells, followed by U2OS cells. *USP10* was detected at a low basal level in all human cell lines, with minimal to non-detectable expression in hTert-immortalized dermal fibroblasts (Figure 8A). qPCR analysis corroborated the presence of mRNA for both *USP10* and *G3BP1* in all human cell lines (Figure 8B). Notably, treatment with IFN- $\alpha$ 2 for 48 hours did not significantly increase the protein or mRNA levels of *USP10* and *G3BP1*. In contrast, *IFIT1*, a well-established prototypic ISG, served as a positive control and was markedly upregulated upon IFN- $\alpha$ 2 treatment. Similarly, AVP treatment did not enhance *USP10* protein expression.

These findings indicate that neither *USP10* nor *G3BP1* is upregulated as part of the immediate ISG response to IFN- $\alpha$ 2. Additionally, the physiological induction of *USP10* expression by AVP may not be applicable to these specific cell lines, potentially due to the lack of V<sub>2</sub> receptor expression (161).

## Results

A



B

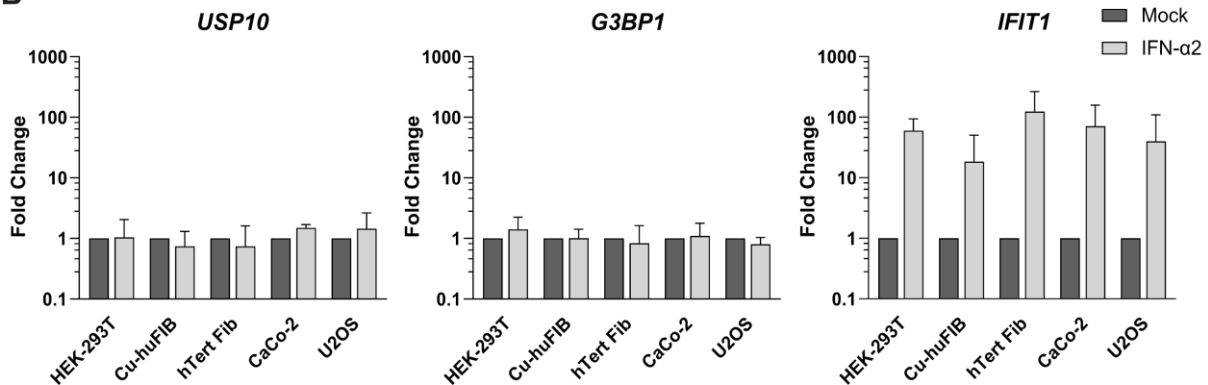


**Figure 8: USP10 and G3BP1 expression profile and response to type I IFN and Vasopressin. (A)** Immunoblot for USP10, G3BP, IFIT1, and  $\beta$ -actin in HEK-293T, CI-huFIB, hTert Fib, CaCo-2, U2OS, and Vero E6 cells after incubation with IFN- $\alpha$ 2 (500 IU/mL) or Vasopressin (10 nM) for 48 hours, respectively. **(B)** RT-qPCR analysis for *USP10*, *G3BP1*, and *IFIT1* mRNA levels in HEK-293T, CI-huFIB, hTert Fib, CaCo-2, and U2OS, either treated with type IFN- $\alpha$ 2 (500 IU/mL), Vasopressin (10 nM) or mock-treated for 48 hours. Error bars represent SD.

### 3.1.5 Conservation of the USP10 FGxF motif among humans and across vertebrates

Single nucleotide polymorphisms (SNPs) are the most common type of genetic variations within a species. Analyzing SNPs can provide insights into the importance of specific regions of a gene and into genetic diversity among individuals. In this context, we investigated the functional relevance of USP10's FGDF motif by analyzing the distribution of SNPs within this region of the human USP10 gene. We focused on the FGDF motif due to its role in G3BP-binding as described in previous studies (99). SNP data was retrieved from NCBI. As demonstrated in Table 2, the FGDF motif is highly conserved within the human population, indicating selective pressure to maintain this motif for the functionality of USP10. Interestingly, non-synonymous SNPs were only identified at the third position of the motif. These specific SNPs result in

amino acid changes that alter the side chain properties from a negatively charged aspartate (D) to either uncharged polar (asparagine, N) or hydrophobic (alanine, A or valine, V). These findings suggest a potential tolerance for changes in the electrochemical properties at the third position. The high conservation of the remaining residues suggests an essential role for the FGx<sub>F</sub> motif in maintaining the structural and functional integrity, potentially through interactions with G3BP or other binding partners.

**Table 2: Human SNP data reveals a strong conservation of the FGx<sub>F</sub> motif in USP10.** SNP data from human FGDF motif. SNPs are highlighted in yellow. The corresponding amino acid sequence is shown on the right. Source: NCBI Genome (TOPMED) (162).

	nucleotide sequence	peptide motif	allele frequency
Consensus <sub>119-130</sub>	5' ...TTTGGAGATTTT...3'	FGDF	99.9992%
rs1909499380 <sub>119-130</sub>	5' ...TTCGGAGATTTT...3'	FGDF	0.0004%
rs1909499616 <sub>119-130</sub>	5' ...TTTGGAAATTTT...3'	FGNF	0.0004%
rs1482511318 <sub>119-130</sub>	5' ...TTTGGAGCTTTT...3'	FGAF	<0.0001%
rs1482511318 <sub>119-130</sub>	5' ...TTTGGAGTTTTT...3'	FGVF	<0.0001%

Extending the analysis to all vertebrates revealed that the FGx<sub>F</sub> motif is remarkably conserved. Almost all mammalian USP10 sequences contain an FGDF motif, with the exception of *Panthera onca*, *Carlito syrichta*, and *Microcebus murinus*. The vast majority of USP10 orthologs in non-mammalian vertebrates contain an FGEF motif (Figure 9).

## Results

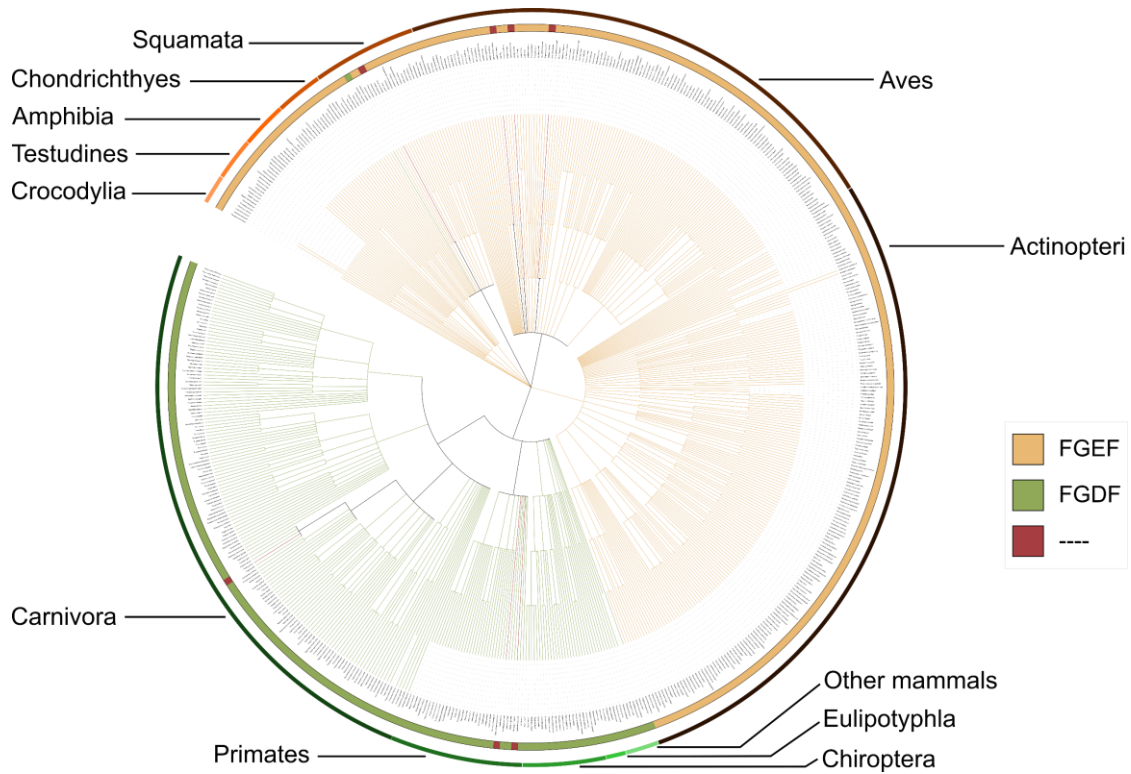


**Figure 9: Multiple sequence alignment reveals a strong conservation of USP10's FGxF motif.** Multiple sequence alignment of USP10 orthologs among vertebrates reveals a strong conservation of the FGDF motif in mammals, which is substituted by an FGEF motif in non-mammalian vertebrates. Created with iTOL v6 and modified with Inkscape 1.3.2.

## 3.2 USP10 in the context of alphavirus infection

### 3.2.1 USP10 overexpression inhibits CHIKV and MAYV infections in a dose-dependent manner

As detailed in chapters 3.1.1 and 3.1.2, tandem mass spectrometry and co-immunoprecipitation analyses indicated a potential interaction between CHIKV nsP3 and USP10 (Figure 6). Building upon these observations, we aimed to investigate the role of USP10 in the context of CHIKV infection. For this study, we used a CHIKV strain from the La Réunion outbreak in 2005, expressing eGFP under the control of a sub-genomic promoter, allowing for the quantification of infected cells via flow cytometry.

USP10 is a ubiquitously expressed cytosolic enzyme that is involved in a wide range of cellular processes through its deubiquitinase activity. To assess the influence of heterologous expression of the protein on CHIKV infections in cell culture, we transiently transfected HEK-293T cells with an N-terminally Flag-tagged USP10 plasmid in increasing amounts. To control for unspecific effects of different plasmid amounts, the total DNA concentration was equalized in the USP10 plasmid dilutions using an empty vector (EV). Transfection with the EV alone served as a control. Figure 10A shows a schematic representation of the experimental setup.

Transfection efficiency at 24 h p.t. was validated via immunoblotting (Figure 10B). The transfected cells were infected with eGFP-tagged CHIKV, using a multiplicity of infection (MOI) of 0.5, and the number of infected cells was quantified at 24 h p.i. As demonstrated in Figure 10C, the infection rate was markedly decreased in cells overexpressing USP10 compared to the empty vector-transfected cells. The observed antiviral effect corresponded to the amount of transfected USP10 plasmid, demonstrating a dose-dependent relationship between USP10 expression and antiviral response in cell culture.

Given the relatively low sequence conservation of the nsP3 protein, we repeated the experiment with MAYV, a New World alphavirus, to compare the effects of USP10 on a diverse range of alphaviruses. Like CHIKV, the MAYV strain used for this experiment expresses eGFP under a sub-genomic promoter. In line with the observed effect on CHIKV, the rate of MAYV-infected cells was decreased in USP10-overexpressing cells in a dose-dependent manner.

## Results

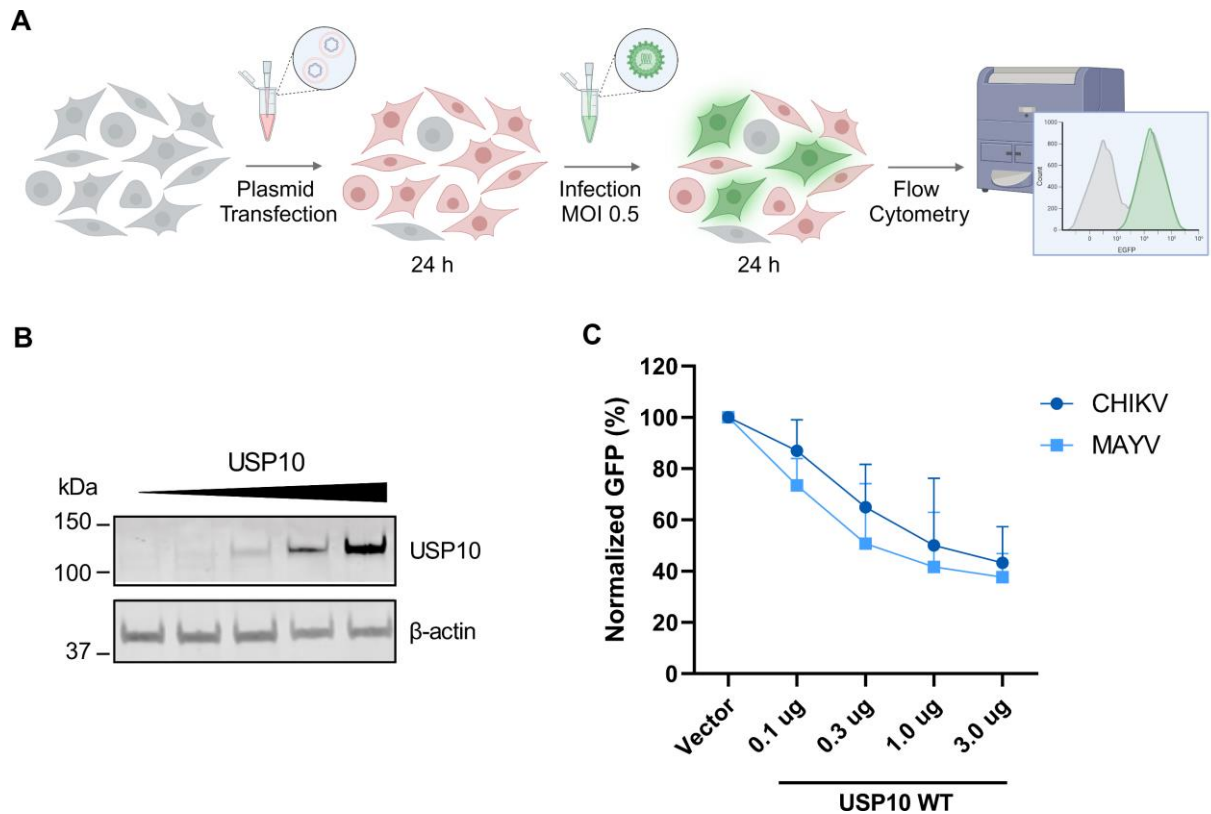


**Figure 10: Heterologous expression of USP10 inhibits CHIKV and MAYV infection in HEK-293T cells in a dose-dependent manner (A)** Schematic representation of the experimental set-up. **(B)** Representative Western blot of HEK-293T cells transfected with titrated amounts of Flag-tagged USP10 (0, 0.1, 0.3, 1 and 3  $\mu$ g) and lysed 24 h p.t. **(C)** Quantification of infected cells transfected with increasing amounts of USP10 vector and infected with eGFP-CHIKV or MAYV-eGFP (MOI 0.5) at 24 h post-infection and 48 h post-transfection (N=3).

### 3.2.2 The G3BP binding capability is essential for the antiviral effect of USP10

To elucidate the specific contribution of USP10's deubiquitinase (DUB) activity and G3BP-binding capability in viral infection, we investigated a G3BP binding-deficient (F10A) and a DUB activity-deficient USP10 mutant (C424A) (Figure 11A).

As described in chapter 3.1.2, USP10 interacts with CHIKV nsP3, via direct binding or indirect interaction. Consequently, this led us to the question whether nsP3 serves as a substrate of USP10's deubiquitinase activity. Our collaborators from Patricia Korn's lab, RWTH Aachen, co-transfected HEK-293 cells with either wild-type USP10 or C424A, alongside Flag-tagged CHIKV nsP3 and His-tagged Ubiquitin. Subsequently, ubiquitinated proteins were enriched via immunoprecipitation targeting the His-tag. As shown in Figure 11B, the detection of the immunoprecipitated proteins revealed that nsP3 underwent ubiquitination in the absence of USP10. Overexpression of wild-type

USP10, but not the C424A mutant, partially reversed the ubiquitination of nsP3. These findings suggest CHIKV nsP3 as a direct target for deubiquitylation by USP10.

We assessed the impact of DUB-deficient and G3BP-binding deficient USP10 mutants on CHIKV and MAYV infections by transfecting HEK-293T cells with USP10 wildtype or the aforementioned mutants. Transfection efficiency was verified 24 h p.t. via immunoblotting (Figure 11C) and the cells were infected with eGFP-expressing CHIKV or MAYV (MOI 0.5). After another 24 hours, we analyzed the cells for eGFP positivity via flow cytometry. In parallel, we extracted intracellular RNA for the quantification of viral RNA through qPCR analysis.

Flow cytometry analysis of CHIKV-infected cells revealed that wild-type USP10 or the DUB-deficient mutant (C424A) overexpression resulted in a five-fold decrease in the infection rates compared to the empty vector controls ( $p \leq 0.0001$ ). In contrast, the G3BP-binding deficient mutant (F10A) did not significantly affect infection rates, underscoring the necessity of USP10-G3BP interaction for the antiviral effect of USP10 (Figure 11D). Similar infection patterns were observed with eGFP-MAYV, where overexpression of wild-type USP10 or C424A led to a comparable reduction in infection rates. However, the F10A mutant overexpression only slightly reduced MAYV infection rates to about 80% of the control. This could be explained by an additional, G3BP-independent inhibitory mechanism of USP10 in the context of MAYV infection (Figure 11D).

In line with these observations, qPCR analysis of intracellular viral RNA revealed a notable reduction in viral RNA levels in cells overexpressing wild-type or DUB-deficient USP10. Interestingly, for both CHIKV and MAYV infections, cells overexpressing the USP10 G3BP-binding deficient mutant (F10A) also showed a slight reduction in viral RNA load compared to controls transfected with the empty vector. However, this reduction did not reach statistical significance, suggesting a minor role of the G3BP-binding capability in the antiviral mechanism of USP10 (Figure 11E).

These data indicate that while CHIKV nsP3 is deubiquitylated by USP10, the antiviral effects against CHIKV and MAYV are independent of the protein's DUB activity. Rather, the interaction with G3BP is crucial for USP10's antiviral potency. Further, while minor differences are indicated for the role of USP10 in CHIKV and MAYV infection, both viruses appear to be affected by the antiviral properties of USP10 in a

## Results

similar fashion. Therefore, for the further characterization of USP10 in the context of alphaviral infection, we decided to focus on CHIKV exclusively.

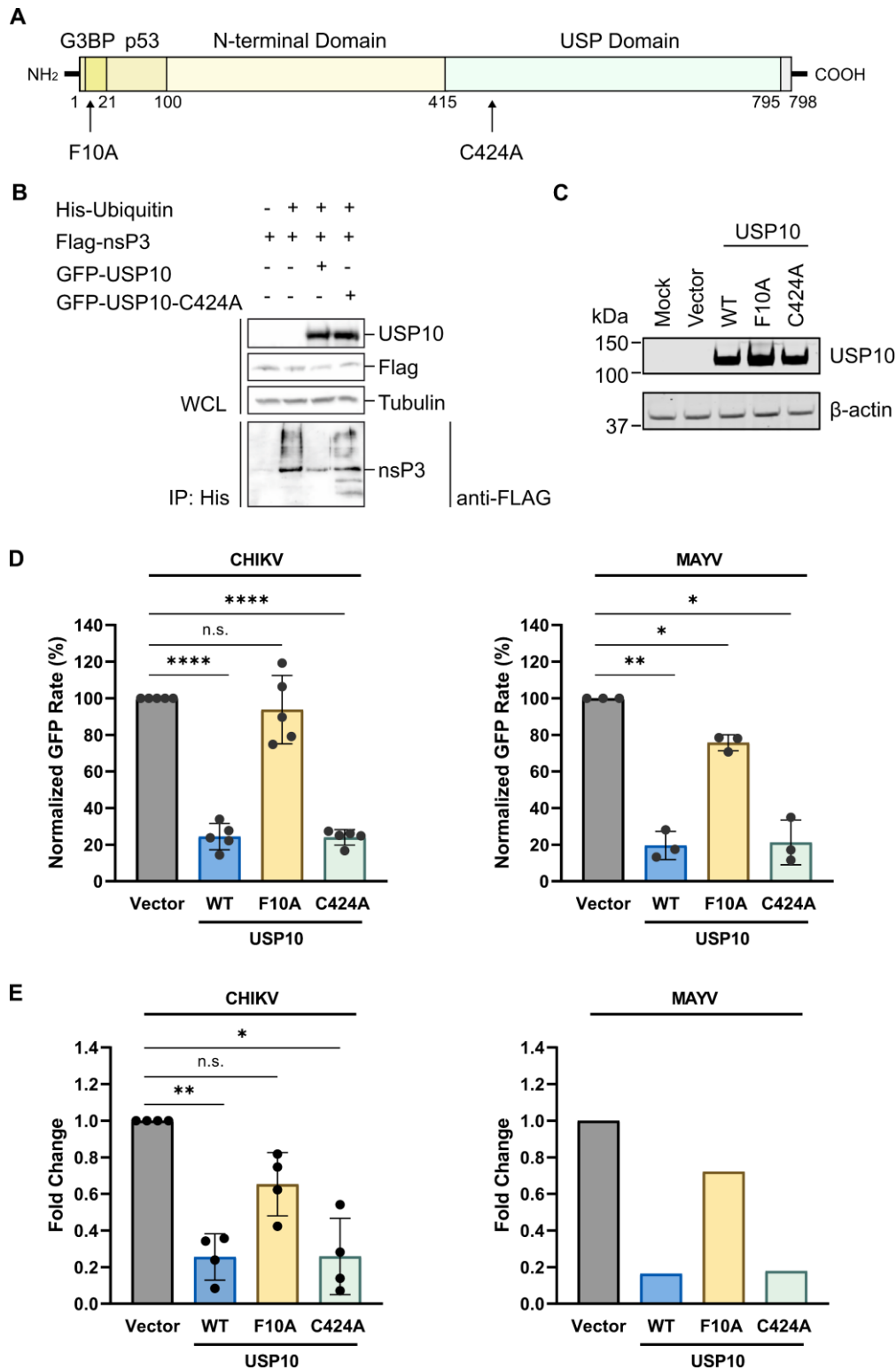


**Figure 11: Heterologous expression of USP10 wildtype and C424A, but not F10A, inhibits CHIKV and MAYV infection in HEK-293T cells. (A)** Schematic overview of the transfected Flag-USP10 plasmid and the position of F10A and C424A mutations. **(B)** Detection of ubiquitinated nsP3 by immunoprecipitation. CHIKV nsP3 and His-Ubiquitin were co-transfected into HEK-293 cells.



Ubiquitinated proteins were enriched using Talon beads, followed by detection with the appropriate antibodies. **(C)** Representative immunoblot of HEK-293T cells transfected with Flag-USP10 wt, F10A, or C424A versus the empty vector. Proteins were extracted from cell lysates 24 h p.t. **(D)** Flow Cytometry analysis of HEK-293T cells transfected with Flag-USP10 wt, F10A, or C424A versus an empty vector control and infected with eGFP-CHIKV (MOI 0.5, N=5) or eGFP-MAYV (MOI 0.5, N=3) for 24 hours. **(E)** qPCR analysis of viral RNA in HEK-293T cells transfected with Flag-USP10 WT, F10A, or C424A versus an empty vector control. Intracellular viral RNA was extracted 24 hours after infection with eGFP-CHIKV (MOI 0.5, N=4) or eGFP-MAYV (MOI 0.5, N=1).

### **3.2.3 USP10 overexpression inhibits the assembly of G3BP condensates at both early and late time of infection**

The interplay between G3BP and alphavirus non-structural protein 3 (nsP3), particularly in the context of stress granule (SG) formation and disassembly, has been increasingly recognized. For instance, Semliki Forest Virus (SFV), an Old World alphavirus, has been shown to initially promote, but later disrupt, SG formation via nsP3-mediated binding and sequestration of G3BP (114). As recent studies suggest, G3BP dynamically switches between the soluble and insoluble state, a balance maintained by interaction with USP10 and Caprin-1, respectively. The promotion of the soluble state through interaction with USP10 could potentially influence SG dynamics during CHIKV infection (99,163).

Aiming to elucidate how USP10 overexpression affects CHIKV-induced SG formation, we transfected HEK-293T cells with Flag-tagged USP10 (wild type and mutants) and subsequently infected the cells with eGFP-CHIKV (MOI 5). We included cells treated with sodium arsenite (0.5  $\mu$ M) for 1 hour as a positive control for SG induction. The cells were fixed at both early (4 h p.i.) and later (8 h p.i.) infection stages in 6% PFA. Fixed cells were labeled with antibodies detecting G3BP1, combined with an AF647-conjugated secondary antibody (red) and TIA-1, in combination with an AF568-conjugated secondary antibody (yellow). Blue DAPI stain was used to stain cell nuclei. Additionally, cells infected for 24 hours were included for transfection control and validation of infection. Those cells were labeled with an anti-G3BP antibody in combination with an AF647-conjugated secondary antibody (red), and an antibody targeting USP10, combined with an AF568-conjugated secondary antibody (yellow) (Figure S 1). Fixed and immunolabelled cells were observed under a confocal microscope, allowing the observation of a single focal plane.

## Results

---

G3BP-positive foci, identified as condensates exerting an intense AF647 signal, were quantified by CellProfiler software, followed by a manual cross-check. The software was further employed to quantify the total number of cells, identified by the number of DAPI stained nuclei. As shown in Figure 12, G3BP foci were induced in empty vector-transfected cells at both infection time points at consistent numbers, as well as in arsenite-treated cells. Further, empty vector-transfected cells did not form G3BP foci in absence of an SG inducer, demonstrating that the transfection itself does not cause SG assembly. At both early and late infection states, the number of foci was significantly reduced in USP10 wild type or USP10 C424A overexpressing cells, compared to the empty vector. The F10A mutant, deficient in G3BP-binding, did not significantly alter foci formation. Sodium arsenite-treated cells displayed the same pattern, indicating that the effect of USP10 on SG formation is independent on the stress inducer.

We observed that arsenite-induced foci were slightly smaller in size (~2  $\mu\text{m}$ ) compared to foci induced by CHIKV infection (~5  $\mu\text{m}$ ). No differences in the size or morphology were observed between four and eight h p.i. Further, we calculated the Manders' correlation coefficient (MCC) to quantify the overlap between two typical SG proteins: G3BP (red channel) with TIA-1 (yellow channel). The coefficient ranges between 0 and 1, with 0 indicating a random distribution, and 1 demonstrating a complete overlap of the two signals. The calculated MCCs were highest (~0.4) for empty vector or USP10 F10A overexpressing cells early after CHIKV infection, and slightly reduced at the later infection timepoint (0.2-0.3). In USP10 wild-type or C424A overexpressing cells, on the other hand, only little signal overlap (~0.1) was measured between G3BP and TIA-1. The pattern was consistent under all stress-inducing conditions compared to the empty vector and USP10 F10A overexpressing cells. Notably, SG formation appeared predominantly in bystander cells or infected cells that do not display detectable eGFP signal. Detectably infected (eGFP-positive) cells, on the other hand, show no foci formation at 8 h p.i. As the overall number of eGFP-positive cells is relatively low at this time of infection, we could not quantify this effect.

In conclusion, our findings illustrate that USP10 potently inhibits the assembly of both bona fide SGs and other G3BP condensates. The effect is observed both under chemical SG induction and CHIKV infection at early and later stages, and mediated through its interaction with G3BP.

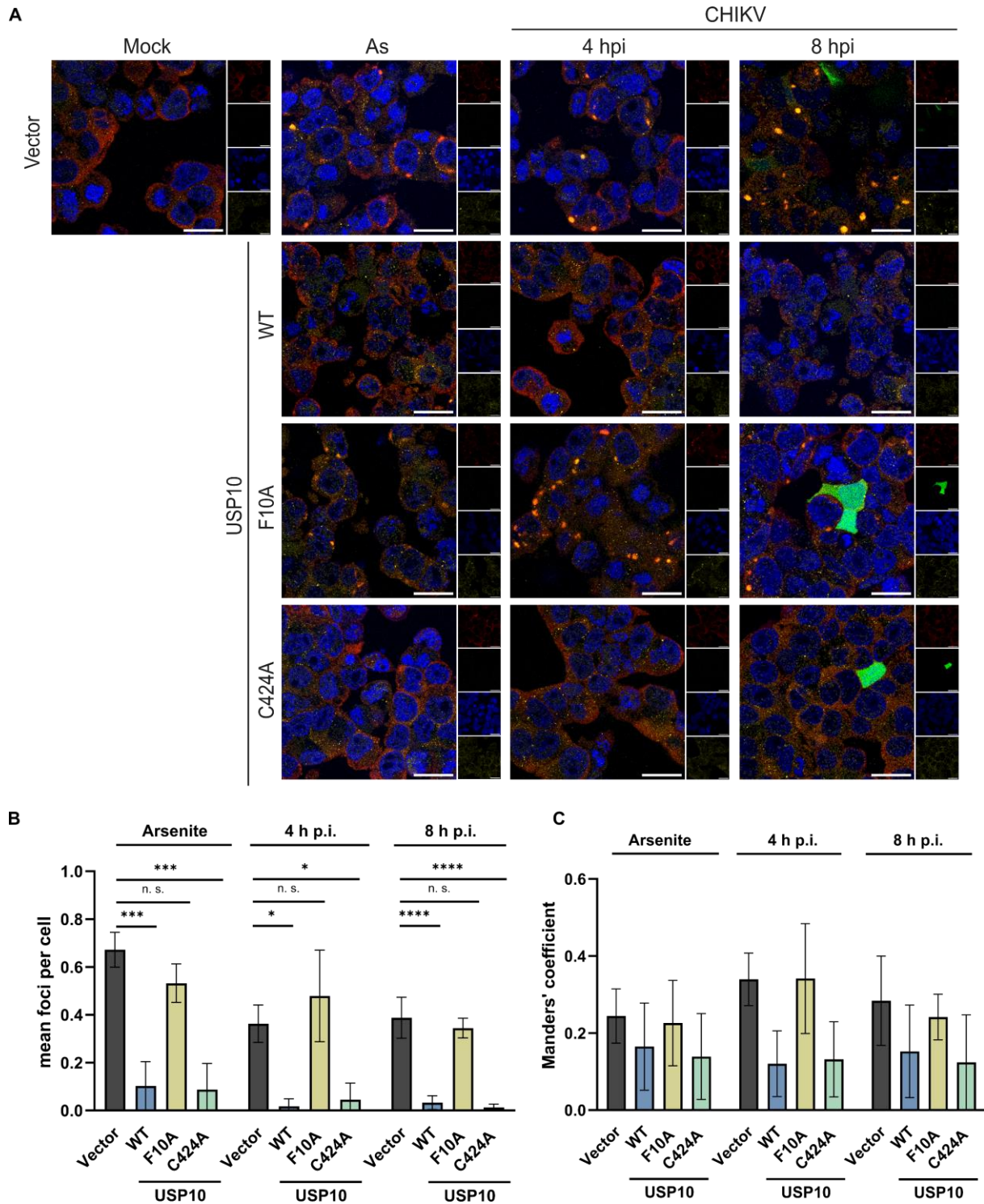


**Figure 12: Stress granule formation in USP10-overexpressing HEK-293T cells upon CHIKV infection or arsenite treatment. (A)** HEK-293T cells were transfected with USP10 WT, F10A, or C424A versus empty vector and infected with CHIKV (MOI 5) or treated with sodium-arsenite. Cells were fixed in 6% PFA at the indicated time points and (immuno)stained against G3BP1 (red), TIA-1 (yellow), and DAPI (blue). Images were taken via confocal microscopy. Scale bar equals 50  $\mu$ m. **(B)** Mean number of foci per cell. **(C)** Manders' coefficient of G3BP1 signal overlap with TIA-1.

### 3.2.4 *USP10* knock-out has no significant effect on CHIKV infection

In chapter 3.2.2, we demonstrated the antiviral effect of overexpressed USP10 in the context of alphaviral infection. To investigate the influence of endogenous levels of USP10 on CHIKV infection, we generated a *USP10* knock-out (KO) HEK-293T clonal cell line using CRISPR/Cas9 technology. We confirmed the successful gene knock-out through Sanger sequencing and Western Blot analysis, as demonstrated in Figure 13A.

We infected *USP10* KO versus parental HEK-293T cells with eGFP-CHIKV (MOI 0.2). At 24 h p.i., we analyzed the abundance of viral proteins via immunoblotting using CHIKV antiserum for the detection of viral capsid (C) and E2 proteins. Additionally, we determined the amount of the cellular housekeeping protein  $\beta$ -actin to account for variations in overall protein quantity. Interestingly, the *USP10* knock-out did not significantly affect CHIKV infection compared to parental HEK-293T cells. Instead, both cell lines displayed similar levels of viral capsid protein normalized to  $\beta$ -actin (Figure 13B).

Flow cytometry analysis of eGFP-CHIKV infected cells corroborated this finding, showing no discernible differences in the percentage of eGFP-positive cells or fluorescence intensity. (Figure 13C). Similarly, qPCR analysis revealed no significant changes in intracellular viral RNA levels between parental and *USP10* KO cells (Figure 13D).

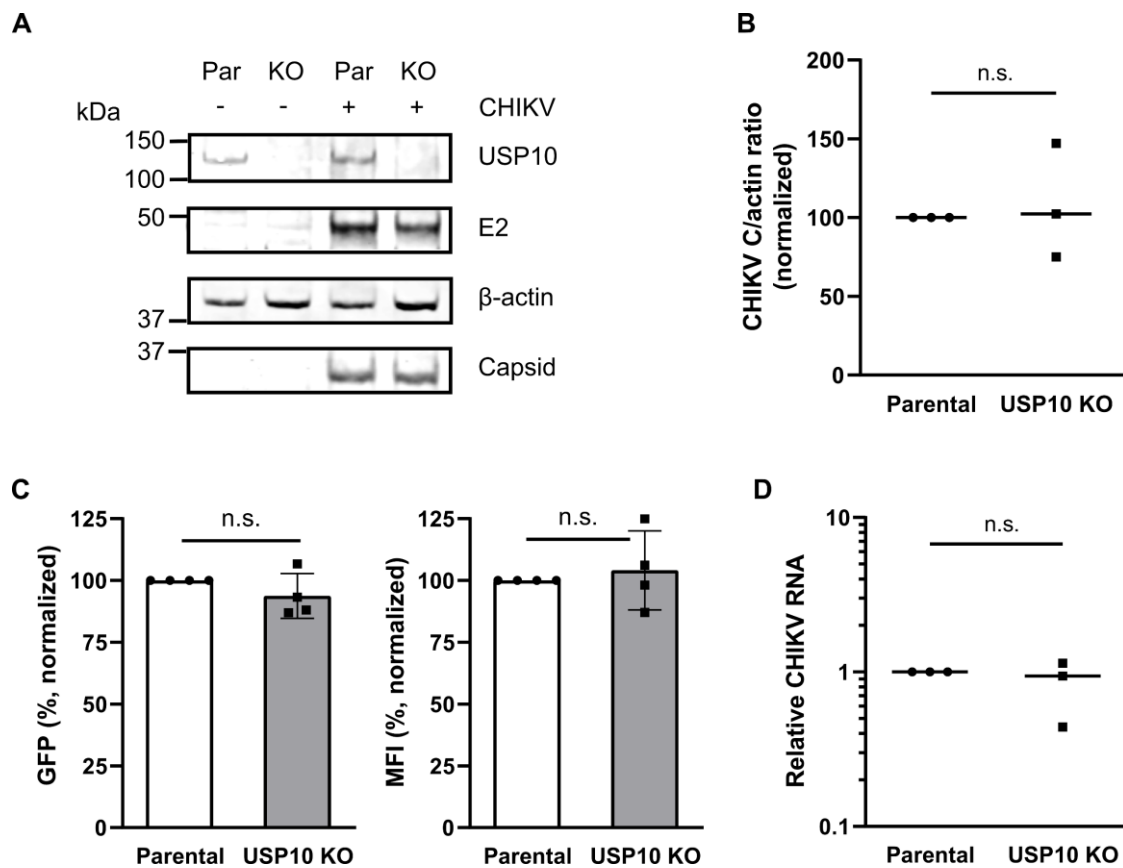


**Figure 13: USP10-knock-out in HEK 293T cells does not affect CHIKV infection.** (A) Representative immunoblot of whole cell lysates from HEK-293T parental vs USP10-knock-out cell lines. Cells were either mock or CHIKV infected (MOI 0.2) and lysed at 24 h p.i.. Viral proteins were detected using CHIKV antiserum. (B) Quantitative analysis of the protein levels detected in immunoblotting. Signal intensity of the viral capsid protein was quantified and normalized to  $\beta$ -actin. (C) Cytometric analysis of HEK-293T parental versus USP10-knock-out cells, infected with eGFP-CHIKV (MOI 0.2) and fixed in 6%PFA at 24 h p.i. for flow cytometry. (D) Quantitative PCR analysis of viral RNA in HEK-293T parental vs USP10-knock-out cells infected with eGFP-CHIKV (MOI 0.2) for 24 hours.

### 3.2.5 C-terminal truncation destabilizes USP10 and attenuates its antiviral effect

Previous data demonstrated that heterologously expressed USP10 exhibits a robust antiviral effect against CHIKV, which requires an intact G3BP-binding site of the protein. We hypothesize that the antiviral property is based on G3BP sequestration by USP10, disrupting the viral interaction with G3BP. This observation could be utilized for the development of therapeutics against CHIKV and related alphaviruses. Therefore, we aimed to identify the shortest essential USP10 peptide for antiviral activity.

To investigate the key antiviral motif, we generated four USP10 fragments with an N-terminal Flag tag and progressively truncated C-termini. The largest fragment, USP10<sub>1-414</sub> encompasses the entire N-terminal domain but lacks the USP domain. USP10<sub>1-100</sub> includes both the G3BP-binding and p53-interacting domains. (164). The third and fourth fragments, USP10<sub>1-26</sub> and USP10<sub>1-17</sub>, are short peptide sequences containing the full or partial G3BP-binding domain, respectively. Successful plasmid cloning was confirmed via Sanger sequencing and gel electrophoresis, as detailed in the Appendix, Figure S 2.

We monitored transfection efficiency by Western Blot and flow cytometry analysis, as shown in Figure 14B. Notably, protein levels significantly decreased in truncated USP10 versions. USP<sub>1-100</sub> was detectable in around 6 %, USP10<sub>1-26</sub>, and USP10<sub>1-17</sub> in less than 2 % of the transfected cells. This suggests rapid degradation of USP10 protein fragments lacking the USP10<sub>100-414</sub> region, indicating the presence of stabilizing motifs within this region.

Next, cells were infected with eGFP-tagged CHIKV (MOI 0.5), and infection rates were quantified at 24 h p.i. via flow cytometry (Figure 14C). Consistent with previous results, wild-type USP10 overexpression significantly reduced infection rates by 5-fold compared to the empty vector control ( $p \leq 0.0001$ ). Heterologous expression of USP10<sub>1-414</sub> exhibited a reduced antiviral effect, with a 2-fold reduced infection rate ( $p \leq 0.001$ ). No reduction in infection rates was observed in cells transfected with USP<sub>1-100</sub>, USP10<sub>1-26</sub>, or USP10<sub>1-17</sub>. These findings suggest that the full-length protein may be necessary for the complete antiviral effect, though it remains unclear whether this requirement is for functional engagement or to maintain protein stability.

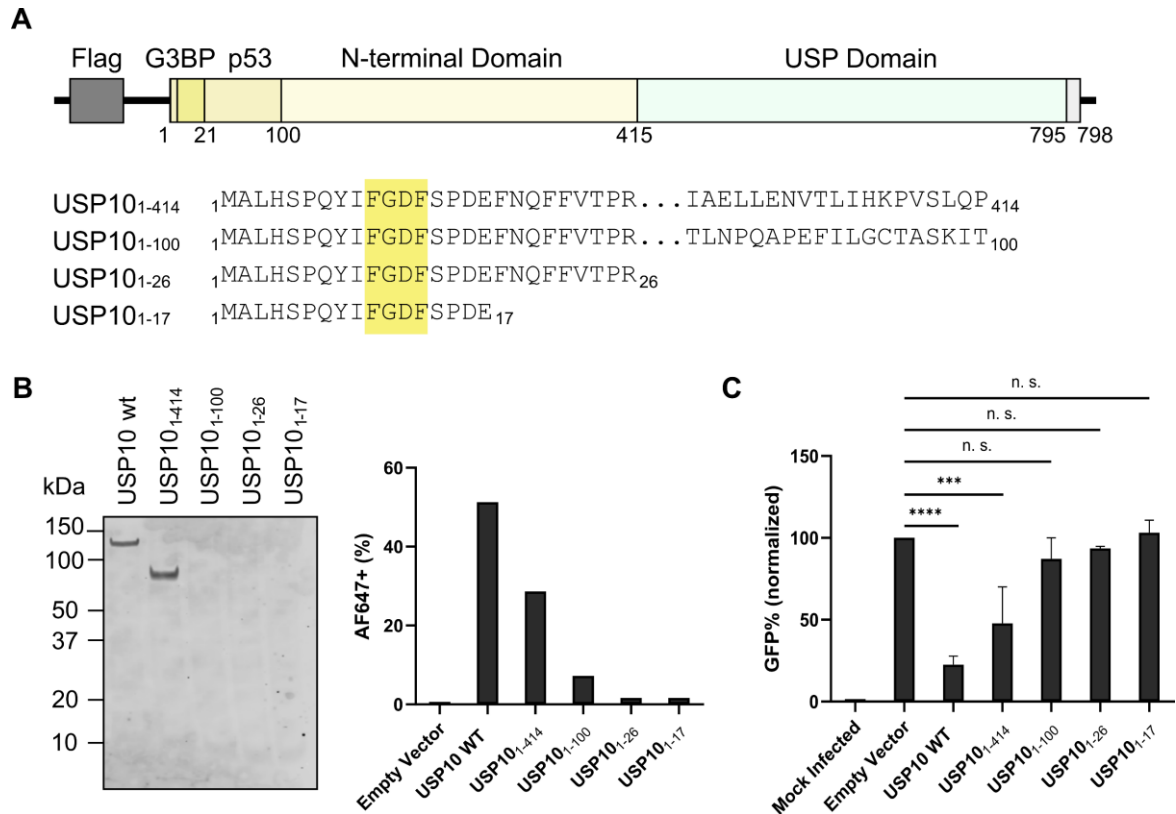


**Figure 14: USP10 fragments in the context of CHIKV infection. (A)** Schematic overview of Flag-tagged USP10 wild-type and truncated versions. The G3BP-binding motif is highlighted in yellow. **(B)** Representative immunoblot (left) and flow cytometry analysis (right) of HEK-293T cells transfected with USP10 wild-type or truncated versions at 24 h p.t. Expected protein sizes are 110 kDa (USP10 WT), 67 kDa (USP10<sub>1-414</sub>), 35 kDa (USP10<sub>1-100</sub>), 27 kDa (USP10<sub>1-26</sub>), 26 kDa (USP10<sub>1-17</sub>). **(C)** Flow cytometry analysis of HEK-293T cells transfected with USP10 (wild-type or truncated versions) for 24 hours, following infection with eGFP-tagged CHIKV (MOI 0.5). Cells were fixed in 6% PFA for cytometric analysis at 24 h p.i. (N=3)

### 3.2.6 *USP10* and *G3BP1* are moderately upregulated upon CHIKV infection

Viral infections trigger an antiviral response, orchestrated by the innate immune system. In chapter 3.1.4, we demonstrated that *USP10* and *G3BP* are not regulated by type I IFN, but their expression might still be influenced by viral infection through other cytokines. Based on this, we investigated the impact of CHIKV infection on *USP10* and *G3BP1* protein expression dynamics over time. We conducted the experiment in U2OS cells, chosen for their robust endogenous levels of *USP10* and *G3BP*, characterized in chapter 3.1.4. Further, U2OS cells maintain intact immune signaling, in contrast to HEK-293T cells, which exhibit an attenuated immune response due to viral transformation.

## Results

---

We monitored CHIKV infection at low (MOI 0.5) and high (MOI 5) multiplicities of infection over 48 hours. The percentage of eGFP-positive cells, indicating productively infected cells, was quantified by flow cytometry (Figure 15A). Low MOI infection displayed a gradual increase in infection over time, while high MOI infection peaked at 24 hours, followed by a decrease at 36 and 48 hours.

Parallel to the assessment of virus kinetics, we examined the mRNA expression of *USP10*, *G3BP1*, and *IFIT1*, serving as an immune response marker, upon CHIKV infection. Cellular mRNA was extracted from cell lysates at defined time points and measured by qPCR. Both *USP10* and *G3BP1* exhibited a steady rise in mRNA levels post-infection at both MOIs, reaching approximately four-fold upregulation compared to mock-infected controls at 48 h p.i. *IFIT1*, as expected, displayed a robust upregulation in response to viral infection, reaching up to a 30-fold increase at 24 hours, which declined afterward (Figure 15B).

This kinetic analysis revealed a moderate, yet consistent upregulation of *USP10* and *G3BP1* mRNA levels upon CHIKV infection in U2OS cells. Overall, these findings highlight the dynamic nature of the cellular antiviral response. The notable elevation in *USP10* and *G3BP1* mRNA levels corroborates a potential involvement of these genes in the innate immune response against CHIKV.



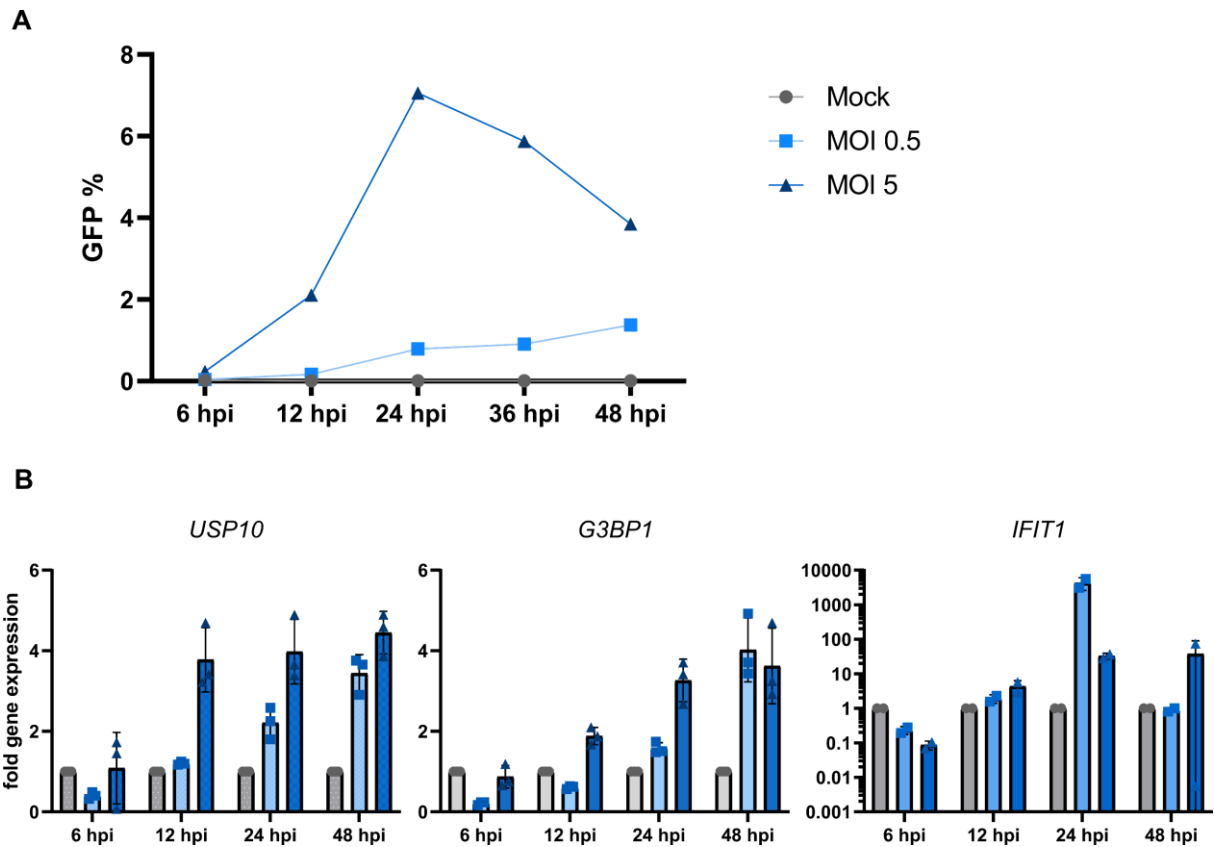


**Figure 15: USP10 and G3BP1 expression is upregulated after CHIKV infection. (A)** Flow cytometry analysis of U2OS cells infected with eGFP-CHIKV (MOI 0.5 and MOI 5) and fixed at indicated time points. **(B)** qPCR analysis of *G3BP1*, *USP10* and *IFIT1* levels at indicated time points.

### 3.3 Antiviral mechanisms of USP10 and viral evasion strategies

To elucidate the mechanisms behind the antiviral effect of USP10 against alphaviruses, we dissected the influence of heterologous USP10 expression on various stages of the viral replication cycle, including entry, RNA replication, and release of de novo-synthesized virions.

#### 3.3.1 Transduction with CHIKV gp-pseudotyped lentiviruses reveals no CHIKV-specific USP10-mediated entry inhibition

USP10 is primarily localized in the cytoplasm and nucleus (129). However, USP10-mediated deubiquitylation plays a role in regulating the expression of multiple membrane proteins, including the epithelial sodium channel (ENaC) and the cystic fibrosis transmembrane regulator (CFTR) (160,165). In analogy to that, an indirect antiviral effect, for example via deubiquitylation of membrane-standing entry factors, is possible.

To assess the impact of heterologous USP10 expression on the cell's susceptibility to CHIKV entry, we generated lentiviral particles pseudotyped with CHIKV glycoproteins, equipped with a luciferase reporter. These CHIKV pseudoparticles utilize the same host cell entry receptor as authentic CHIKV virions but lack the alphaviral replication system. This setup allowed us to isolate and evaluate the entry phase of infection, independent of viral replication. In accordance with previous experiments with the CHIKV full-length virus, we used HEK-293T cells transfected with plasmids encoding wild-type or mutants of USP10, as described in chapter 3.2.2. We included IFITM3-expressing cells, serving as a positive control for entry inhibition (166). The cells were transduced with CHIKV pseudotyped particles and incubated for 48 hours. We measured cell entry efficiency via luciferase assay on cell lysates. A schematic overview of the experiment setup is given in Figure 16.

Our findings, illustrated in Figure 16B, indicate a slight decrease in CHIKV glycoprotein-mediated entry in cells overexpressing wild-type USP10 compared to controls. However, this effect was absent in cells expressing either USP10 mutant. Notably, similar results were observed with VSV-G pseudotyped particles, suggesting that the reduction in luminescence observed in USP10 wild-type overexpressing cells

is based on the inhibition of post-entry viral processes rather than specifically targeting Chikungunya virus (CHIKV) glycoprotein-mediated entry. Potential post-entry steps that USP10 overexpression might inhibit include viral reverse transcription, nuclear import, and integration of the viral genome. The absence of lentiviral inhibition in USP10 F10A and C424A overexpressing cells suggests that both the G3BP binding and DUB activity are crucial for the observed effect

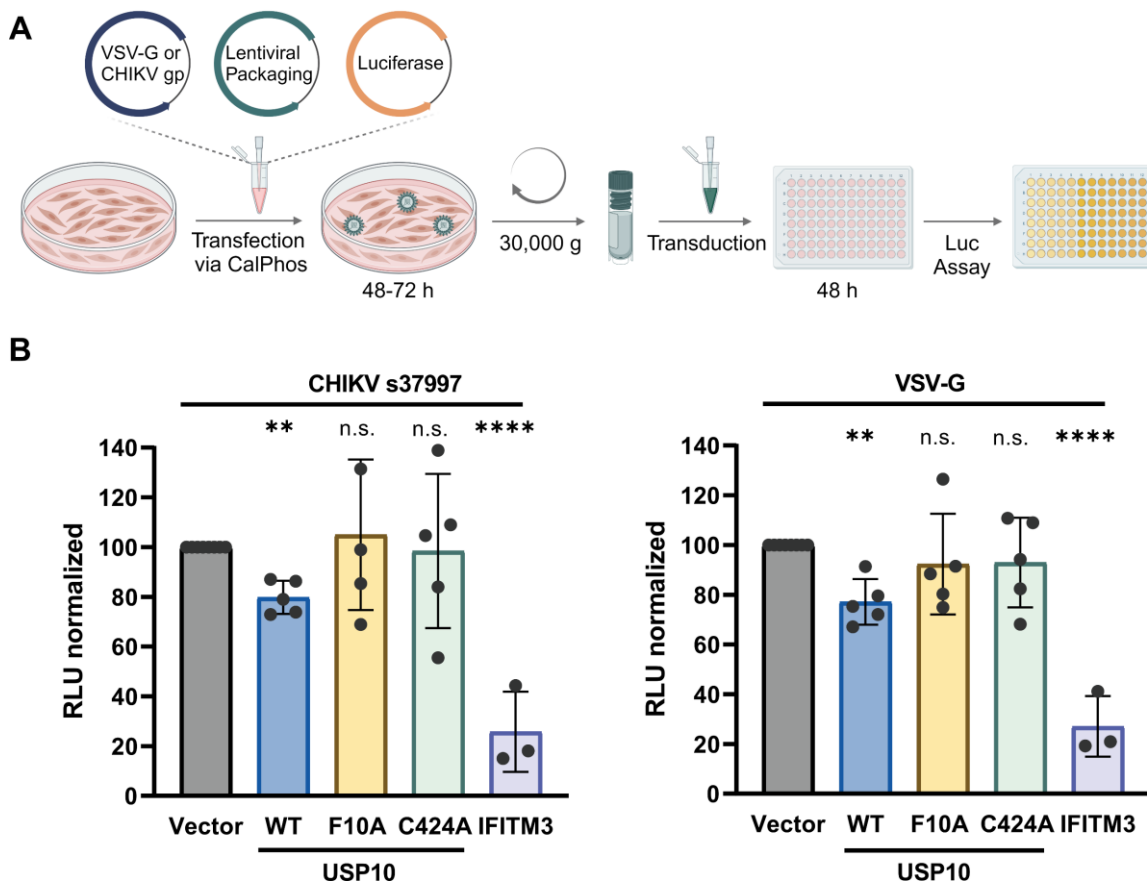


**Figure 16: Impact of heterologous USP10 expression on CHIKV glycoprotein-mediated cell entry.** (A) Schematic representation of lentiviral particle production and experiment set-up. Created with Biorender. (B) Luciferase assay of HEK-293T cells transfected with USP10 wild-type or mutant and at 24 h p.t. transduced with lentiviral particles pseudotyped either with CHIKV s37997 glycoprotein or VSV-G and containing a firefly luciferase-expressing reporter. After incubation for 48 hours, luciferase activity in lysed cells was quantified luminometrically and normalized to vector control cells.

## Results

### 3.3.2 Replication and protein translation in the CHIKV replicon system are unaffected by USP10 overexpression

To assess the impact of USP10 on the later stages of the viral replication cycle, we employed a CHIKV replicon system in HEK-293T cells. These replicons mimic the viral genome but lack structural components, enabling the study of post-entry viral processes (141).

As described in Chapter 3.2.2, cells were transfected with USP10 wild-type or mutant constructs and incubated for 24 hours, followed by the transfection of *in vitro* transcribed RNA encoding a GFP-expressing CHIKV replicon. 24 hours after the second transfection, we quantified the GFP-positive cell percentage via flow cytometry. Remarkably, we observed no significant differences in the percentage of GFP-positive cells between cells overexpressing USP10 wild-type or either mutant, compared to the empty vector control (Figure 17). These findings suggest that USP10 overexpression does not markedly influence viral RNA replication and protein translation.

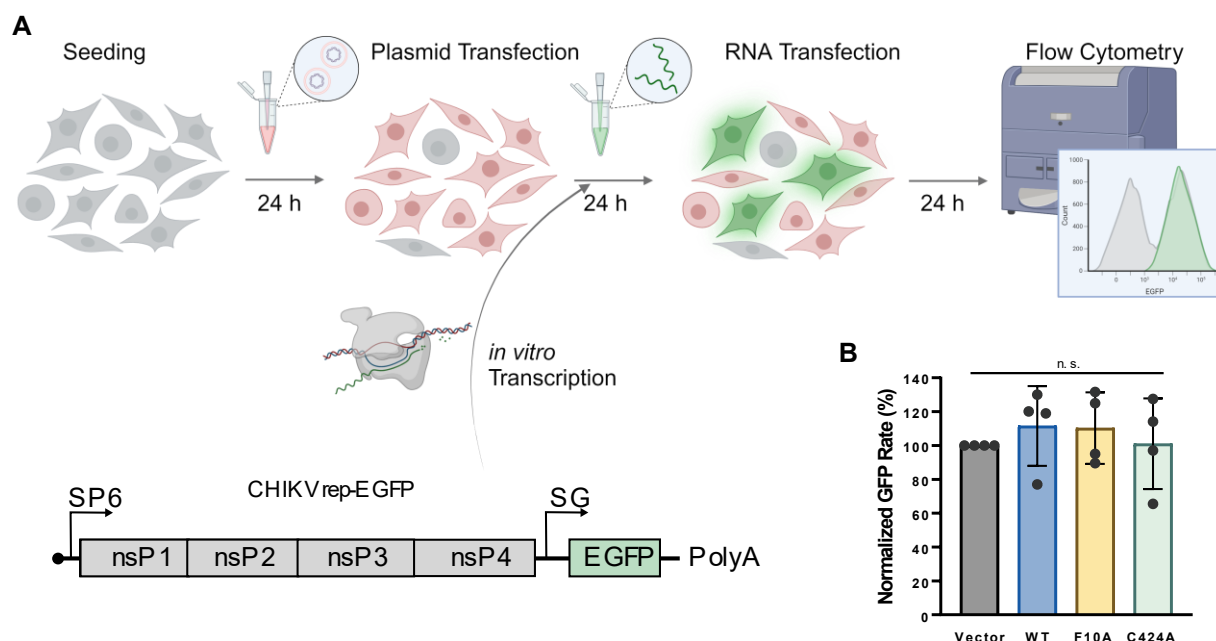


**Figure 17: Impact of heterologous USP10 expression on virus replication. (A)** Schematic overview of *in vitro* transcribed CHIKV replicon transfection. Created with Biorender and Inkscape 1.3.2. **(B)** Cytometric analysis of GFP-positive cells after transfection with GFP-tagged CHIKV replicon RNA. HEK-293T cells were transfected with USP10 wild type or mutant, and after 24 hours *in vitro*, transcribed GFP-CHIKV replicon was introduced via RNA transfection. GFP-positive cell rate was quantified 24 hours after the second transfection via flow cytometry and normalized to empty vector-transfected control cells.

### 3.3.3 Virus progeny is decreased in cells overexpressing wild type and DUB-deficient, but not G3BP-binding deficient USP10

To assess the impact of USP10 on virus progeny, we infected HEK-293T cells overexpressing USP10 wild-type or one of the mutants using a low viral titer (MOI 0.1) and collected the infectious supernatants 48 hours after infection for titration on naïve HEK-293T cells for an eGFP reporter-based analysis via flow cytometry, and on naïve Vero E6 cells for a conventional plaque assay. Furthermore, we quantified the viral proteins in the supernatant via Western blot and the viral RNA via qPCR. A schematic overview of the experiment procedure is given in Figure 18A.

Immunoblotting of whole cell lysates versus supernatant samples at 48 h p.i. MOI 0.1 demonstrated an overall reduction in viral structural proteins (capsid and E2) both intracellular and in the supernatant of HEK-293Ts overexpressing USP10 wild-type or the DUB-defective C424A mutant, but not the G3BP binding-deficient F10A mutant, compared to the empty vector. Tetherin, a release inhibitor, served as a positive control (Figure 18B). Accordingly, quantitative PCR analysis of viral RNA in the supernatant 48 hours after infection with CHIKV or MAYV (MOI 0.1) demonstrated a significant increase in viral RNA in supernatants of USP10 wild-type and C424A overexpressing cells compared to the empty vector. However, a moderate reduction of viral RNA was detected in the supernatant of USP10 F10A transfected cells. These data indicate that while G3BP-binding is crucial for the major part of the antiviral activity, USP10 may inhibit viral RNA release through an additional, G3BP1-binding independent mechanism (Figure 18C).

Titration of the infectious supernatant on naïve HEK-293T cells for an eGFP signal-based flow cytometry analysis demonstrated a significant decrease in the amount of virus progeny in cells overexpressing USP10 wild-type or the C424A mutant, while no significant effects were observed in cells overexpressing the F10A mutant. Similarly, the number of infectious particles was decreased approximately by factor 10 in plaque assay (Figure 18D+E).

Collectively, these findings indicate an antiviral effect of USP10 on the later stages of the replication cycle, leading to reduced virus progeny. The infectivity of virions, as well as the total number of released particles, is decreased by USP10 overexpression, independent of the protein's DUB activity.

## Results

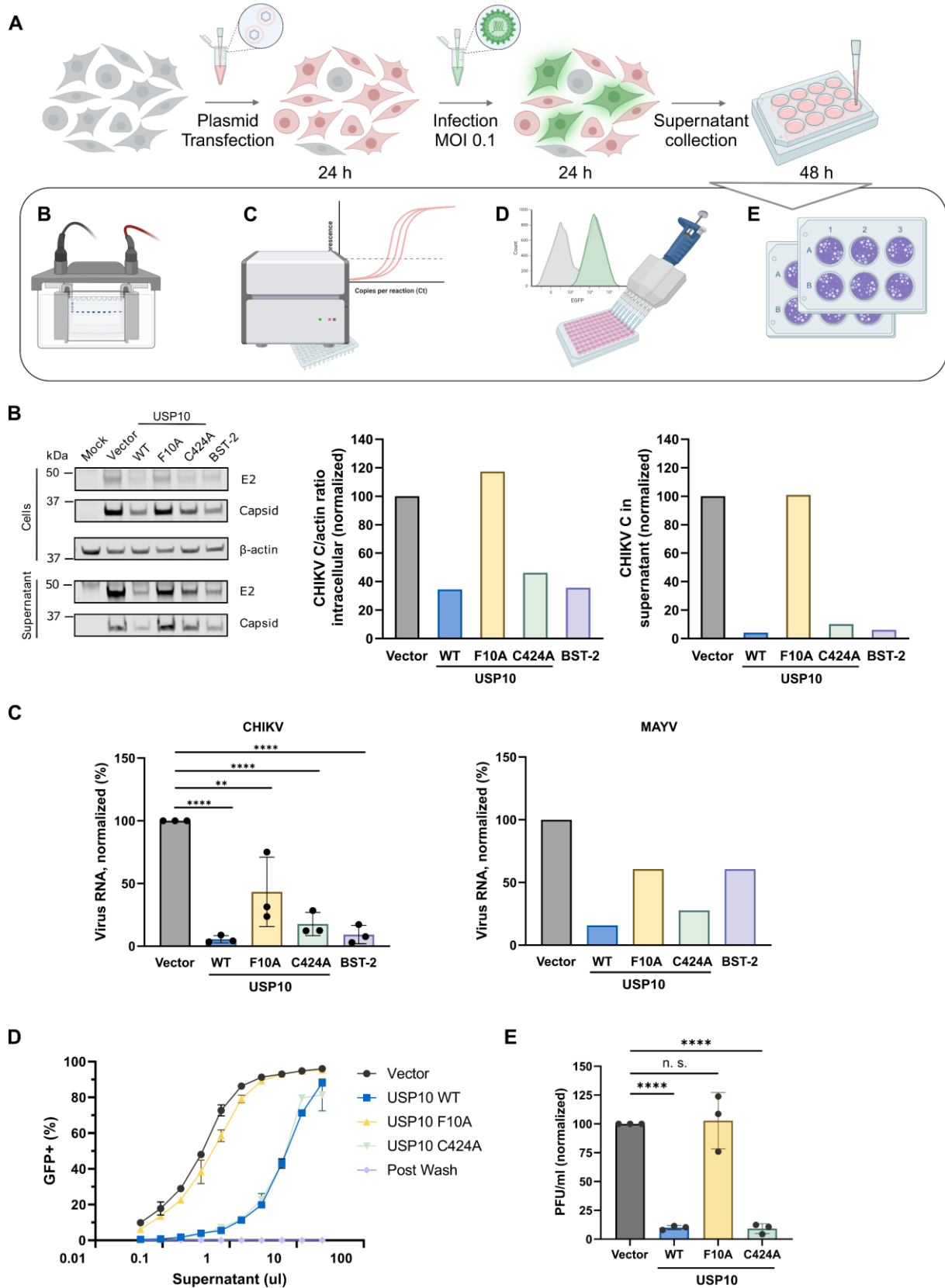


**Figure 18: Impact of USP10 overexpression on virus progeny.** (A) Schematic overview of the experiment procedure (created with biorender.com). (B) Representative immunoblot of whole cell lysates and supernatants of infected cells (MOI 0.1, 48 h p.i.) (left), quantification of CHIKV C/actin ratio in whole cell lysates (middle), quantitative analysis of CHIKV C in the supernatant (right). Viral proteins

were detected using CHIKV antiserum. Cellular  $\beta$ -actin was detected for normalization. **(C)** Quantitative PCR analysis of viral RNA in the supernatant of HEK-293T cells infected with CHIKV (MOI 0.1, N=3) or MAYV (MOI 0.1, N=1) at 48 h. p.i.. **(D)** Flow cytometry analysis of infectious supernatant titration on naïve HEK-293T cells. Supernatants were derived from HEK-293T cells, heterologously expressing USP10 wild-type or mutant, infected with CHIKV (MOI 0.1, 48 h p.i., N=3). Titration was performed on naïve HEK-293T for an eGFP-reporter-based cytometric assay **(E)** Plaque assay on naïve Vero E6 cells using supernatants from eGFP-CHIKV-infected HEK-293T cells (MOI 0.1, 48 h p.i., N=3), heterologously expressing USP10 wild-type or mutant versus an empty vector control.

### 3.3.4 Influence of G3BP-binding deficiency in CHIKV nsP3 on virus kinetics and USP10-mediated antiviral response

Previous chapters established the importance of G3BP binding for USP10's antiviral activity against CHIKV. Notably, a similar motif is found in the hypervariable domain of many alphaviruses, including CHIKV, which has even two FGDF motifs (115). Here, we investigate how mutations in the CHIKV nsP3 protein that attenuate G3BP binding affect viral dynamics and the USP10-mediated antiviral response.

Through site-directed mutagenesis, we generated two CHIKV mutants harboring a single phenylalanine-to-alanine substitution in each FGDF motif (F1812A and F1830A), and a double mutant with substitutions in both motifs. Mutations are schematically represented in Figure 19A. After confirmation of successful plasmid cloning via Sanger sequencing, we used *in vitro* transcription to obtain viral RNA. BHK-21 cells were electroporated with viral RNA via electroporation, and incubated for 48 hours for virus production. We monitored the virus growth via fluorescence microscopy and cytometric analysis of the eGFP signal in the producer cells. Notably, cells transfected with the double mutant did not exhibit any observable eGFP signal or cytopathic effect after 48 hours, indicating a lack of viability of this virus. The CHIKV mutant with an F $\rightarrow$ A exchange in the first motif (F1812A) displayed moderate CPE and eGFP signal (8.6%), while the mutant with an F $\rightarrow$ A exchange in the second motif (F1830A) displayed relatively high CPE and eGFP signal (94.0%). In accordance, virus titration on naïve HEK-293T cells displayed the highest virus titer for CHIKV ORF1 F1830A, followed by CHIKV ORF1 F1812A. The double mutant lacked any evidence of detectable viral infection and was therefore excluded from further experiments. Infection rates in BHK-21 cells after 48 hours and virus titration on HEK-293T cells are represented in the Appendix, Figure S 3.

## Results

---

To assess virus kinetics, we infected U2OS cells with wild-type CHIKV, CHIKV ORF1 F1812A, or CHIKV ORF1 F1830A at a multiplicity of infection of 0.5. Infection rates were monitored over 72 hours by measuring eGFP-positive cells via flow cytometry (Figure 19B).

An initial appearance of eGFP-positive cells was noted at 12 h p.i. for all virus types, with variations in early infection rates attributed to MOI calculations based on a different cell line (HEK-293T). Notably, the infection rate of G3BP-binding mutants peaked at 24 h p.i. and declined thereafter. In some replicates, a second peak was observed at 72 h p.i., potentially reflecting the emergence of adaptive mutations that restore G3BP binding. These findings suggest that impairments in the G3BP-binding ability of nsP3 disrupt the virus's ability to counteract innate immune responses. Additionally, the potential for mutations that revert to wild-type characteristics by restoring G3BP-binding capability must be considered. Therefore, further experiments were conducted with maximum 24-hour infection time, to avoid multiple rounds of infection.

To explore the interplay between USP10 expression and infection with G3BP binding-deficient CHIKV, we transfected HEK-293T cells with USP10 wild-type, F10A, or C424A mutants. After 24 hours, we infected the cells with the aforementioned CHIKV mutants (MOI 0.5) and determined the infection rates at 24 h p.i. by flow cytometry (Figure 19C). We observed no significant differences in infection rates among USP10 expressing cells and empty vector controls. These observations contrast with the clear impact of USP10 on wild-type CHIKV infection (Chapter 3.2.2), further emphasizing the critical role of G3BP binding in exerting an antiviral effect of USP10.



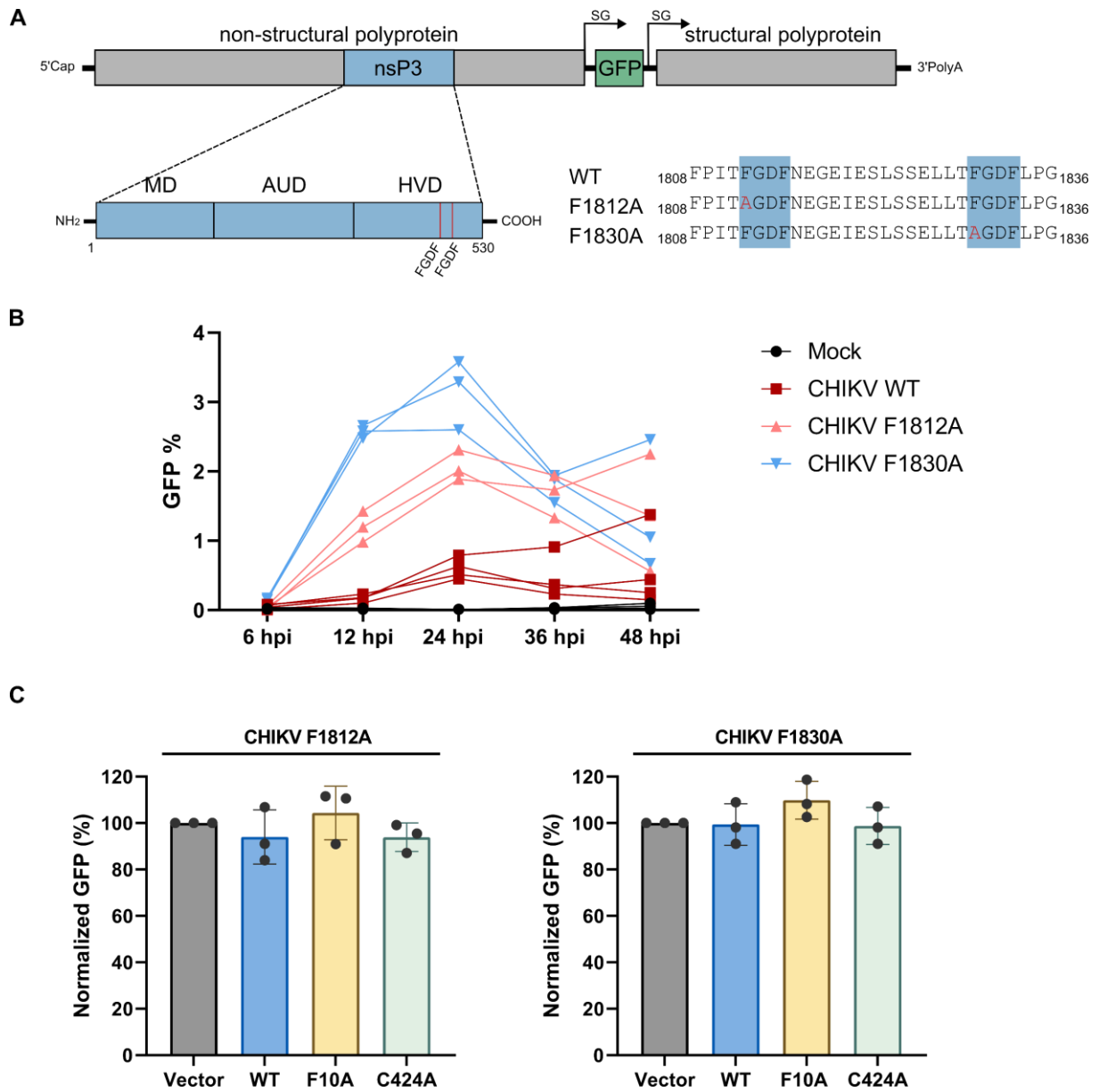


**Figure 19: Impact of USP10 on G3BP binding-deficient CHIKV mutants. (A)** Schematic overview of the CHIKV genome. The nonstructural protein 3 is sub-organized in Macrodomain (MD), Alphavirus Unique Domain (AUD), and Hypervariable Domain (HVD). The two G3BP-binding FGDF motifs are highlighted. **(B)** Cytometric analysis of U2OS cells infected with eGFP-CHIKV WT, eGFP-CHIKV F1812A, or eGFP-CHIKV-F1830A (MOI 0.5). Cells were fixed in PFA 6% at indicated time points (6, 12, 24, 48, 72 h). eGFP-positive cell rate was measured via Flow Cytometry **(C)** Cytometric analysis of HEK-293T cells transfected with USP10 wild-type, F10A or C424A, and infected 24 h p.t. with eGFP-tagged wild type CHIKV, CHIKV ORF1 F1812A or CHIKV ORF1 F1830A (MOI 0.5). Cells were fixed in 6% PFA at 24 h p.i. and analyzed via flow cytometry.

### 3.3.5 Mutation analysis under selective pressure

Many viruses, including CHIKV, exhibit strong adaptability to selective pressures, often caused by environmental changes and immunologic pressure. This adaptability can lead to the emergence of escape mutations that allow the virus to circumvent host antiviral mechanisms. Resistance mutations have been described for example for HIV in the context of antiretroviral therapy, or for Hepatitis C virus against protease inhibitors (167,168). The accuracy of viral polymerases, particularly RNA-dependent RNA polymerases (RdRp), plays a crucial role in this process. The CHIKV RdRp has a low fidelity with around 1 error per  $10^4$  nucleotides, which provides a reservoir of genetic variability for potential adaptation under selective pressures (169).

To explore the evolutionary adaptation of CHIKV in response to the antiviral activity of USP10, we passaged eGFP-CHIKV ten times under the selection pressure exerted by USP10 overexpression. Given the dependency of USP10's antiviral effect on its interaction with G3BP, we employed the G3BP binding-deficient mutant, USP10 F10A, as a reference. A schematic overview of the experimental procedure is given in Figure 20. This setup aimed to discern whether continuous exposure to USP10's antiviral action would lead to the emergence of CHIKV strains resistant to this specific host defense mechanism. For transfection, an intermediate amount of USP10 wild-type or F10A plasmid input was chosen, to ensure selection pressure, while at the same time avoiding a too strong antiviral effect, bearing the risk that it suppresses initial virus infection and spread before it was able to form adaptive mutations for immune evasion. The initial infection was carried out with eGFP-CHIKV at an MOI of 0.1. Every 48 hours, infectious supernatant was passaged onto naïve HEK-293T cells, previously transfected with USP10 wild-type or F10A, until ten passages were reached. Additionally, cell and supernatant samples were collected for flow cytometry and qPCR analysis, respectively.

Flow cytometric analysis demonstrated an initial decrease of viral infection in USP10 wild-type expressing cells compared to F10A by around 30% (60% infection rate in F10A expressing cells versus 40% in USP10 expressing cells). Further, a rapid decrease in GFP-positive cells is observed after 4-5 passages in five out of six samples, indicating the spontaneous emergence of mutations in the eGFP reporter

(Figure 20B). However, quantitative PCR of the viral RNA in the supernatant demonstrated the presence of viral RNA in all ten passages (Figure 20C).

NGS analysis of viral RNA after ten passages revealed an interesting mutation pattern. For both viruses passaged over USP10 WT and USP10 F10A overexpressing HEK-293T cells, all nucleotide exchanges were limited to three proteins: nsP2, C, and E2 (Figure 20D). Additionally, we found mutations in the eGFP cassette, including large deletions in five out of six samples (Figure S 4). All of the nucleotide exchanges with the corresponding mutations are detailed in the Appendix, Table S 2.

Nonsynonymous mutations that exclusively occur in USP10 WT but not F10A are: D420G and N643K in nsP2, and E166K, M171V, N187D and N238S in E2. Although no mutations occurred in nsP3, therefore did not directly affect G3BP-binding, their emergence might indicate an indirect escape from the antiviral effects of USP10.

## Results

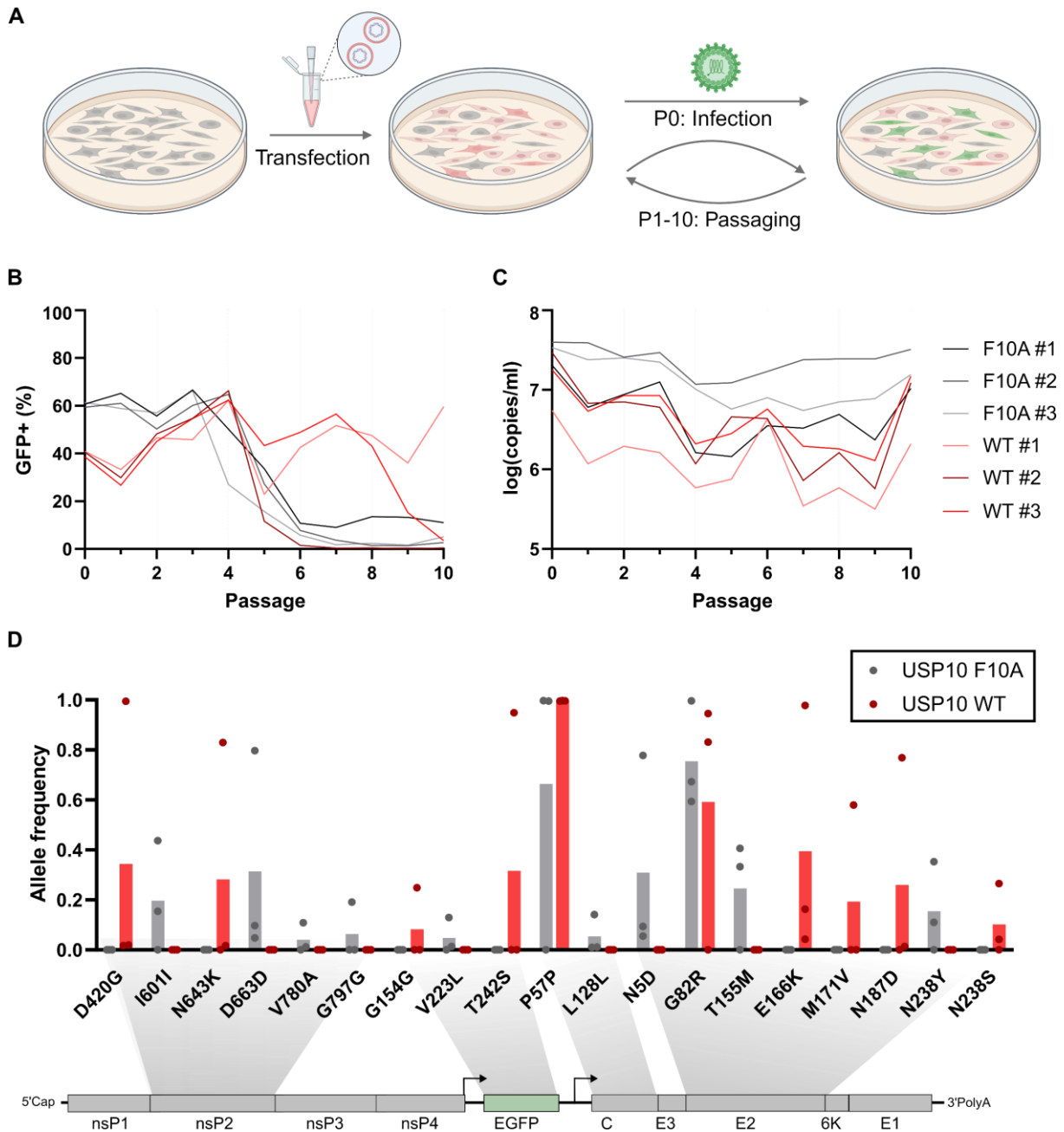


**Figure 20: Mutation analysis under selective pressure exerted by heterologous USP10. (A)** Schematic representation of the experiment procedure. Created with Biorender. **(B)** Flow cytometry and **(C)** qPCR analysis of eGFP-CHIKV, passaged over ten times on USP10 wild type vs. F10A overexpressing HEK-293T cells **(D)** NGS analysis of eGFP-CHIKV after ten passages in USP10 wild type vs. F10A overexpressing HEK-293T cells.

## 4 Discussion

### 4.1 Characterization of USP10 and G3BP expression and inducibility

USP10 and G3BP are multifunctional proteins with ubiquitous cytoplasmic expression. G3BP is involved in regulating cellular homeostasis, mRNA stability, and immune signaling via the cGAS-STING pathway. Further, G3BP plays a dual role in viral infection. While it is a key initiator for SG formation upon viral infection, some viruses, including alphaviruses and SARS-CoV-2, have evolved mechanisms to exploit G3BP for their own replication (82,128).

USP10, in addition to its role in the ubiquitin-proteasome pathway for protein degradation and various other functions related to deubiquitylation of target proteins, is a crucial regulator of G3BP-mediated SG nucleation. It interacts with the NTF2-like domain of G3BP, antagonizing Caprin-1 binding. While Caprin-1 promotes the oligomerization and RNA binding of G3BP, USP10 acts as a valence cap, lacking both RNA-binding and oligomerization domains. The balance between G3BP interaction with USP10 or Caprin-1, favoring either the soluble or condensed state, respectively, is driven by cellular pH (99,163). Our collaboration partners from Patrica Korn's lab at RWTH Aachen conducted tandem MS and Co-IP analysis, demonstrating an interaction between USP10 and CHIKV-nsP3, which may be mediated via G3BP binding. This is in line with previous reports on the interaction between nsP3 and G3BP in related alphaviruses (83,114).

Analysis of USP10 and G3BP in numerous cell lines demonstrated the abundance of both proteins. Further, we examined the regulation of USP10 and G3BP1 by type I interferon (IFN) and vasopressin (AVP) in various human cell lines. The canonical USP10 inducer AVP did not increase USP10 expression in the tested cell lines, which might be due to the lack of V<sub>2</sub> receptor expression (161).

The interferon response is a cornerstone of the innate immune system's defense against viral invaders. Interferon stimulation triggers the upregulation of various interferon-stimulated genes (ISGs) with diverse antiviral functions. Our results revealed that USP10 and G3BP1 protein levels were not significantly upregulated following treatment with IFN- $\alpha$ 2 for 48 hours. This suggests that *USP10* and *G3BP1* are not ISGs, in line with findings collected in the interferome database (170). Further, we

## Discussion

---

investigated the regulation of *USP10* and *G3BP1* mRNA expression by infecting U2OS cells, a cell line with robust endogenous levels of these proteins and intact antiviral signaling, with CHIKV. The observed CHIKV infection kinetics aligned with previously reported virus growth kinetics (171,172), exhibiting a gradual increase at low MOI and a peak at 24 hours followed by a decline at high MOI. We observed a moderate but consistent upregulation of *USP10* and *G3BP1* mRNA in U2OS cells following CHIKV infection. In combination with our previous results, showing USP10 and G3BP not to be ISGs, their upregulation after CHIKV infection suggests an IFN-independent induction mechanism. Pathways that are upregulated independently of IFN signaling include for instance NF- $\kappa$ B activation by PRRs or inflammasome activation and subsequent secretion of inflammatory cytokines (85,173).

Conservation of genes among and across species can provide insights into their biological importance. The interaction between USP10 and G3BP is mediated via an FGDF motif in USP10. We analyzed the distribution of single nucleotide polymorphisms (SNPs) within the FGDF motif of the human USP10 gene. Our analysis revealed a high degree of conservation within the FGDF motif, suggesting its functional importance. Non-synonymous SNPs were only identified at the third position of the motif, indicating a tolerance for changes in the electrochemical properties at this position. However, these SNPs occur in less than 0.001% of the dataset, which could hint at selective pressures maintaining the original motif. The conservation of the remaining residues (F10, G11, and F13) suggests an essential role of the FGx F motif in maintaining USP10's structural and functional integrity, likely through interactions with G3BP.

Notably, nearly all mammalian USP10 sequences harbor an FGDF motif, with only the exception of *Panthera onca* (jaguar), *Carlito syrichta* (Philippine tarsier), and *Microcebus murinus* (mouse lemur). Among non-mammalian vertebrates, the motif contains a single amino acid exchange at the third position from Aspartate (D) to Glutamate (E). Since these two amino acids possess comparable electrochemical properties, the exchange most likely maintains the properties of the motif. Overall, the conservation of the motif within humans and across vertebrates underlines the biological importance of an intact G3BP-binding site.

The multiple sequence alignment was conducted on USP10 orthologs across 590 species. While these encompass a majority of the 630 available vertebrate full genomes, there are 40 species in the database that do not have an annotated USP10 ortholog. This could be due to limitations in the ortholog identification algorithm, or a genuine lack of USP10 homologues in these species.

### 4.2 Impact of USP10 on alphavirus infection and SG formation

Our collaborators from Patricia Korn's Lab (RWTH Aachen) identified USP10 as an interaction partner of CHIKV nsP3 in tandem MS analysis. Co-immunoprecipitation confirmed the interaction and indicated G3BP as an additional binding partner. Further, analysis of the ubiquitination status of CHIKV nsP3 in the presence of wild-type versus DUB-deficient USP10 suggested that nsP3 is a target of the DUB activity. The interaction between USP10 and G3BP is well-established in the literature (137,174). However, to date, the interaction between USP10 and CHIKV nsP3, and the impact on CHIKV and other alphaviruses, have not been studied.

We examined the role of USP10 overexpression on infection with CHIKV, an Old World alphavirus, and MAYV, a New World alphavirus, to investigate potential conservation of USP10's antiviral effect across diverse alphaviruses with relatively low sequence homology of nsP3 (115). Our findings indicate a notable dose-dependent decrease in CHIKV and MAYV infection rates in HEK-293T cells overexpressing USP10. This antiviral effect was further confirmed by a reduction in viral RNA levels as measured by qPCR. The effects on CHIKV and MAYV were similar, suggesting a general antiviral activity of USP10 against alphaviruses.

A recent study by Ravindran et al. reported potential antiviral properties of USP10 in the context of SARS-CoV-2 infection. Moreover, they demonstrated the deubiquitinase inhibitor spautin-1 to enhance SARS-CoV-2 infection, suggesting the antiviral role of USP10 to be mediated by its deubiquitinase activity (175). Considering the ubiquitin-proteasome system's pivotal role in regulating viral replication and host antiviral responses, USP10 could be interfering with the ubiquitination of viral components or modulating host proteins essential for viral replication. Accordingly, we initially hypothesized the antiviral effect of USP10 in alphaviruses to be based on its DUB activity. This hypothesis is supported by the findings of Patricia Korn's lab, indicating that CHIKV nsP3 is a target of USP10's DUB function. Hence, we examined the impact of a DUB-deficient USP10 mutant (C424A) on CHIKV and MAYV infection. Notably, our findings indicate that the DUB-inactive mutant maintained its ability to inhibit viral infection to a similar extent as wild-type USP10. Thus, we concluded that the deubiquitinating activity is not the primary mechanism for the antiviral effect of USP10.



Further, we investigated the relevance of G3BP-binding for the antiviral effect of USP10. Infection of cells heterologously expressing USP10 F10A, a G3BP binding-deficient mutant, displayed no significant reduction in viral infection rates. This finding demonstrates a critical role of the USP10-G3BP interaction in mediating the antiviral response. Both CHIKV and MAYV infection were significantly inhibited by wild-type USP10 overexpression, suggesting an antiviral effect on various alphaviruses. However, we noticed a subtle difference in the antiviral properties of the G3BP-binding deficient mutant (F10A) between CHIKV and MAYV. While the mutant displayed no antiviral effect against CHIKV, a slight infection reduction was observed in MAYV-infected cells. These findings suggest that, in addition to the G3BP-dependent antiviral properties, USP10 might utilize additional G3BP-independent mechanisms to restrict MAYV infection. To date, all functions of USP10 are attributed to either DUB activity or G3BP binding. Therefore, an antiviral effect that is based on a non-canonical function of USP10 remains to be investigated.

Building on the observation that the antiviral effect of USP10 is mediated via G3BP-binding, we further explored the impact of USP10 on the interplay between G3BP and CHIKV nsP3. Previous studies demonstrated that G3BP dynamically switches between its soluble and insoluble state, a balance maintained by interaction with USP10 and Caprin-1, respectively. Therefore, we hypothesized an effect of USP10 on SG condensation in the context of alphavirus infection (99,163). We investigated the role of USP10 in regulating SG formation during CHIKV infection via confocal microscopy. Our findings demonstrate that G3BP foci were robustly induced by CHIKV infection at four and eight h p.i., as well as in arsenite-treated cells. Interestingly, SG formation mainly occurred in eGFP-negative cells. The reporter gene is expressed under a subgenomic promoter, therefore eGFP signal is presumably absent in early infection stages. Due to the high virus inoculum (MOI of 5), the vast majority of cells can be assumed to be infected despite not having reached sufficient eGFP levels. This assumption is supported by a large fraction of cells being eGFP-positive 24 h p.i. (see Figure S 1). The absence of foci in eGFP-positive cells suggests an induction of SG formation at early stages post infection and a subsequent virus-mediated disassembly, a finding that has been previously reported during SINV infection (117).

At both early and late infection stages, the number of foci was significantly reduced in USP10 wild-type or USP10 C424A overexpressing cells, compared to the empty

## Discussion

---

vector. The F10A mutant, deficient in G3BP-binding, did not significantly reduce foci formation. Sodium arsenite-treated cells displayed the same pattern, indicating that the effect of USP10 on SG formation is independent of the stress inducer. The modulation of SG formation by USP10 observed through the reduction of G3BP-positive foci in USP10 overexpressing cells, aligns with previous studies demonstrating that USP10 maintains G3BP in its soluble state (99). The insoluble state of G3BP, formed by a network with mRNA-binding proteins, is crucial for SG condensation. Our data indicates that USP10 overexpression disrupts the formation of SGs during CHIKV infection. This disruption likely stems from USP10's sequestration of G3BP, preventing its aggregation into SGs (99). Interestingly, USP10 reduces viral infection despite facilitating the disassembly of SGs, a structure that is generally considered to be antiviral (176). We hypothesize that the disassembly of SGs by USP10 does not contribute to its antiviral nature but may rather be a side-effect of its efficient G3BP recruitment.

As the literature suggests, G3BP-containing foci do not exclusively represent *bona fide* SGs. Instead, G3BP and CHIKV-nsP3 form foci that differ from *bona fide* SGs in size, morphology and lack in composition of other key SG components (82). Typically, SG foci size ranges from 0.1 to 2.0  $\mu\text{m}$  in diameter (177). Accordingly, our microscopic analysis indicated that arsenite-induced foci measured  $\sim 2 \mu\text{m}$  in diameter. In contrast, foci induced by CHIKV infection measured  $\sim 5 \mu\text{m}$  in diameter at both time points. The larger foci size may indicate that the infection-induced condensates are not *bona fide* SGs. Manders' correlation coefficient (MCC) analysis revealed a moderate colocalization between G3BP and TIA-1 in the empty vector or USP10 F10A expressing cells upon cellular stress (arsenite or CHIKV infection). The signal correlation was markedly decreased in USP10 wild-type or C424A-expressing cells. This underlines that USP10 might disrupt the formation of *bona fide* SGs. We observed a minor reduction of aggregate co-localization from the early to late infection stage, which indicates a shift from *bona fide* SGs toward the formation of nsP3-G3BP complexes. Notably, the measured MCCs had a high variance between experiments, therefore these results are statistically not significant but rather mark a trend.

In conclusion, our study illustrates that USP10 potently inhibits the assembly of both *bona fide* SGs and other G3BP condensates. The effect is observed under both chemical SG induction and CHIKV infection at early and later stages, and mediated

through its interaction with G3BP. The previously described proviral role of G3BP in CHIKV replication provides a plausible pathway through which USP10 could act in an antiviral manner (82).

The role of SG formation upon alphavirus infection has been subject to multiple studies in the past. While SG assembly is induced early after infection, many viruses counteract SGs at later stages of infection (113). Three hypotheses for the inhibition mechanism have been discussed in the literature: (i) the hypervariable domain (HVD) of CHIKV nsP3 binds the pivotal SG initiation factors G3BP. The nsP3-G3BP complexes sequester the entire pool of G3BPs, thereby hindering SG development and indirectly promoting viral replication. (114,115) (ii) the macro domain of CHIKV nsP3 reduced ADP-ribosylation of G3BP1, resulting in the downregulating of SG formation. (116) (iii) SG formation is blocked by alphavirus-induced transcriptional and translational shutoffs, independent of the interaction with G3BP (117). Our findings provide another piece of the puzzle, by showing that USP10 inhibits SG formation in a G3BP-dependent mechanism. The disassembly of SGs by G3BP sequestration via the USP10 FGDF motif provides a plausible mechanism for the SG disassembly via the FGDF motif of alphaviral nsP3, favoring the first hypothesis.

In contrast to the antiviral effects observed during USP10 overexpression, the knock-out of endogenous *USP10* in HEK-293T cells displayed no significant effect on CHIKV infection. Instead, our findings demonstrated equal infection rates, as well as viral protein and RNA levels, between USP10 KO and parental cells. There are several possible explanations for this discrepancy:

(i) The absence of a detectable effect of the knock-out may indicate compensatory mechanisms for the loss of USP10, maintaining the defense against CHIKV infection. The ubiquitin-proteasome pathway is noted for considerable redundancy, with multiple enzymes targeting the same substrates (178,179). For example, the tumor suppressor p53 is a substrate of several DUBs, including USP10 (180). An analogous compensatory mechanism might exist for the interaction between USP10 and G3BP, possibly through alternative binding partners yet to be identified.

(ii) The antiviral mechanism could require a threshold level of USP10. Heterologous expression may allow to exceed the threshold, while physiological levels of USP10 in HEK-293T cells might be insufficient to exert a detectable antiviral effect. In this case,

## Discussion

---

the endogenous expression is geared more toward maintaining cellular homeostasis rather than mounting an antiviral response. The significant antiviral activity observed with USP10 overexpression might result from activating unexploited antiviral pathways, providing novel targets for antiviral strategies.

(iii) Considering the critical role of G3BP binding in mediating the antiviral effect of USP10, as detailed in previous chapters, a requisite USP10 level may need to be surpassed to bind and sequester G3BP effectively, hence exerting an antiviral effect.

In conclusion, the absence of a significant effect of the knock-out underscores the complex role of USP10 in the antiviral defense mechanism against CHIKV infection, rather than the initially anticipated model where USP10 serves as a straightforward antiviral factor. Mirroring the USP10-G3BP interaction could be an ideal approach for drug development, as it does not rely on the modulation of USP10 activity, which might interfere with maintaining cellular homeostasis.

Rational drug design often utilizes small molecules or peptidomimetics based on key protein sequences. To develop such therapeutics against CHIKV, we aimed to identify the minimal USP10 peptide sequence essential for its antiviral activity. Previously, the importance of phenylalanine at position 10 (F10) was established. To elucidate the role of other residues and required peptide length, we expressed four C-terminally truncated fragments of USP10 in eukaryotic cells. Only the largest peptide, encompassing the entire N-terminal domain of USP10, displayed moderate stability and antiviral properties. All other fragments exhibited minimal expression levels, indicating rapid degradation. Consequently, the antiviral effect of the smaller truncated USP10 peptides could not be assessed.

The rapid degradation of USP10 fragments, especially when truncated within the N-terminal domain, underlines the importance of the C-terminal domain of USP10 for its stability. While the previous experiments suggest that the antiviral properties of USP10 rely on G3BP binding, the instability of a minimal peptide chain complicates its use as a therapeutic agent. A more comprehensive approach to improving the metabolic stability via (macro-)cyclization, L to D amino acid substitution, or the incorporation of unnatural amino acids might be necessary for successful drug development (181).

### 4.3 Antiviral mechanisms of USP10 and viral evasion strategies

We explored the impact of heterologous USP10 expression on different stages of the viral replication cycle.

Infection with CHIKV gp-pseudotyped luciferase reporter lentiviruses revealed a modest decrease in luminescence in cells overexpressing wild-type USP10. The effect was absent in cells overexpressing the G3BP binding-deficient or DUB-inactive USP10 mutant. Notably, similar results were observed with VSV-G-pseudotyped particles. The consistency across different pseudotyped lentiviruses suggests that the decreased luminescence in wild-type USP10-overexpressing cells is attributable to an inhibition of post-entry steps rather than the CHIKV glycoprotein-mediated entry. Post-entry steps that might be inhibited by USP10 include reverse transcriptase, nuclear import, and integration. The absence of lentiviral inhibition in the USP10 mutants suggests that both the G3BP binding and DUB activity are crucial for the observed effect. Previous studies demonstrated that G3BP's cellular function is dependent on its ubiquitination status (182). Therefore, we hypothesize, that USP10 utilizes its G3BP-binding motif to recruit and efficiently deubiquitinate G3BP, leading to a reduction in pseudovirus transduction. It is important to note that the observed effect is distinct from USP10's antiviral function in the context of alphavirus infection, which we consistently observed to be independent of USP10's DUB activity.

We examined the effect of USP10 on viral replication and translation by employing a CHIKV replicon system. Interestingly, flow cytometry analysis 24 hours after replicon RNA transfection revealed no significant deviation in GFP-positive cell rates across cells overexpressing wild-type USP10, its mutants, or the empty vector control. This suggests that USP10 overexpression does not markedly influence CHIKV replication at the stage of RNA replication and protein translation. However, the lack of structural proteins in the replicon system limits the transferability of these results to the full virus context. Structural proteins in other viruses have been described to interfere with intracellular functions. For example, the nucleocapsid protein of SARS-CoV-2 was found to interfere with SG formation by sequestering G3BP (183). Similarly, the structural proteins of CHIKV might interact with G3BP or parts of the viral replication machinery, which are targeted by USP10.

## Discussion

---

Next, we assessed the impact of USP10 on the release of new virions. Western blot analysis showed reduced quantities of viral structural proteins (capsid and E2) intracellularly and in the supernatant of HEK-293T cells overexpressing wild-type USP10 or the DUB-deficient C424A mutant. This effect was not observed in cells expressing the G3BP binding-deficient F10A mutant. Similarly, qPCR analysis revealed a significant decrease of viral RNA in the supernatant of USP10 wild type and C424A cells compared to controls, while F10A cells showed a moderate reduction. These findings suggest that G3BP binding is essential for USP10's major antiviral effect, but there might be a minor, G3BP-independent mechanism affecting virion formation. However, titration of the infectious supernatant from cells overexpressing USP10 wild type or C424A, but not F10A, demonstrated a significant decrease in viral progeny.

These findings on viral entry, replication, and release collectively suggest that the antiviral capacity of USP10 is affecting predominantly the later stages of the viral replication cycle. The decreased viral titers in the supernatant of USP10 overexpressing cells in combination with the absence of an effect on the replicon, suggest that USP10 acts either on virion assembly, budding, or on translation of structural proteins which are not contained in the replicon system. The observed decrease of intracellular levels of E2 and C after USP10 overexpression hints at inhibition of translation of the structural proteins. This is in line with previous studies, showing that G3BP supports viral replication and translation in the context of SFV (83). As an alternative hypothesis, USP10 might interfere with virion assembly and budding. Since the protein levels are measured at 48 h p.i. the reduction of intracellular structural protein levels is potentially an effect of previous rounds of viral replication with decreased virion release. The markedly stronger reduction in viral protein levels after USP10 overexpression in the supernatant, compared to cellular levels, supports the hypothesis that USP10 interferes with particle formation or budding. The observed antiviral effect of USP10 is independent of the protein's DUB activity. Additionally, we hypothesize that USP10 mediates a G3BP binding- and DUB-dependent anti-lentiviral effect, that is distinct from its antiviral role in alphavirus infection.

Most alphaviruses harbor one or two G3BP-binding motifs, similar to the FGDF motif in USP10. A comparative analysis by Nowee et al. demonstrated the presence of one or two FGDF motifs in the nsP3-HVD of 16 out of 20 studied alphaviruses (115). A

conserved FGDF motif was found in all studied Old World alphaviruses including two insect-specific viruses, and some New World alphaviruses, such as MAYV. Notably, the encephalitic alphaviruses of the (V/W/E)EEV complex seemed to follow a different evolutionary path. These viruses do not harbor an FGDF motif and either bind G3BP through an alternative binding site or, in the case of VEEV, completely lack interaction with G3BP (115).

We assessed how CHIKV nsP3 mutants, impaired in their ability to bind G3BP, impact viral dynamics and USP10-mediated antiviral responses. Notably, a double mutant with phenylalanine-to-alanine substitutions in both FGDF motifs (CHIKV ORF1 F1812A+F1830A) was not replication-competent in cell culture. Single mutations of either FGDF motif displayed viral activity at varying levels, with the F1812A mutation showing limited CPE and eGFP signal, while the F1830A mutation exhibited a much higher level of both. These findings align with previous studies on the FGDF motifs in the context of the SFV virus, demonstrating that single mutations of the motif lead to viable viruses with limited G3BP-binding abilities, while a double mutation strongly attenuated viral growth (120,184). Accordingly, a double-mutated CHIKV *trans*-replicase with mutations in both FGDF motifs (F1812A and F1830A) resulted in nearly a total loss of replication and transcription (84). Further, they found a 29-amino acid deletion which created a novel FGDF motif in the double mutant at 72 h p.i., leading to a restoration of viral replication. These observations suggest a critical role of G3BP binding in CHIKV replication. We postulate the FGDF motif to be of major importance for G3BP binding, while the second motif plays a minor role. However, single mutations in each motif can be compensated by the remaining G3BP-binding site, to a varying extent. The complete lack of G3BP binding, as in the double mutant, renders the virus replication defective. Further, heterologous USP10 expression in HEK-293T cells did not significantly impact the infection rates of CHIKV mutants with attenuated G3BP-binding abilities. These findings indicate that USP10's inhibition of CHIKV relies on the intact interaction between nsP3 and G3BP. This is in line with our hypothesis, that the antiviral effect of USP10 is due to binding and sequestration of G3BP, thereby making it inaccessible for CHIKV nsP3. The role of G3BP in the context of alphavirus infection has been the subject of research in various studies in the past decade, with evidence for proviral and antiviral roles (82–84,122). The here presented findings emphasize the importance of G3BP as a proviral factor for CHIKV.

## Discussion

---

Congruently, we explored the potential for CHIKV to develop escape mutations against the antiviral activity of USP10, by employing serial passaging of eGFP-CHIKV under selective pressure exerted by USP10 overexpression. An initial decrease in viral infection was observed in USP10-overexpressing cells, in accordance with previous results. To minimize the risk of complete viral elimination after ten passages, the cells were transfected with significantly less USP10 plasmid, compared to previous experiments. As anticipated, this resulted in a less pronounced antiviral effect, compared to overexpression with higher amounts of USP10. The loss of the antiviral effect of USP10 after several passages could indicate the emergence of escape variants. Since the viral titer in the supernatant used for inoculation of passages two to ten was not determined, a direct comparison of infection rates between USP10 WT and F10A is not feasible. Moreover, a rapid decrease in eGFP-positive cells was observed in most samples, suggesting mutations in the eGFP reporter cassette. In fact, the number of mapped reads is starkly decreased in the genomic region of eGFP compared to the rest of the viral genome in 5 out of 6 samples, suggesting deletions in the eGFP-encoding cassette. Since expressing eGFP imposes an additional and non-essential burden on the virus, mutations deleting the cassette are advantageous for viral fitness. However, the presence of viral RNA in all ten passages confirms ongoing viral replication despite USP10 overexpression.

NGS analysis revealed mutations in the viral genome after ten passages. These mutations were restricted to three proteins: nsP2, capsid (C), and envelope protein E2. Notably, mutations specific to USP10 wild type overexpression were identified only in nsP2 and E2, suggesting a potential escape mechanism mediated by these proteins. While the detected mutations are not directly related to G3BP-binding in nsP3, their emergence might indicate an alternative pathway for evading USP10's effects.

In a study by Götte et al., the sensitivity of alphaviruses to G3BP knock-out has been determined to depend on a single arginine residue close to the nsP1-nsP2 cleavage site (nsP1 532R) (84), a position previously described to influence nsP1-nsP2 processing efficiency (185). Functionally, the sequestration of G3BP by USP10 overexpression likely has a comparable outcome to a knock-out of G3BP. Since the viral dependence on G3BP is related to the nsP2-mediated cleavage of nsP1 and nsP2, it is conceivable that the nsP2 mutations we detected after ten passages, D420G and N643K, modulate nsP2's protease activity, thereby exerting a partial G3BP



independence. Further, nsP2 has been found in complexes with G3BP, hinting at a direct interaction, which might be augmented by the observed mutations (186). In accordance, the recruitment of G3BP by nsP2, modified with an artificial FGDF motif, has been shown to enhance viral replication (187). To our knowledge, there are no studies indicating a modulation of the host cell by E2. However, it is known in other viruses that structural proteins also play a role in modulating the stress response. For instance, SARS-CoV-2 nucleocapsid disrupts SG formation by G3BP binding (183). Similarly, the mutations in E2 might target an unknown function of the glycoprotein.

In summary, the research conducted for this thesis establishes USP10 as a potent inhibitor of alphavirus infection by disrupting the G3BP-nsP3 interaction. Targeting the G3BP-nsP3 interaction analogously to USP10 offers a promising approach for the development of novel antiviral strategies.

## References

1. Costa LB, Barreto FKDA, Barreto MCA, Santos THPD, Andrade MDMOD, Farias LABG, et al. Epidemiology and Economic Burden of Chikungunya: A Systematic Literature Review. *Trop Med Infect Dis*. 2023 May 31;8(6):301.
2. Caicedo EY, Charniga K, Rueda A, Dorigatti I, Mendez Y, Hamlet A, et al. The epidemiology of Mayaro virus in the Americas: A systematic review and key parameter estimates for outbreak modelling. Corrales-Aguilar E, editor. *PLoS Negl Trop Dis*. 2021 Jun 3;15(6):e0009418.
3. Mehand MS, Al-Shorbaji F, Millett P, Murgue B. The WHO R&D Blueprint: 2018 review of emerging infectious diseases requiring urgent research and development efforts. *Antiviral Res*. 2018 Nov;159:63–7.
4. Cunha RVD, Trinta KS. Chikungunya virus: clinical aspects and treatment - A Review. *Mem Inst Oswaldo Cruz*. 2017 Aug;112(8):523–31.
5. Robinson MC. An epidemic of virus disease in Southern Province, Tanganyika territory, in 1952–1953. *Trans R Soc Trop Med Hyg*. 1955 Jan;49(1):28–32.
6. Lumsden WHR. An epidemic of virus disease in Southern Province, Tanganyika territory, in 1952–1953 II. General description and epidemiology. *Trans R Soc Trop Med Hyg*. 1955 Jan;49(1):33–57.
7. Chikungunya [Internet]. [cited 2024 Feb 14]. Available from: <https://www.who.int/health-topics/chikungunya>
8. World Health Organization. Global vector control response 2017-2030 [Internet]. Geneva: World Health Organization; 2017 [cited 2023 Mar 20]. 51 p. Available from: <https://apps.who.int/iris/handle/10665/259205>
9. Powers AM, Brault AC, Tesh RB, Weaver SC. Re-emergence of chikungunya and o'nyong-nyong viruses: evidence for distinct geographical lineages and distant evolutionary relationships. *Microbiology*. 2000 Feb 1;81(2):471–9.
10. Cassadou S, Boucau S, Petit-Sinturel M, Huc P, Leparç-Goffart I, Ledrans M. Emergence of chikungunya fever on the French side of Saint Martin island, October to December 2013. *Eurosurveillance* [Internet]. 2014 Apr 3 [cited 2024 Feb 14];19(13). Available from: <https://www.eurosurveillance.org/content/10.2807/1560-7917.ES2014.19.13.20752>
11. Van Bortel W, Dorleans F, Rosine J, Blateau A, Rousset D, Matheus S, et al. Chikungunya outbreak in the Caribbean region, December 2013 to March 2014, and the significance for Europe. *Eurosurveillance* [Internet]. 2014 Apr 3 [cited 2024 Feb 14];19(13). Available from: <https://www.eurosurveillance.org/content/10.2807/1560-7917.ES2014.19.13.20759>
12. Schuffenecker I, Iteman I, Michault A, Murri S, Frangeul L, Vaney MC, et al. Genome Microevolution of Chikungunya Viruses Causing the Indian Ocean Outbreak. *PLoS Med*. 2006 May 23;3(7):e263.

13. Tsetsarkin KA, Vanlandingham DL, McGee CE, Higgs S. A Single Mutation in Chikungunya Virus Affects Vector Specificity and Epidemic Potential. Holmes EC, editor. *PLoS Pathog.* 2007 Dec 7;3(12):e201.
14. De Oliveira EC, Fonseca V, Xavier J, Adelino T, Morales Claro I, Fabri A, et al. Short report: Introduction of chikungunya virus ECSA genotype into the Brazilian Midwest and its dispersion through the Americas. Forshey BM, editor. *PLoS Negl Trop Dis.* 2021 Apr 16;15(4):e0009290.
15. Reyna RA, Weaver SC. Sequelae and Animal Modeling of Encephalitic Alphavirus Infections. *Viruses.* 2023 Jan 28;15(2):382.
16. Kolimenakis A, Heinz S, Wilson ML, Winkler V, Yakob L, Michaelakis A, et al. The role of urbanisation in the spread of Aedes mosquitoes and the diseases they transmit—A systematic review. Kittayapong P, editor. *PLoS Negl Trop Dis.* 2021 Sep 9;15(9):e0009631.
17. Rezza G, Weaver SC. Chikungunya as a paradigm for emerging viral diseases: Evaluating disease impact and hurdles to vaccine development. Diemert DJ, editor. *PLoS Negl Trop Dis.* 2019 Jan 17;13(1):e0006919.
18. NCBI Virus [Internet]. [cited 2024 May 9]. Available from: [https://www.ncbi.nlm.nih.gov/labs/virus/vssi/#/virus?SeqType\\_s=Nucleotide&VirusLineage\\_ss=Chikungunya%20virus,%20taxid:37124](https://www.ncbi.nlm.nih.gov/labs/virus/vssi/#/virus?SeqType_s=Nucleotide&VirusLineage_ss=Chikungunya%20virus,%20taxid:37124)
19. Letunic I, Bork P. Interactive Tree of Life (iTOL) v6: recent updates to the phylogenetic tree display and annotation tool. *Nucleic Acids Res.* 2024 Apr 13;gkae268.
20. Moloney RM, Kmush B, Rudolph KE, Cummings DAT, Lessler J. Incubation Periods of Mosquito-Borne Viral Infections: A Systematic Review. *Am J Trop Med Hyg.* 2014 May 7;90(5):882–91.
21. Gordon A, Gresh L, Ojeda S, Chowell G, Gonzalez K, Sanchez N, et al. Differences in Transmission and Disease Severity Between 2 Successive Waves of Chikungunya. *Clin Infect Dis.* 2018 Nov 13;67(11):1760–7.
22. Suhrbier A. Rheumatic manifestations of chikungunya: emerging concepts and interventions. *Nat Rev Rheumatol.* 2019 Oct;15(10):597–611.
23. Matusali G, Colavita F, Bordi L, Lalle E, Ippolito G, Capobianchi M, et al. Tropism of the Chikungunya Virus. *Viruses.* 2019 Feb 20;11(2):175.
24. Diagnostic Testing | Chikungunya virus | CDC [Internet]. 2023 [cited 2024 Feb 14]. Available from: <https://www.cdc.gov/chikungunya/hc/diagnostic.html>
25. Natrajan MS, Rojas A, Waggoner JJ. Beyond Fever and Pain: Diagnostic Methods for Chikungunya Virus. Kraft CS, editor. *J Clin Microbiol.* 2019 Jun;57(6):e00350-19.
26. Ly H. Ixchiq (VLA1553): The first FDA-approved vaccine to prevent disease caused by Chikungunya virus infection. *Virulence.* 2024 Dec 31;15(1):2301573.

## Discussion

---

27. Wressnigg N, Hochreiter R, Zoihs O, Fritzer A, Bézay N, Klingler A, et al. Single-shot live-attenuated chikungunya vaccine in healthy adults: a phase 1, randomised controlled trial. *Lancet Infect Dis.* 2020 Oct;20(10):1193–203.
28. Schneider M, Narciso-Abraham M, Hadl S, McMahon R, Toepfer S, Fuchs U, et al. Safety and immunogenicity of a single-shot live-attenuated chikungunya vaccine: a double-blind, multicentre, randomised, placebo-controlled, phase 3 trial. *The Lancet.* 2023 Jun;401(10394):2138–47.
29. Zhu FC, Guan XH, Li YH, Huang JY, Jiang T, Hou LH, et al. Immunogenicity and safety of a recombinant adenovirus type-5-vectored COVID-19 vaccine in healthy adults aged 18 years or older: a randomised, double-blind, placebo-controlled, phase 2 trial. *The Lancet.* 2020 Aug;396(10249):479–88.
30. Voysey M, Clemens SAC, Madhi SA, Weckx LY, Folegatti PM, Aley PK, et al. Safety and efficacy of the ChAdOx1 nCoV-19 vaccine (AZD1222) against SARS-CoV-2: an interim analysis of four randomised controlled trials in Brazil, South Africa, and the UK. *The Lancet.* 2021 Jan;397(10269):99–111.
31. Sadoff J, Gray G, Vandebosch A, Cárdenas V, Shukarev G, Grinsztejn B, et al. Safety and Efficacy of Single-Dose Ad26.COV2.S Vaccine against Covid-19. *N Engl J Med.* 2021 Jun 10;384(23):2187–201.
32. Logunov DY, Dolzhikova IV, Shcheblyakov DV, Tukhvatulin AI, Zubkova OV, Dzharullaeva AS, et al. Safety and efficacy of an rAd26 and rAd5 vector-based heterologous prime-boost COVID-19 vaccine: an interim analysis of a randomised controlled phase 3 trial in Russia. *The Lancet.* 2021 Feb;397(10275):671–81.
33. Volkmann A, Williamson AL, Weidenthaler H, Meyer TPH, Robertson JS, Excler JL, et al. The Brighton Collaboration standardized template for collection of key information for risk/benefit assessment of a Modified Vaccinia Ankara (MVA) vaccine platform. *Vaccine.* 2021 May;39(22):3067–80.
34. Reisinger EC, Tschismarov R, Beubler E, Wiedermann U, Firbas C, Loebermann M, et al. Immunogenicity, safety, and tolerability of the measles-vectored chikungunya virus vaccine MV-CHIK: a double-blind, randomised, placebo-controlled and active-controlled phase 2 trial. *The Lancet.* 2018 Dec;392(10165):2718–27.
35. Sun S, Xiang Y, Akahata W, Holdaway H, Pal P, Zhang X, et al. Structural analyses at pseudo atomic resolution of Chikungunya virus and antibodies show mechanisms of neutralization. *eLife.* 2013 Apr 2;2:e00435.
36. Tiwari M, Parida M, Santhosh SR, Khan M, Dash PK, Rao PVL. Assessment of immunogenic potential of Vero adapted formalin inactivated vaccine derived from novel ECSA genotype of Chikungunya virus. *Vaccine.* 2009 Apr;27(18):2513–22.
37. Huang Z, Zhang Y, Li H, Zhu J, Song W, Chen K, et al. Vaccine development for mosquito-borne viral diseases. *Front Immunol.* 2023 May 12;14:1161149.

38. Tretyakova I, Hearn J, Wang E, Weaver S, Pushko P. DNA Vaccine Initiates Replication of Live Attenuated Chikungunya Virus In Vitro and Elicits Protective Immune Response in Mice. *J Infect Dis.* 2014 Jun 15;209(12):1882–90.
39. Muthumani K, Block P, Flingai S, Muruganantham N, Chaaithanya IK, Tingey C, et al. Rapid and Long-Term Immunity Elicited by DNA-Encoded Antibody Prophylaxis and DNA Vaccination Against Chikungunya Virus. *J Infect Dis.* 2016 Aug 1;214(3):369–78.
40. Shaw C, Panther L, August A, Zaks T, Smolenov I, Bart S, et al. Safety and immunogenicity of a mRNA-based chikungunya vaccine in a phase 1 dose-ranging trial. *Int J Infect Dis.* 2019 Feb;79:17.
41. Mukhopadhyay S, Zhang W, Gabler S, Chipman PR, Strauss EG, Strauss JH, et al. Mapping the Structure and Function of the E1 and E2 Glycoproteins in Alphaviruses. *Structure.* 2006 Jan;14(1):63–73.
42. Voss JE, Vaney MC, Duquerroy S, Vonnrhein C, Girard-Blanc C, Crublet E, et al. Glycoprotein organization of Chikungunya virus particles revealed by X-ray crystallography. *Nature.* 2010 Dec;468(7324):709–12.
43. Khan AH, Morita K, Parquet MDC, Hasebe F, Mathenge EGM, Igarashi A. Complete nucleotide sequence of chikungunya virus and evidence for an internal polyadenylation site. *J Gen Virol.* 2002 Dec 1;83(12):3075–84.
44. Hyde JL, Chen R, Trobaugh DW, Diamond MS, Weaver SC, Klimstra WB, et al. The 5' and 3' ends of alphavirus RNAs – Non-coding is not non-functional. *Virus Res.* 2015 Aug;206:99–107.
45. Hardy WR, Strauss JH. Processing the nonstructural polyproteins of sindbis virus: nonstructural proteinase is in the C-terminal half of nsP2 and functions both in cis and in trans. *J Virol.* 1989 Nov;63(11):4653–64.
46. De Groot RJ, Hardy WR, Shirako Y, Strauss JH. Cleavage-site preferences of Sindbis virus polyproteins containing the non-structural proteinase. Evidence for temporal regulation of polyprotein processing in vivo. *EMBO J.* 1990 Aug;9(8):2631–8.
47. Ahola T, Kääriäinen L. Reaction in alphavirus mRNA capping: formation of a covalent complex of nonstructural protein nsP1 with 7-methyl-GMP. *Proc Natl Acad Sci.* 1995 Jan 17;92(2):507–11.
48. Zhang K, Law MCY, Nguyen TM, Tan YB, Wirawan M, Law YS, et al. Molecular basis of specific viral RNA recognition and 5'-end capping by the Chikungunya virus nsP1. *Cell Rep.* 2022 Jul;40(4):111133.
49. Vasiljeva L, Merits A, Auvinen P, Kääriäinen L. Identification of a Novel Function of the Alphavirus Capping Apparatus. *J Biol Chem.* 2000 Jun;275(23):17281–7.

## Discussion

---

50. Rikkonen M, Peränen J, Kääriäinen L. ATPase and GTPase activities associated with Semliki Forest virus nonstructural protein nsP2. *J Virol.* 1994 Sep;68(9):5804–10.
51. Gomez De Cedrón M, Ehsani N, Mikkola ML, García JA, Kääriäinen L. RNA helicase activity of Semliki Forest virus replicase protein NSP2. *FEBS Lett.* 1999 Apr 2;448(1):19–22.
52. Vasiljeva L, Valmu L, Kääriäinen L, Merits A. Site-specific Protease Activity of the Carboxyl-terminal Domain of Semliki Forest Virus Replicase Protein nsP2. *J Biol Chem.* 2001 Aug;276(33):30786–93.
53. McPherson RL, Abraham R, Sreekumar E, Ong SE, Cheng SJ, Baxter VK, et al. ADP-ribosylhydrolase activity of Chikungunya virus macrodomain is critical for virus replication and virulence. *Proc Natl Acad Sci.* 2017 Feb 14;114(7):1666–71.
54. Barton DJ, Sawicki SG, Sawicki DL. Demonstration in vitro of temperature-sensitive elongation of RNA in Sindbis virus mutant ts6. *J Virol.* 1988 Oct;62(10):3597–602.
55. Rubach JK, Wasik BR, Rupp JC, Kuhn RJ, Hardy RW, Smith JL. Characterization of purified Sindbis virus nsP4 RNA-dependent RNA polymerase activity in vitro. *Virology.* 2009 Feb;384(1):201–8.
56. Uchime O, Fields W, Kielian M. The Role of E3 in pH Protection during Alphavirus Assembly and Exit. *J Virol.* 2013 Sep 15;87(18):10255–62.
57. Snyder AJ, Mukhopadhyay S. The Alphavirus E3 Glycoprotein Functions in a Clade-Specific Manner. *J Virol.* 2012 Dec 15;86(24):13609–20.
58. Firth AE, Chung BY, Fleeton MN, Atkins JF. Discovery of frameshifting in Alphavirus 6K resolves a 20-year enigma. *Virol J.* 2008;5(1):108.
59. Ramsey J, Mukhopadhyay S. Disentangling the Frames, the State of Research on the Alphavirus 6K and TF Proteins. *Viruses.* 2017 Aug 18;9(8):228.
60. Cross RK. Identification of a unique guanine-7-methyltransferase in Semliki forest virus (SFV) infected cell extracts. *Virology.* 1983 Oct;130(2):452–63.
61. Spuul P, Salonen A, Merits A, Jokitalo E, Kääriäinen L, Ahola T. Role of the Amphipathic Peptide of Semliki Forest Virus Replicase Protein nsP1 in Membrane Association and Virus Replication. *J Virol.* 2007 Jan 15;81(2):872–83.
62. Weiss B, Geigenmüller-Gnirke U, Schlesinger S. Interactions between Sindbis virus RNAs and a 68 amino acid derivative of the viral capsid protein further defines the capsid binding site. *Nucleic Acids Res.* 1994;22(5):780–6.
63. Choi HK, Tong L, Minor W, Dumas P, Boege U, Rossmann MG, et al. Structure of Sindbis virus core protein reveals a chymotrypsin-like serine proteinase and the organization of the virion. *Nature.* 1991 Nov 7;354(6348):37–43.

64. Lobigs M, Zhao HX, Garoff H. Function of Semliki Forest virus E3 peptide in virus assembly: replacement of E3 with an artificial signal peptide abolishes spike heterodimerization and surface expression of E1. *J Virol.* 1990 Sep;64(9):4346–55.
65. Smith TJ, Cheng RH, Olson NH, Peterson P, Chase E, Kuhn RJ, et al. Putative receptor binding sites on alphaviruses as visualized by cryoelectron microscopy. *Proc Natl Acad Sci.* 1995 Nov 7;92(23):10648–52.
66. Lusa S, Garoff H, Lieström P. Fate of the 6K membrane protein of semliki forest virus during virus assembly. *Virology.* 1991 Dec;185(2):843–6.
67. Snyder JE, Kulcsar KA, Schultz KLW, Riley CP, Neary JT, Marr S, et al. Functional Characterization of the Alphavirus TF Protein. *J Virol.* 2013 Aug;87(15):8511–23.
68. Wahlberg JM, Bron R, Wilschut J, Garoff H. Membrane fusion of Semliki Forest virus involves homotrimers of the fusion protein. *J Virol.* 1992 Dec;66(12):7309–18.
69. Gibbons DL, Ahn A, Chatterjee PK, Kielian M. Formation and Characterization of the Trimeric Form of the Fusion Protein of Semliki Forest Virus. *J Virol.* 2000 Sep;74(17):7772–80.
70. Wintachai P, Wikan N, Kuadkitkan A, Jaimipuk T, Ubol S, Pulmanausahakul R, et al. Identification of prohibitin as a Chikungunya virus receptor protein. *J Med Virol.* 2012 Nov;84(11):1757–70.
71. Zhang R, Kim AS, Fox JM, Nair S, Basore K, Klimstra WB, et al. Mxra8 is a receptor for multiple arthritogenic alphaviruses. *Nature.* 2018 May;557(7706):570–4.
72. Reyes Ballista JM, Miazgowiec KL, Acciani MD, Jimenez AR, Belloli RS, Havranek KE, et al. Chikungunya virus entry and infectivity is primarily facilitated through cell line dependent attachment factors in mammalian and mosquito cells. *Front Cell Dev Biol.* 2023 Jan 20;11:1085913.
73. Fongsaran C, Jirakanwisal K, Kuadkitkan A, Wikan N, Wintachai P, Thepparit C, et al. Involvement of ATP synthase  $\beta$  subunit in chikungunya virus entry into insect cells. *Arch Virol.* 2014 Dec;159(12):3353–64.
74. Chain MMT, Doane FW, McLean DM. MORPHOLOGICAL DEVELOPMENT OF CHIKUNGUNYA VIRUS. *Can J Microbiol.* 1966 Oct 1;12(5):895–900.
75. Abraham R, Hauer D, McPherson RL, Utt A, Kirby IT, Cohen MS, et al. ADP-ribosyl-binding and hydrolase activities of the alphavirus nsP3 macrodomain are critical for initiation of virus replication. *Proc Natl Acad Sci U S A.* 2018 Oct 30;115(44):E10457–66.
76. Gao Y, Goonawardane N, Ward J, Tuplin A, Harris M. Multiple roles of the non-structural protein 3 (nsP3) alphavirus unique domain (AUD) during Chikungunya virus genome replication and transcription. Kuhn RJ, editor. *PLOS Pathog.* 2019 Jan 22;15(1):e1007239.

## Discussion

---

77. Götte B, Liu L, McInerney G. The Enigmatic Alphavirus Non-Structural Protein 3 (nsP3) Revealing Its Secrets at Last. *Viruses*. 2018 Feb 28;10(3):105.
78. Meertens L, Hafirassou ML, Couderc T, Bonnet-Madin L, Kril V, Kümmerer BM, et al. FHL1 is a major host factor for chikungunya virus infection. *Nature*. 2019 Oct 10;574(7777):259–63.
79. Meertens L, Hafirassou ML, Couderc T, Bonnet-Madin L, Kril V, Kümmerer BM, et al. FHL1 is a key player of chikungunya virus tropism and pathogenesis. *C R Biol*. 2021 Apr 21;343(4):79–89.
80. Kim DY, Reynaud JM, Rasaloukaya A, Akhrymuk I, Mobley JA, Frolov I, et al. New World and Old World Alphaviruses Have Evolved to Exploit Different Components of Stress Granules, FXR and G3BP Proteins, for Assembly of Viral Replication Complexes. Heise MT, editor. *PLOS Pathog*. 2016 Aug 10;12(8):e1005810.
81. Frolov I, Kim DY, Akhrymuk M, Mobley JA, Frolova EI. Hypervariable Domain of Eastern Equine Encephalitis Virus nsP3 Redundantly Utilizes Multiple Cellular Proteins for Replication Complex Assembly. Perlman S, editor. *J Virol*. 2017 Jul 15;91(14):e00371-17.
82. Scholte FEM, Tas A, Albulescu IC, Žusinaite E, Merits A, Snijder EJ, et al. Stress Granule Components G3BP1 and G3BP2 Play a Proviral Role Early in Chikungunya Virus Replication. Diamond MS, editor. *J Virol*. 2015 Apr 15;89(8):4457–69.
83. Götte B, Panas MD, Hellström K, Liu L, Samreen B, Larsson O, et al. Separate domains of G3BP promote efficient clustering of alphavirus replication complexes and recruitment of the translation initiation machinery. Heise MT, editor. *PLOS Pathog*. 2019 Jun 14;15(6):e1007842.
84. Götte B, Utt A, Fragkoudis R, Merits A, McInerney GM. Sensitivity of Alphaviruses to G3BP Deletion Correlates with Efficiency of Replicase Polyprotein Processing. Heise MT, editor. *J Virol*. 2020 Mar 17;94(7):e01681-19.
85. Nelemans T, Kikkert M. Viral Innate Immune Evasion and the Pathogenesis of Emerging RNA Virus Infections. *Viruses*. 2019 Oct 18;11(10):961.
86. Jensen S, Thomsen AR. Sensing of RNA Viruses: a Review of Innate Immune Receptors Involved in Recognizing RNA Virus Invasion. *J Virol*. 2012 Mar 15;86(6):2900–10.
87. Neighbours LM, Long K, Whitmore AC, Heise MT. Myd88-Dependent Toll-Like Receptor 7 Signaling Mediates Protection from Severe Ross River Virus-Induced Disease in Mice. *J Virol*. 2012 Oct;86(19):10675–85.
88. Akhrymuk I, Frolov I, Frolova EI. Both RIG-I and MDA5 detect alphavirus replication in concentration-dependent mode. *Virology*. 2016 Jan;487:230–41.



89. Sanchez David RY, Combredet C, Sismeiro O, Dillies MA, Jagla B, Coppée JY, et al. Comparative analysis of viral RNA signatures on different RIG-I-like receptors. *eLife*. 2016 Mar 24;5:e11275.
90. De Andrade Vieira Alves F, Nunes PCG, Arruda LV, Salomão NG, Rabelo K. The Innate Immune Response in DENV- and CHIKV-Infected Placentas and the Consequences for the Fetuses: A Minireview. *Viruses*. 2023 Sep 6;15(9):1885.
91. Schoggins JW, Rice CM. Interferon-stimulated genes and their antiviral effector functions. *Curr Opin Virol*. 2011 Dec;1(6):519–25.
92. Schoggins JW, Wilson SJ, Panis M, Murphy MY, Jones CT, Bieniasz P, et al. A diverse range of gene products are effectors of the type I interferon antiviral response. *Nature*. 2011 Apr 28;472(7344):481–5.
93. Schmidt-Supprian M, Courtois G, Tian J, Coyle AJ, Israël A, Rajewsky K, et al. Mature T Cells Depend on Signaling through the IKK Complex. *Immunity*. 2003 Sep;19(3):377–89.
94. Taniguchi K, Karin M. NF- $\kappa$ B, inflammation, immunity and cancer: coming of age. *Nat Rev Immunol*. 2018 May;18(5):309–24.
95. Panas MD, Ivanov P, Anderson P. Mechanistic insights into mammalian stress granule dynamics. *J Cell Biol*. 2016 Nov 7;215(3):313–23.
96. Anderson P, Kedersha N. RNA granules. *J Cell Biol*. 2006 Mar 13;172(6):803–8.
97. Kim WJ, Kim JH, Jang SK. Anti-inflammatory lipid mediator 15d-PGJ2 inhibits translation through inactivation of eIF4A. *EMBO J*. 2007 Dec 12;26(24):5020–32.
98. Fros J, Pijlman G. Alphavirus Infection: Host Cell Shut-Off and Inhibition of Antiviral Responses. *Viruses*. 2016 Jun 11;8(6):166.
99. Kedersha N, Panas MD, Achorn CA, Lyons S, Tisdale S, Hickman T, et al. G3BP–Caprin1–USP10 complexes mediate stress granule condensation and associate with 40S subunits. *J Cell Biol*. 2016 Mar 28;212(7):e201508028.
100. Li J, Zhang Y, Chen X, Ma L, Li P, Yu H. Protein phase separation and its role in chromatin organization and diseases. *Biomed Pharmacother*. 2021 Jun;138:111520.
101. Cirillo L, Cieren A, Barbieri S, Khong A, Schwager F, Parker R, et al. UBAP2L Forms Distinct Cores that Act in Nucleating Stress Granules Upstream of G3BP1. *Curr Biol*. 2020 Feb;30(4):698-707.e6.
102. Matheny T, Van Treeck B, Huynh TN, Parker R. RNA partitioning into stress granules is based on the summation of multiple interactions. *RNA*. 2021 Feb;27(2):174–89.

## Discussion

---

103. Ozeki K, Sugiyama M, Akter KA, Nishiwaki K, Asano-Inami E, Senga T. FAM98A is localized to stress granules and associates with multiple stress granule-localized proteins. *Mol Cell Biochem.* 2019 Jan;451(1–2):107–15.
104. Kedersha N, Cho MR, Li W, Yacono PW, Chen S, Gilks N, et al. Dynamic Shuttling of Tia-1 Accompanies the Recruitment of mRNA to Mammalian Stress Granules. *J Cell Biol.* 2000 Dec 11;151(6):1257–68.
105. Nonhoff U, Ralser M, Welzel F, Piccini I, Balzereit D, Yaspo ML, et al. Ataxin-2 Interacts with the DEAD/H-Box RNA Helicase DDX6 and Interferes with P-Bodies and Stress Granules. Weissman J, editor. *Mol Biol Cell.* 2007 Apr;18(4):1385–96.
106. Li L, Garg M, Wang Y, Wang W, Godbout R. DEAD box 1 (DDX1) protein binds to and protects cytoplasmic stress response mRNAs in cells exposed to oxidative stress. *J Biol Chem.* 2022 Aug;298(8):102180.
107. Tourrière H, Chebli K, Zekri L, Courselaud B, Blanchard JM, Bertrand E, et al. The RasGAP-associated endoribonuclease G3BP mediates stress granule assembly. *J Cell Biol.* 2023 Nov 6;222(11):e200212128072023new.
108. Matsuki H, Takahashi M, Higuchi M, Makokha GN, Oie M, Fujii M. Both G3BP1 and G3BP2 contribute to stress granule formation. *Genes Cells.* 2013 Feb;18(2):135–46.
109. Law LMJ, Razooky BS, Li MMH, You S, Jurado A, Rice CM, et al. ZAP's stress granule localization is correlated with its antiviral activity and induced by virus replication. Randall G, editor. *PLOS Pathog.* 2019 May 22;15(5):e1007798.
110. Onomoto K, Jogi M, Yoo JS, Narita R, Morimoto S, Takemura A, et al. Critical Role of an Antiviral Stress Granule Containing RIG-I and PKR in Viral Detection and Innate Immunity. Kanai A, editor. *PLoS ONE.* 2012 Aug 13;7(8):e43031.
111. Luo L, Li Z, Zhao T, Ju X, Ma P, Jin B, et al. SARS-CoV-2 nucleocapsid protein phase separates with G3BPs to disassemble stress granules and facilitate viral production. *Sci Bull.* 2021 Jun;66(12):1194–204.
112. Liu H, Bai Y, Zhang X, Gao T, Liu Y, Li E, et al. SARS-CoV-2 N Protein Antagonizes Stress Granule Assembly and IFN Production by Interacting with G3BPs to Facilitate Viral Replication. Subbarao K, editor. *J Virol.* 2022 Jun 22;96(12):e00412-22.
113. Yang P, Mathieu C, Kolaitis RM, Zhang P, Messing J, Yurtsever U, et al. G3BP1 Is a Tunable Switch that Triggers Phase Separation to Assemble Stress Granules. *Cell.* 2020 Apr;181(2):325-345.e28.
114. Panas MD, Varjak M, Lulla A, Er Eng K, Merits A, Karlsson Hedestam GB, et al. Sequestration of G3BP coupled with efficient translation inhibits stress granules in Semliki Forest virus infection. Wolin S, editor. *Mol Biol Cell.* 2012 Dec 15;23(24):4701–12.

115. Nowee G, Bakker JW, Geertsema C, Ros VID, Göertz GP, Fros JJ, et al. A Tale of 20 Alphaviruses; Inter-species Diversity and Conserved Interactions Between Viral Non-structural Protein 3 and Stress Granule Proteins. *Front Cell Dev Biol.* 2021 Feb 11;9:625711.
116. Jayabalan AK, Adivarahan S, Koppula A, Abraham R, Batish M, Zenklusen D, et al. Stress granule formation, disassembly, and composition are regulated by alphavirus ADP-ribosylhydrolase activity. *Proc Natl Acad Sci.* 2021 Feb 9;118(6):e2021719118.
117. Frolova EI, Palchevska O, Dominguez F, Frolov I. Alphavirus-induced transcriptional and translational shutoffs play major roles in blocking the formation of stress granules. Heise MT, editor. *J Virol.* 2023 Nov 30;97(11):e00979-23.
118. Kang W, Wang Y, Yang W, Zhang J, Zheng H, Li D. Research Progress on the Structure and Function of G3BP. *Front Immunol.* 2021 Aug 30;12:718548.
119. Vognsen T, Møller IR, Kristensen O. Crystal Structures of the Human G3BP1 NTF2-Like Domain Visualize FxFG Nup Repeat Specificity. Xu W, editor. *PLoS ONE.* 2013 Dec 4;8(12):e80947.
120. Schulte T, Liu L, Panas MD, Thaa B, Dickson N, Götte B, et al. Combined structural, biochemical and cellular evidence demonstrates that both FGDF motifs in alphavirus nsP3 are required for efficient replication. *Open Biol.* 2016 Jul;6(7):160078.
121. Guillén-Boixet J, Kopach A, Holehouse AS, Wittmann S, Jahnel M, Schlüßler R, et al. RNA-Induced Conformational Switching and Clustering of G3BP Drive Stress Granule Assembly by Condensation. *Cell.* 2020 Apr;181(2):346-361.e17.
122. Reineke LC, Lloyd RE. The Stress Granule Protein G3BP1 Recruits Protein Kinase R To Promote Multiple Innate Immune Antiviral Responses. Sandri-Goldin RM, editor. *J Virol.* 2015 Mar;89(5):2575–89.
123. Tourrière H, Gallouzi I eddine, Chebli K, Capony JP, Mouaikel J, Van Der Geer P, et al. RasGAP-Associated Endoribonuclease G3BP: Selective RNA Degradation and Phosphorylation-Dependent Localization. *Mol Cell Biol.* 2001 Nov 1;21(22):7747–60.
124. Parker F, Maurier F, Delumeau I, Duchesne M, Faucher D, Debussche L, et al. A Ras-GTPase-Activating Protein SH3-Domain-Binding Protein. *Mol Cell Biol.* 1996 Jun 1;16(6):2561–9.
125. Annibaldi A, Dousse A, Martin S, Tazi J, Widmann C. Revisiting G3BP1 as a RasGAP Binding Protein: Sensitization of Tumor Cells to Chemotherapy by the RasGAP 317–326 Sequence Does Not Involve G3BP1. Buday L, editor. *PLoS ONE.* 2011 Dec 19;6(12):e29024.
126. Liu ZS, Cai H, Xue W, Wang M, Xia T, Li WJ, et al. G3BP1 promotes DNA binding and activation of cGAS. *Nat Immunol.* 2019 Jan;20(1):18–28.

## Discussion

---

127. Yang Z, Johnson BA, Meliopoulos VA, Ju X, Zhang P, Hughes MP, et al. Interaction between host G3BP and viral nucleocapsid protein regulates SARS-CoV-2 replication [Internet]. *Cell Biology*; 2023 Jun [cited 2024 Feb 16]. Available from: <http://biorxiv.org/lookup/doi/10.1101/2023.06.29.546885>
128. Murigneux E, Softic L, Aubé C, Grandi C, Judith D, Bruce J, et al. Proteomic analysis of SARS-CoV-2 particles unveils a key role of G3BP proteins in viral assembly. *Nat Commun*. 2024 Jan 20;15(1):640.
129. Bhattacharya U, Neizer-Ashun F, Mukherjee P, Bhattacharya R. When the chains do not break: the role of USP10 in physiology and pathology. *Cell Death Dis*. 2020 Dec 4;11(12):1033.
130. Mapa CE, Arsenault HE, Conti MM, Poti KE, Benanti JA. A balance of deubiquitinating enzymes controls cell cycle entry. Solomon MJ, editor. *Mol Biol Cell*. 2018 Nov 15;29(23):2821–34.
131. Kee Y, Huang TT. Role of Deubiquitinating Enzymes in DNA Repair. *Mol Cell Biol*. 2016 Feb 1;36(4):524–44.
132. Hu M, Li P, Li M, Li W, Yao T, Wu JW, et al. Crystal Structure of a UBP-Family Deubiquitinating Enzyme in Isolation and in Complex with Ubiquitin Aldehyde. *Cell*. 2002 Dec;111(7):1041–54.
133. Yuan J, Luo K, Zhang L, Cheville JC, Lou Z. USP10 Regulates p53 Localization and Stability by Deubiquitinating p53. *Cell*. 2010 Feb;140(3):384–96.
134. Lin Z, Yang H, Tan C, Li J, Liu Z, Quan Q, et al. USP10 Antagonizes c-Myc Transcriptional Activation through SIRT6 Stabilization to Suppress Tumor Formation. *Cell Rep*. 2013 Dec;5(6):1639–49.
135. Zhang M, Hu C, Tong D, Xiang S, Williams K, Bai W, et al. Ubiquitin-specific Peptidase 10 (USP10) Deubiquitinates and Stabilizes MutS Homolog 2 (MSH2) to Regulate Cellular Sensitivity to DNA Damage. *J Biol Chem*. 2016 May;291(20):10783–91.
136. Takayama K ichi, Suzuki T, Fujimura T, Takahashi S, Inoue S. Association of USP10 with G3BP2 Inhibits p53 Signaling and Contributes to Poor Outcome in Prostate Cancer. *Mol Cancer Res*. 2018 May 1;16(5):846–56.
137. Song D, Kuang L, Yang L, Wang L, Li H, Li X, et al. Yin and yang regulation of stress granules by Caprin-1. *Proc Natl Acad Sci*. 2022 Nov;119(44):e2207975119.
138. Biswal M, Lu J, Song J. SARS-CoV-2 Nucleocapsid Protein Targets a Conserved Surface Groove of the NTF2-like Domain of G3BP1. *J Mol Biol*. 2022 May;434(9):167516.
139. Li X, Zhang H, Zhang Y, Li J, Wang Z, Deng C, et al. Development of a rapid antiviral screening assay based on eGFP reporter virus of Mayaro virus. *Antiviral Res*. 2019 Aug;168:82–90.

140. Weber C, König R, Niedrig M, Emmerich P, Schnierle BS. A neutralization assay for chikungunya virus infections in a multiplex format. *J Virol Methods*. 2014 Jun;201:7–12.
141. Fros JJ, Liu WJ, Prow NA, Geertsema C, Ligtenberg M, Vanlandingham DL, et al. Chikungunya Virus Nonstructural Protein 2 Inhibits Type I/II Interferon-Stimulated JAK-STAT Signaling. *J Virol*. 2010 Oct 15;84(20):10877–87.
142. Tyanova S, Temu T, Cox J. The MaxQuant computational platform for mass spectrometry-based shotgun proteomics. *Nat Protoc*. 2016 Dec;11(12):2301–19.
143. Lipps C, Klein F, Wahlicht T, Seiffert V, Butueva M, Zauers J, et al. Expansion of functional personalized cells with specific transgene combinations. *Nat Commun*. 2018 Mar 8;9(1):994.
144. Zhang X, Bogunovic D, Payelle-Brogard B, Francois-Newton V, Speer SD, Yuan C, et al. Human intracellular ISG15 prevents interferon- $\alpha/\beta$  over-amplification and auto-inflammation. *Nature*. 2015 Jan 1;517(7532):89–93.
145. Waggoner JJ, Ballesteros G, Gresh L, Mohamed-Hadley A, Tellez Y, Sahoo MK, et al. Clinical evaluation of a single-reaction real-time RT-PCR for pan-dengue and chikungunya virus detection. *J Clin Virol*. 2016 May;78:57–61.
146. Waggoner JJ, Rojas A, Mohamed-Hadley A, De Guillén YA, Pinsky BA. Real-time RT-PCR for Mayaro virus detection in plasma and urine. *J Clin Virol*. 2018 Jan;98:1–4.
147. Fronhoffs S, Totzke G, Stier S, Wernert N, Rothe M, Brüning T, et al. A method for the rapid construction of cRNA standard curves in quantitative real-time reverse transcription polymerase chain reaction. *Mol Cell Probes*. 2002 Apr;16(2):99–110.
148. Martin M. Cutadapt removes adapter sequences from high-throughput sequencing reads. *EMBnet.journal*. 2011 May 2;17(1):10.
149. Li H. Aligning sequence reads, clone sequences and assembly contigs with BWA-MEM [Internet]. arXiv; 2013 [cited 2024 Feb 28]. Available from: <http://arxiv.org/abs/1303.3997>
150. Danecek P, Bonfield JK, Liddle J, Marshall J, Ohan V, Pollard MO, et al. Twelve years of SAMtools and BCFtools. *GigaScience*. 2021 Jan 29;10(2):giab008.
151. Wilm A, Aw PPK, Bertrand D, Yeo GHT, Ong SH, Wong CH, et al. LoFreq: a sequence-quality aware, ultra-sensitive variant caller for uncovering cell-population heterogeneity from high-throughput sequencing datasets. *Nucleic Acids Res*. 2012 Dec 1;40(22):11189–201.
152. The pandas development team. pandas-dev/pandas: Pandas [Internet]. Zenodo; 2024 [cited 2024 Feb 28]. Available from: <https://zenodo.org/doi/10.5281/zenodo.3509134>
153. Hunter JD. Matplotlib: A 2D Graphics Environment. *Comput Sci Eng*. 2007;9(3):90–5.

## Discussion

---

154. Waskom M. seaborn: statistical data visualization. *J Open Source Softw.* 2021 Apr 6;6(60):3021.
155. Madeira F, Pearce M, Tivey ARN, Basutkar P, Lee J, Edbali O, et al. Search and sequence analysis tools services from EMBL-EBI in 2022. *Nucleic Acids Res.* 2022 Jul 5;50(W1):W276–9.
156. Sievers F, Higgins DG. Clustal Omega for making accurate alignments of many protein sequences. *Protein Sci.* 2018 Jan;27(1):135–45.
157. Krieg S, Pott F, Potthoff L, Verheirstraeten M, Bütepage M, Goltzmann A, et al. Mono-ADP-ribosylation by PARP10 inhibits Chikungunya virus nsP2 proteolytic activity and viral replication. *Cell Mol Life Sci.* 2023 Mar;80(3):72.
158. Eckeï L, Krieg S, Bütepage M, Lehmann A, Gross A, Lippok B, et al. The conserved macrodomains of the non-structural proteins of Chikungunya virus and other pathogenic positive strand RNA viruses function as mono-ADP-ribosylhydrolases. *Sci Rep.* 2017 Feb 2;7(1):41746.
159. Brylinski M. Aromatic interactions at the ligand–protein interface: Implications for the development of docking scoring functions. *Chem Biol Drug Des.* 2018 Feb;91(2):380–90.
160. Boulkroun S, Ruffieux-Daidié D, Vitagliano JJ, Poirot O, Charles RP, Lagnaz D, et al. Vasopressin-inducible ubiquitin-specific protease 10 increases ENaC cell surface expression by deubiquitylating and stabilizing sorting nexin 3. *Am J Physiol-Ren Physiol.* 2008 Oct;295(4):F889–900.
161. ARCHS4 [Internet]. [cited 2024 May 1]. Available from: <https://maayanlab.cloud/archs4/gene/AVPR2#tissueexpression>
162. NCBI Gene. USP10 - ubiquitin specific peptidase 10 (human) [Internet]. [cited 2024 May 1]. Available from: <https://pubchem.ncbi.nlm.nih.gov/gene/USP10/human>
163. Sheehan CT, Hampton TH, Madden DR. Tryptophan mutations in G3BP1 tune the stability of a cellular signaling hub by weakening transient interactions with Caprin1 and USP10. *J Biol Chem.* 2022 Dec;298(12):102552.
164. Yuan J, Luo K, Zhang L, Cheville JC, Lou Z. USP10 Regulates p53 Localization and Stability by Deubiquitinating p53. *Cell.* 2010 Feb;140(3):384–96.
165. Bomberger JM, Barnaby RL, Stanton BA. The Deubiquitinating Enzyme USP10 Regulates the Post-endocytic Sorting of Cystic Fibrosis Transmembrane Conductance Regulator in Airway Epithelial Cells. *J Biol Chem.* 2009 Jul;284(28):18778–89.
166. Franz S, Pott F, Zillinger T, Schüler C, Dapa S, Fischer C, et al. Human IFITM3 restricts chikungunya virus and Mayaro virus infection and is susceptible to virus-mediated counteraction. *Life Sci Alliance.* 2021 Jul;4(7):e202000909.
167. Rong L, Dahari H, Ribeiro RM, Perelson AS. Rapid Emergence of Protease Inhibitor Resistance in Hepatitis C Virus. *Sci Transl Med* [Internet]. 2010 May 5 [cited

2024 Mar 21];2(30). Available from:  
<https://www.science.org/doi/10.1126/scitranslmed.3000544>

168. Clutter DS, Jordan MR, Bertagnolio S, Shafer RW. HIV-1 drug resistance and resistance testing. *Infect Genet Evol.* 2016 Dec;46:292–307.
169. Drake JW, Holland JJ. Mutation rates among RNA viruses. *Proc Natl Acad Sci.* 1999 Nov 23;96(24):13910–3.
170. Rusinova I, Forster S, Yu S, Kannan A, Masse M, Cumming H, et al. INTERFEROME v2.0: an updated database of annotated interferon-regulated genes. *Nucleic Acids Res.* 2012 Nov 29;41(D1):D1040–6.
171. Rathore APS, Ng ML, Vasudevan SG. Differential unfolded protein response during Chikungunya and Sindbis virus infection: CHIKV nsP4 suppresses eIF2 $\alpha$  phosphorylation. *Virology J.* 2013 Dec;10(1):36.
172. Sudeep A, Vyas P, Parashar D, Shil P. Differential susceptibility & replication potential of Vero E6, BHK-21, RD, A-549, C6/36 cells & *Aedes aegypti* mosquitoes to three strains of chikungunya virus. *Indian J Med Res.* 2019;149(6):771.
173. Jenster LM, Lange KE, Normann S, vom Hemdt A, Wuerth JD, Schiffelers LDJ, et al. P38 kinases mediate NLRP1 inflammasome activation after ribotoxic stress response and virus infection. *J Exp Med.* 2022 Oct 31;220(1):e20220837.
174. Soncini C, Berdo I, Draetta G. Ras–GAP SH3 domain binding protein (G3BP) is a modulator of USP10, a novel human ubiquitin specific protease. *Oncogene.* 2001 Jun 28;20(29):3869–79.
175. Ravindran V, Wagoner J, Athanasiadis P, Den Hartigh AB, Sidorova JM, Ianevski A, et al. Discovery of host-directed modulators of virus infection by probing the SARS-CoV-2–host protein–protein interaction network. *Brief Bioinform.* 2022 Nov 19;23(6):bbac456.
176. Miller CL. Stress Granules and Virus Replication. *Future Virol.* 2011 Nov;6(11):1329–38.
177. Hirose T, Ninomiya K, Nakagawa S, Yamazaki T. A guide to membraneless organelles and their various roles in gene regulation. *Nat Rev Mol Cell Biol.* 2023 Apr;24(4):288–304.
178. Beckley JanelR, Chen JS, Yang Y, Peng J, Gould KathleenL. A Degenerate Cohort of Yeast Membrane Trafficking DUBs Mediates Cell Polarity and Survival\*. *Mol Cell Proteomics.* 2015 Dec;14(12):3132–41.
179. Han Y, Yun CC. Ubiquitin-specific peptidase 7 (USP7) and USP10 mediate deubiquitination of human NHE3 regulating its expression and activity. *FASEB J.* 2020 Dec;34(12):16476–88.

## Discussion

---

180. Kwon SK, Saindane M, Baek KH. p53 stability is regulated by diverse deubiquitinating enzymes. *Biochim Biophys Acta BBA - Rev Cancer*. 2017 Dec;1868(2):404–11.
181. Qvit N, Rubin SJS, Urban TJ, Mochly-Rosen D, Gross ER. Peptidomimetic therapeutics: scientific approaches and opportunities. *Drug Discov Today*. 2017 Feb;22(2):454–62.
182. Gwon Y, Maxwell BA, Kolaitis RM, Zhang P, Kim HJ, Taylor JP. Ubiquitination of G3BP1 mediates stress granule disassembly in a context-specific manner. *Science*. 2021 Jun 25;372(6549):eabf6548.
183. Kruse T, Benz C, Garvanska DH, Lindqvist R, Mihalic F, Coscia F, et al. Large scale discovery of coronavirus-host factor protein interaction motifs reveals SARS-CoV-2 specific mechanisms and vulnerabilities. *Nat Commun*. 2021 Nov 19;12(1):6761.
184. Panas MD, Schulte T, Thaa B, Sandalova T, Kedersha N, Achour A, et al. Viral and Cellular Proteins Containing FGDF Motifs Bind G3BP to Block Stress Granule Formation. Heise MT, editor. *PLOS Pathog*. 2015 Feb 6;11(2):e1004659.
185. Saul S, Ferguson M, Cordonin C, Fragkoudis R, Ool M, Tamberg N, et al. Differences in Processing Determinants of Nonstructural Polyprotein and in the Sequence of Nonstructural Protein 3 Affect Neurovirulence of Semliki Forest Virus. Diamond MS, editor. *J Virol*. 2015 Nov;89(21):11030–45.
186. Atasheva S, Gorchakov R, English R, Frolov I, Frolova E. Development of Sindbis Viruses Encoding nsP2/GFP Chimeric Proteins and Their Application for Studying nsP2 Functioning. *J Virol*. 2007 May 15;81(10):5046–57.
187. Wang S, Merits A. G3BP/Rin-Binding Motifs Inserted into Flexible Regions of nsP2 Support RNA Replication of Chikungunya Virus. Williams BRG, editor. *J Virol*. 2022 Nov 9;96(21):e01278-22.



## 5 Abbreviations

Abbreviation	Full name
AMPK $\alpha$	AMP-Activated Protein Kinase Alpha
ATPS $\beta$	ATP Synthase $\beta$ Subunit
ATXN2	Ataxin-2
AUD	Alphavirus Unique Domain
AVP	Arginine Vasopressin
BHK-21	Baby Hamster Kidney Cells
C	Capsid Protein
CBP	Calmodulin-Binding Peptide
CFTR	Cystic Fibrosis Transmembrane Conductance Regulator
cGAS	cyclic GMP-AMP Synthase
CHIKV	Chikungunya Virus
Co-IP	Co-Immunoprecipitation
CPE	Cytopathic Effect
DAPI	4',6-Diamidino-2-Phenylindole
DDX1	DEAD box 1
DMEM	Dulbecco's Modified Eagles Medium
DNA	Deoxyribonucleic Acid
DUB	Deubiquitinase
E	Envelope Protein
ECSA	East Central South African
EDTA	Ethylene Diamine Tetraacetic Acid
EEEV	Eastern Equine Encephalitis Virus
eGFP	Enhanced Green Fluorescent Protein
EGTA	Ethylene Glycol Tetraacetic Acid
eIF2 $\alpha$	eukaryotic initiation factor 2 $\alpha$
ER	Endoplasmatic Reticulum
EV	Empty Vector
FACS	Fluorescence Activated Cell Sorting
FCS	Fetal Calf Serum
FHL1	Four and a Half LIM Domain Protein 1 Gene

## Abbreviations

---

FMRP	Fragile X mental retardation protein
G3BP	Ras-GAP SH3 Domain Binding Protein
G3BP	Ras-GTPase-activating protein SH3-domain-binding protein
gp	Glycoprotein
h. p.i.	hours post-infection
h. p.t.	hours post-transfection
HEK-293T	Human Embryonic Kidney cell line
HVD	Hypervariable Domain
IF	Immunofluorescence
IFIT1	Interferon Induced Protein With Tetratricopeptide Repeats 1 Gene
IFITM	Interferon Induced Transmembrane Protein
IFN	Interferon
IFNAR	Interferon Alpha/Beta Receptor
IFNAR	Interferon Lambda Receptor
IL	Interleukin
IOL	Indian Ocean lineage
IRF	Interferon Regulatory Factor
IRF	Interferon Regulatory Factor
ISG	Interferon-Stimulated Gene
JAK	Janus Kinase
KO	Knock-out
LLPS	Liquid-Liquid Phase Separation
m7GMP	7-Methyl-Guanosine-5'-Monophosphate
MAYV	Mayaro Virus
MCC	Manders' Correlation Coefficient
MD	Macro Domain
MDA5	Melanoma Differentiation-Associated protein 5
MOI	Multiplicity of Infection
mRNA	messenger RNA
MS	Mass Spectrometry
MXRA8	Matrix Remodeling Associated 8 Protein
NEMO	NF- $\kappa$ B-Essential Modulator
NF $\kappa$ B	Nuclear Factor Kappa-B Kinase

---

NGS	Next Generation Sequencing
nsP	non-structural protein
NTF2	Nuclear Transport Factor 2
NUFIP2	FMR1 Interacting Protein 2
ORF	Open Reading Frame
p1234	non-structural polyprotein
PABP1	Poly(A) Binding Protein Cytoplasmic 1
PAM	Protospacer Adjacent Motif
PBS	Phosphate Buffered Saline
PCR	Polymerase Chain Reaction
PFA	Paraformaldehyd
PFU	Plaque Forming Units
PKR	Protein Kinase R
PRNT	Plaque Reduction Neutralization Test
PRR	Pattern Recognition Receptor
qPCR	quantitative PCR
RasGAP	Ras-GTPase-activating protein
RBP	RNA-binding Protein
RIG-I	Retinoic Acid Inducible Gene I
RLR	RIG-I-like Receptor
RNA	Ribonucleic Acid
RT-PCR	Reverse Transcription Polymerase Chain Reaction
SARS-CoV-2	Severe Acute Respiratory Syndrome Coronavirus 2
SD	Standard Deviation
SDS	Sodium Dodecyl Sulphate
SFV	Semliki Forest Virus
SG	Stress Granule
SINV	Sindbis Virus
SNP	Single Nucleotide Polymorphism
SOC	Super Optimal broth with Catabolite repression
STAT	Signal Transducer and Activator of Transcription
TAE	Tris-Acetate Ethylene diamine tetraacetic acid
TAP	Tandem affinity purification

---

## Abbreviations

---

TCEP	Tris(2-carboxyethyl)phosphine
TEV	Tobacco Etch Virus
TF	Trans-Frame protein
TIA-1	T-cell restricted intracellular antigen-1
TIA-1/R	T-cell restricted intracellular antigen-1-related protein
TLR	Toll-Like Receptor
TNF- $\alpha$	Tumor Necrosis Factor $\alpha$
U2OS	Human Osteosarcoma Cells
UBAP2L	Ubiquitin Associated Protein 2 Like
USP10	Ubiquitin-Specific Peptidase 10
UTR	Untranslated Region
VEEV	Venezuelan Equine Encephalitis Virus
vRC	viral Replication Complex
vRNA	viral RNA
VSV	Vesicular Stomatitis Virus
VSV-G	Vesicular Stomatitis Virus Glycoprotein
WA	West African
WB	Western Blot
WCL	Whole Cell Lysate
WEEV	Western Equine Encephalitis Virus
WHO	World Health Organization
WT	Wild Type

---

## 6 Acknowledgments

First, I would like to thank Prof. Dr. Christine Goffinet and Prof. Dr. Christian Drosten for giving me the opportunity and providing the resources to delve into this fascinating work at the Institute of Virology at Charité Berlin.

My profound gratitude goes to Prof. Dr. Christine Goffinet, my supervisor and mentor, for the unparalleled support and guidance throughout the years. Your insight, inspiration, and attention to detail have been the cornerstone of this thesis.

I am deeply thankful to Prof. Dr. Gerhard Wolber, for his co-supervision, his support, and encouragement.

I would like to thank all the people whose contribution was vital to the completion of this work. Special thanks go to Dr. Patricia Korn and her lab for their indispensable contributions. Many thanks to Dr. Fabian Pott for his invaluable advice during the initial phase of this project. Special thanks to Jenny Jansen for her exceptional technical assistance, and Niklas Endres for his guidance in biomedical analyses.

Thank you to the entire Goffinet Lab for providing a uniquely open and friendly work environment and to all my colleagues and friends at the Institute of Virology at the Charité.

Lastly, I would like to thank my family and friends for their constant support.

This journey has been more than an academic endeavor. It has been a transformative experience, made possible by each of you.

## 7 Curriculum Vitae

### Education

---

- Since 06/2019 **Charité Universitätsmedizin Berlin and Freie Universität Berlin**  
Doctoral Student, Institute of Virology  
Doctoral Thesis “The Antiviral Role of USP10 in Response to Chikungunya and Mayaro Virus Infections”, under the supervision of Prof. Dr. Christine Goffinet
- 10/2017 – 11/2018 **Freie Universität Berlin**  
Study of Pharmaceutical Sciences (M.Sc.)  
Master Thesis “Exploring Flaviviral Resistance: A Dynamic Hotspot Analysis” under the supervision of Prof. Dr. Gerhard Wolber
- 11/2013 – 06/2017 **Johannes Gutenberg-Universität Mainz**  
Study of Pharmacy (2<sup>nd</sup> and 3<sup>rd</sup> state examination)
- 10/2011 – 09/2013 **Philipps Universität Marburg**  
Study of Pharmacy (1<sup>st</sup> state examination)

### Research and Work Experience

---

- 06/2019 – 01/2024 **Charité Universitätsmedizin Berlin**  
Doctoral Candidate at the Goffinet Lab, Institute of Virology
- 08/2021 – 10/2021 **University of Rijeka**  
Research Stay at the Jonjić Lab, University of Rijeka, Croatia
- 11/2018 – 04/2019 **Freie Universität Berlin**  
Teaching Assistant in the lab course “General and Analytical Chemistry of Inorganic Pharmaceutical Agents, Excipients and Toxicants” at the Institute of Pharmacy
- 11/2017 – 11/2018 **Freie Universität Berlin**  
Masters Candidate at the Wolber Lab, Department of Pharmaceutical and Medicinal Chemistry, Institute of Pharmacy
- 11/2016 – 05/2017 **University of Vermont, Burlington, VT**  
Research Internship in the Dostmann Lab, Department of Pharmacology, College of Medicine
- 05/2016 – 10/2016 **Roemerapotheke Mainz**  
Pharmaceutical Internship
- 03/2015 – 04/2015 **Sanofi Frankfurt**  
Student Employee

## 8 Appendix

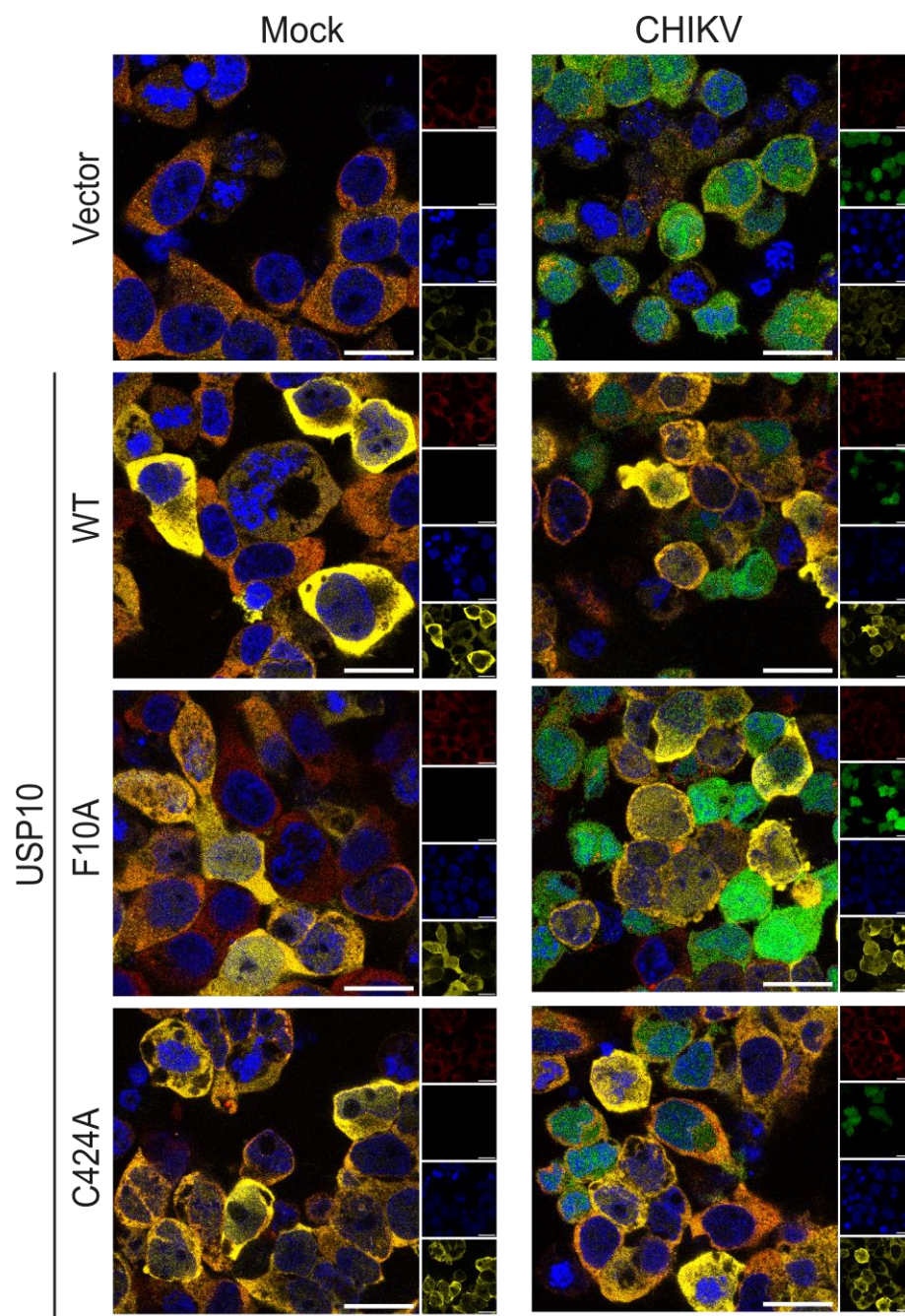
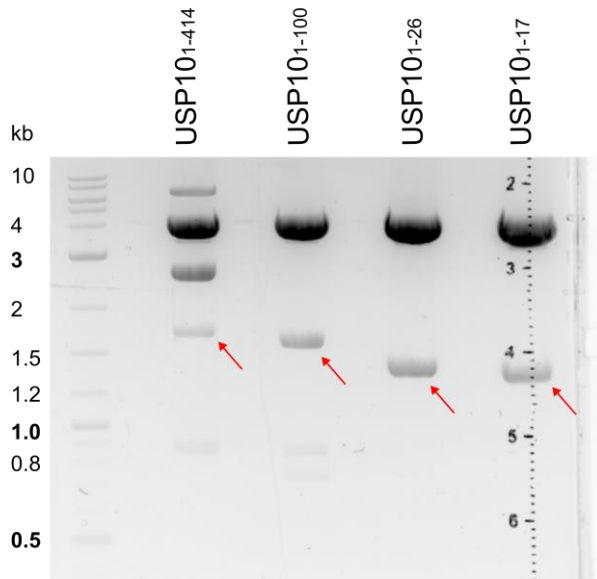
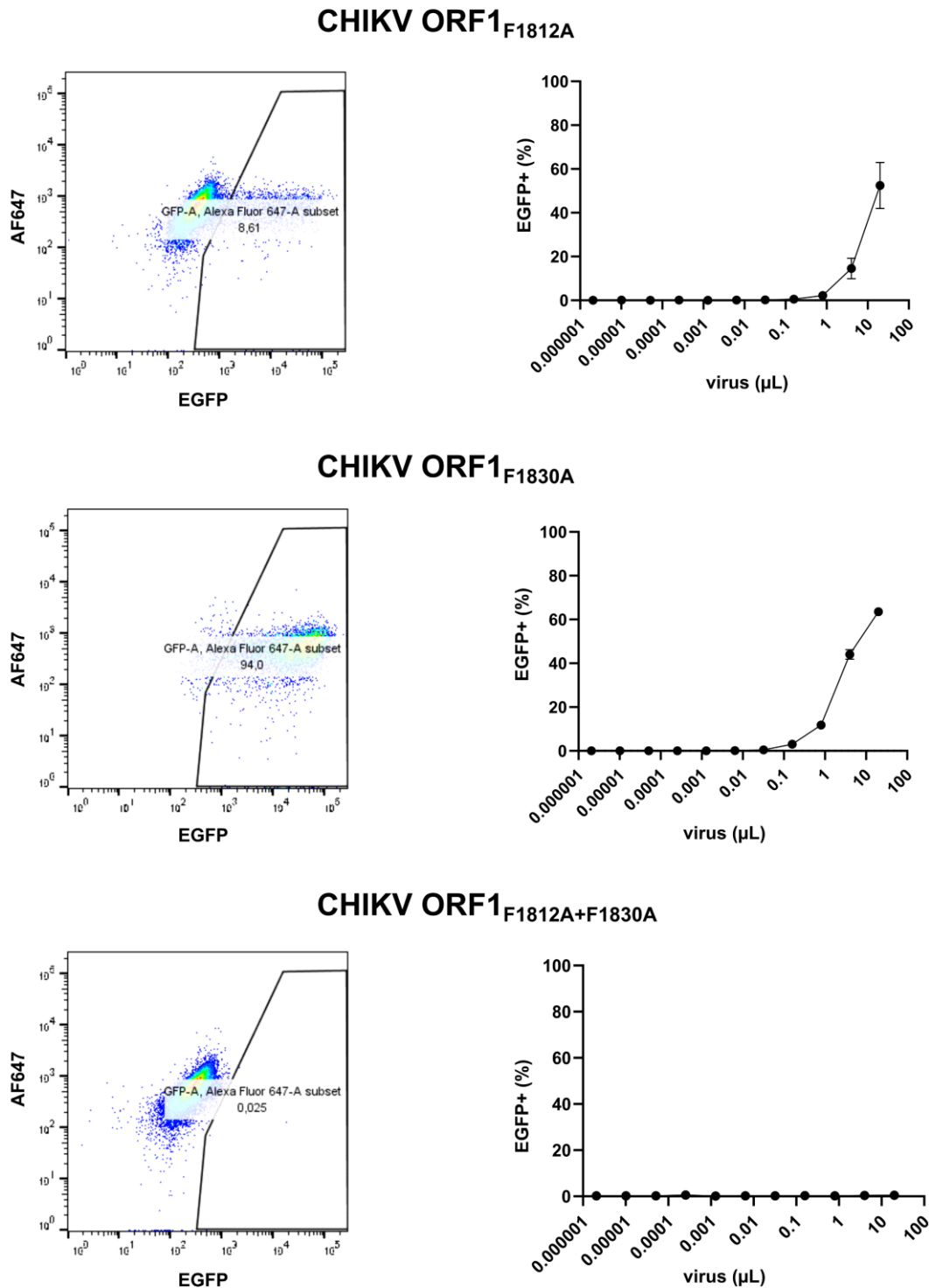


Figure S 1: Microscopy of CHIKV-infected USP10-overexpressing HEK-293T cells



**Figure S 2: Gel electrophoresis of double-digested USP10 fragments.** Plasmids containing Flag-tagged USP10 fragments were cut with the restriction enzymes MluI-HF and XbaI at 37 °C overnight and separated on a 1% agarose gel. Expected band sizes were 4129 and 2627 base pairs for USP10<sub>1-414</sub>, 4129 + 1685 base pairs for USP10<sub>1-100</sub>, 4129 + 1464 base pairs for USP10<sub>1-26</sub>, and 4129 + 1437 base pairs for USP10<sub>1-17</sub>.





**Figure S 3: Growth kinetics of CHIKV mutants.** Infection rate of CHIKV ORF1 F1812A, CHIKV ORF1 F1830A, and CHIKV ORF1 F1812A+F1813A in BHK-21 cells. 48 hours after electroporation, cells were fixed in 6% PFA and analyzed via flow cytometry (left). Virus stocks were titrated on naïve HEK-293T cells. 24 h p.i. cells were fixed in 6% PFA for cytometric analysis (right).

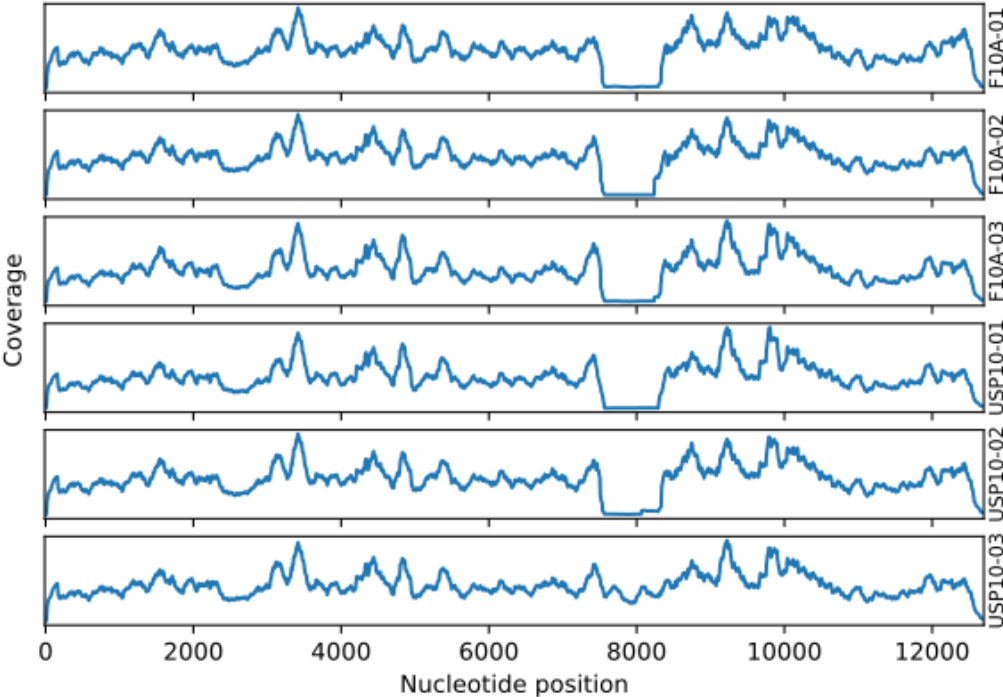


Figure S 4: Coverage plot of next generation sequencing analysis.

Table S 1: Potential interaction partners of CHIKV nsP3 in Affinity Purified MS/MS

	nsP3 WT		nsP3 MD	
	BirA > 10	TAP > 10	TAP > 5	BirA >10
ATXN2	+	+	+	+
CD2AP	+	+	+	+
FHL1	+	+	+	+
FXR2	+	+	+	+
G3BP1	+	+	+	+
LARP1	+	+	+	+
MAGED2	+	+	+	+
NAP1L1	+	+	+	+
NUFIP2	+	+	+	+
ATXN2L	+		+	+
DDX1	+		+	+
PRPF31	+		+	+
PRRC2C	+		+	+
CSNK1E	+	+	+	
DDX6	+	+	+	
G3BP2	+	+	+	
USP10	+	+	+	
UPF3B	+		+	

## Appendix

**Table S 2: Nucleotide exchanges in eGFP-CHIKV after ten passages on USP10 WT vs F10A overexpressing HEK-293T cells.**

	Location	Nucleotide exchange	Mutation
<b>ORF1</b>	nsP1	-	-
	nsP2	A2940G	D420G
		C3484T	I601I
		C3610A	N643K
		C3670T	D663D
		T4020C	V780A
		A4072G	G797G
		nsP3	-
	nsP4	-	-
	<b>eGFP</b>	eGFP	C8032T
G8237C			V223L
A8294T			T242S
A8613C			P57P
<b>ORF2</b>	C	C8827T	L128L
	E3	-	-
		A9430G	N5D
		G9661A	G82R
		C9881T	T155M
		G9913A	E166K
		A9928G	M171V
		A9976G	N187D
		A10129T	N238Y
	E2	A10130G	N238S
	6K	-	-
	E1	-	-